Doctoral Dissertation

Structure, stability and activity of metagenome-derived LC-cutinase with polyethylene terephthalate (PET) degrading ability

（ポリエチレンテレフタレート（PET）分解能を有するメタゲノム由来 LC—クチナーゼの構造、安定性、活性）

Sintawee Sulaiman

June 2014

Graduate School of Engineering
Osaka University

Contents

Abbreviations

Bc-Lip:	*Burkholderia cepacia* lipase
BHET:	*bis*(2-hydroxyethyl)terephthalate
CBB:	Coomassie brilliant blue
CD:	Circular dichroism
Coot:	Crystallographic Object-Oriented Toolkit
Cr-Lip:	*Candida rugosa* lipase
DTT:	Dithiothreidol
EDTA:	Ethylenediaminetetraacetic acid
GdnHCl:	Guanidine hydrochloride
IPTG:	Isopropyl thio-β-D-galactoside
LCC:	LC-cutinase
MHET:	mono(2-hydroxyethyl)terephthalate
PCL:	Poly(ε-caprolactone)
PCR:	Polymerase chain reaction
PDB:	Protein data bank
PEG:	Polyethyleneglycol
PET:	Polyethyl terephthalate
*p*NP:	*p*-nitrophenol
RMSD:	Root-mean-square deviation
SDS-PAGE:	Sodium dodecyl sulfate-polyacrylamide gel electrophoresis
TaC:	*Thermobifida alba* cutinase
TfC:	*Thermobifida fusca* cutinase
TPA:	Terephthalic acid

CHAPTER 1

General introduction

1.1 Cutinase

Cutinase (3.1.1.74) is a lipolytic/esterolytic enzyme that hydrolyzes cutin as a natural substrate. Cutin is an insoluble lipid polyester composed of hydroxyl and hydroxyepoxy fatty acids (Kolattukudy, 1980, 1981). The most common major components of cutin (Fig. 1-1A) are derivatives of saturated palmitic (C_{16}) and stearic (C_{18}) acids (Kolattukudy, 2001). Cutin is the major constituent of the cuticle (Fig. 1-1B), which protects plants from dehydration, and is a barrier to pathogenic infections.

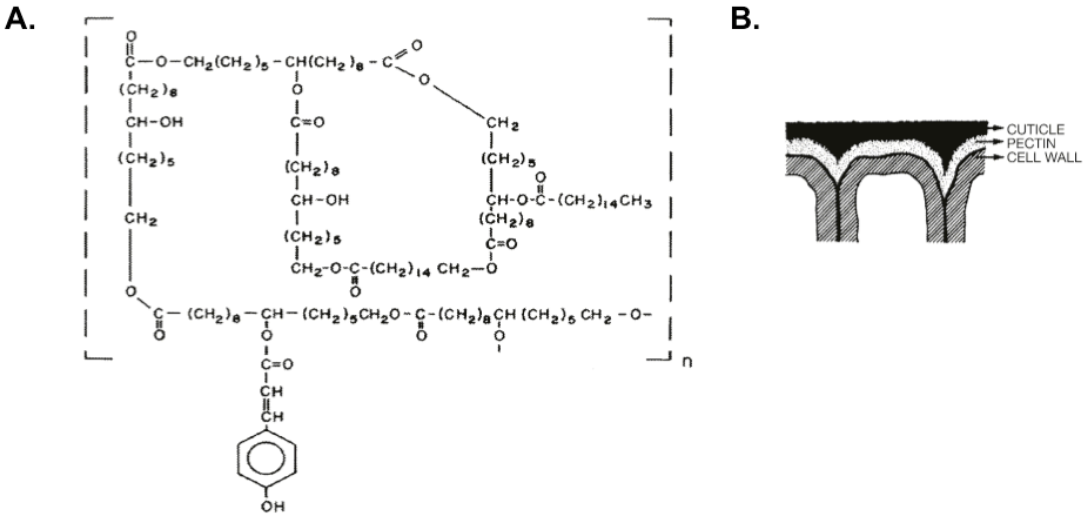

Fig. 1-1 Models showing structures present in cutin polymers and cutin location. (A) Cutin contains C_{16} and C_{18} acids as major components of this complex structure. (B) Schematic representation of cutin in plant. This insoluble cuticular polymer of plants is composed of interesterified hydroxyl and hydroxyepoxy fatty acids derived from common cellular fatty acids and attached to the cell's outer epidermal layer by a pectinaceous layer (Kolattukudy, 2001).

Early work focused on the role of cutinase in plant fungal infections. Cutinases are enzymes produced by several phytopathogenic fungi, such as *Fusarium solani, Colletotrichum capsici*, and *C. gloeosporioides* (Soliday *et al*., 1984; Ettinger *et al*., 1987). Germinating fungal spores of phytopathogens secrete cutinase to assist in penetrating the cuticular barrier, and inhibition of this enzyme prevents infection through intact cuticular barriers (Kolattukudy *et al*., 1985). Cutinase is induced in spores of virulent pathogenic fungi soon after contact with cutin (Fig. 1-2; Woloshuk & Kolattukudy, 1986).

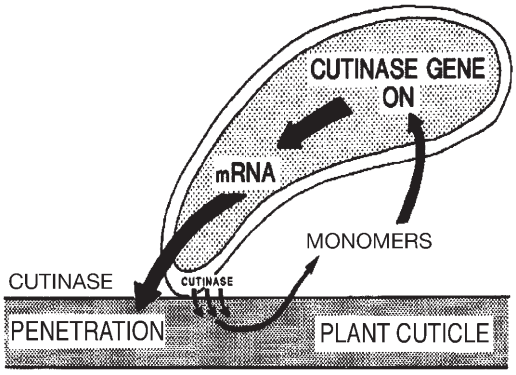

Fig. 1-2 Schematic representation of plant cuticle induction of cutinase in a fungal spore (Kolattukudy, 2001).

Later work with *Alternaria brassicicola* has demonstrated that cutinases are a diverse group of enzymes, in which some cutinases are essential for pathogenicity, while others are expressed during saprophytic growth on cutin as a carbon source (Fan and Köller, 1998; St Leger *et al*., 1997). More recent research has demonstrated that both pathogenic and saprophytic microorganisms express cutinases, that the genomes of individual species might harbor several different putative cutinases, and that these enzymes are expressed at different times during the microbial life cycle (Skamnioti *et al*., 2008[a], 2008[b]). Cutinase was first purified in the 1970s from *F. solani* grown on

cutin as a sole carbon source (Purdy and Kolattukudy, 1975). The molecular weight and subunit composition of most fungal cutinases thus far purified show that they are single peptides with a molecular weight range of 20–25 kDa. Although originally found in pathogenic fungi, cutinases have subsequently been isolated and characterized from bacteria, such as *Thermobifida fusca* (Chen *et al*., 2008), *T. alba* (Hu *et al*., 2010), and *T. cellulosilytica* (Herrero Acero *et al*., 2011), and from a variety of both pathogenic and nonpathogenic fungi, including the yeast *Cryptococcus* (Masaki *et al*., 2005). There is evidence suggesting that the activities of cutinase-producing saprophytic bacteria, such as *Pseudomonas putida*, might provide a carbon source to a wider microbial community (Sebastian *et al*., 1987). This particular bacterial cutinase is a 30-kDa protein with an amino acid composition distinctly different from that of fungal cutinases and does not show an immunological relationship with fungal cutinases (Kolattukudy, 2001). The microbial strains that have been shown to produce cutinases are listed in Table 1-1.

Table 1-1. Microbial cutinases

Organism	Genus	Species	Reference
Fungi	*Fusarium*	*solani*	Purdy and Kolattukudy, 1975
		oxysporum	Nimchua *et al*., 2007
		roseum culmorum	Soliday and Kolattukudy, 1976
		roseum	Lin and Kolattukudy, 1980
		sambucinum	

Table 1-1. (Continued) Microbial cutinases

Organism	Genus	Species	Reference
Fungi	*Ulocladium*	*consortiale*	Lin and Kolattukudy, 1980
	Helminthosporium	*sativum*	Lin and Kolattukudy, 1980
	Aspergillus	*nidulans*	Castro-Ochoa *et al*., 2012
		niger	Nyyssola *et al*., 2013
	Monilinia	*fructicola*	Wang *et al*., 2000
	Alternaria	*brassicicola*	Trail and Köller, 1993
	Pyrenopeziza	*brassicae*	Davies *et al*., 2000
	Botrytis	*cinerea*	Shishiyama *et al*., 1970
	Magnaporthe	*grisea*	Sweigard *et al*., 1992
	Colletotrichum	*gloeosporioides*	Ettinger *et al*., 1987
		kahawae	Chen *et al*., 2007
		capsici	Hijden *et al*., Unilever patent WO 9403578.94.02
	Cochliobolus	*heterostrophus*	Trail and Köller, 1990
	Rhizoctonia	*solani*	Trail and Köller, 1990
	Venturia	*inaequalis*	Köller and Parker, 1989
	Penicillium	sp.	Nimchua *et al*., 2008
		citrinum	Liebminger *et al*., 2007
	Aspergillus	*oryzae*	Ohnishi *et al*., 1995
	Pseudomonas	*antarctica*	Susuki *et al*., 2012
	Phytopthora	*cactorum*	Egmond *et al*., 1997
	Coprinopsis	*cinerea*	Kontkanen *et al*., 2009

Table 1-1. (Continued) Microbial cutinases

Organism	Genus	Species	Reference
Fungi	*Humicola*	*insolens*	Ronkvist *et al*., 2009
	Thielavia	*terrestris*	Yang *et al*., 2013
Bacteria	*Streptomyces*	*scabies*	Lin and Kolattukudy, 1980
		acidiscabies	Fett *et al*., 1992a
		badius	Fett *et al*., 1992a
	Thermobifida	*fusca*	Kleeberg *et al*., 1998
		alba	Hu *et al*., 2010
		cellulosilytica	Herrero Acero *et al*., 2011
	Thermoactinomyces	*vulgaris*	Fett *et al*., 2000
	Pseudomonas	*putida*	Sebastian *et al*., 1987
		aeruginosa	Fett *et al*., 1992b
		mendocina	Degani *et al*., 2006
Yeast	*Cryptococcus*	sp.	Masaki *et al*., 2005
Pollen (Nasturtiumpollen)	*Tropaeolum*	*majus*	Maiti *et al*., 1979

1.2 Cutinase diversity

Relatively recent work on the molecular taxonomy of fungal cutinases (Skamnioti *et al*., 2008a) has suggested that fungal cutinases can be divided into two ancient subfamilies. This partition is likely to have resulted from gene duplication event before the divergence of the Basidiomycota and Ascomycota. Furthermore, the cutinase families of all sequenced fungal genomes display extreme coding divergence, much

more so than the significantly larger fungal families of P450 monooxygenases (Deng *et al*., 2007). This could reflect the diversity of roles attributed to cutinases, ranging from host-signal perception and transduction to fungal penetration of a host and subsequent carbon acquisition, and which could have contributed to fungal adaptation to diverse ecological niches. Furthermore, no cutinase sequences have been found in the *Saccharomycotina* (true yeasts), which might indicate that the enzyme family has not been maintained by selection in nonplant-infecting nonfilamentous hemiascomycete or archaeascomycete yeasts. A similar comparative study of the cutinase sequence from *Phytophthora*, a genus of phytopathogenic oomycetes (water mold), identified related cutinase sequences in three genera of *Actinobacteria* and suggested lateral gene transfer (LGT) between ancient bacteria and oomycetes (Belbahri *et al*., 2008). In contrast to this speculation, a phylogenetic analysis of the cutinases from five filamentous *Ascomycete* fungi *(Magnaphorthe grisea*, *Neurospora crassa*, *Aspergillus nidulans*, *Botrytis cinerea*, and *Fusarium graminearum*) and cutinases from Mycobacteria reveals a distinct clade with a long branch carrying only the bacterial sequences (Skamnioti *et al*., 2008b). This suggests that no fungal genes are closely related to mycobacterial cutinases and that lateral gene transfer has not been a major factor in the evolution of the cutinase gene family. Additionally, the phylogenetic analysis shows the high degree of sequence diversity within the fungal cutinase genes due to the significant copy number variation of cutinases and there are no intron positions are shared across the deepest divergences in the phylogeny. The total lack of conservation in intron positioning among their fungal cutinase genes further suggests that these genes have undergone ancient and extensive sequence diversification (Skamnioti *et al*., 2008b). Transcription analysis of 14 putative cutinases from *M. grisea* strain Guy11 has

revealed that four of them are constitutively expressed and that one gene has elevated expression only during early differentiation. Six genes have elevated expression during plant penetration and, finally, three genes have elevated expression *in planta*. There is no correlation between the phylogenetic clades of these putative cutinases and some phylogenetic group contains cutinases homologous to bacterial acetylxylan esterases, which suggested the functional divergence of these cutinases. Therefore, it is possible that cutinase-like proteins from the important human bacterial pathogen *Mycobacterium tuberculosis*, which share high sequence homology with fungal cutinase and exhibits strong esterase activity, do not possess cutinase activity (West *et al*., 2009).

The Genbank accession numbers of genes that have been shown to encode true cutinases are presented in Table 1-1. Aligning all of true cutinase sequences allows construction of a true cutinase phylogenetic tree (Fig. 1-3) and reveals that the prokaryotic cutinases are distinct from eukaryotic cutinases. Their low sequence identity indicates that they have undergone extensive evolutionary differentiation. The eukaryotic family appears to fall into three subgroups, two of which contain fungal sequences, and the other of which contains true cutinases from yeast-like fungi (*Cryptococcus* sp. and *Pseudozyma antarctica*). The two fungal subgroups share roughly 30% similarity, while the yeast-like sequences share approximately 19% similarity with the two fungal groups. It appears that the known true cutinases provide a diverse sample of the cutinase families, identified through broad phylogenetic analysis of genome sequences.

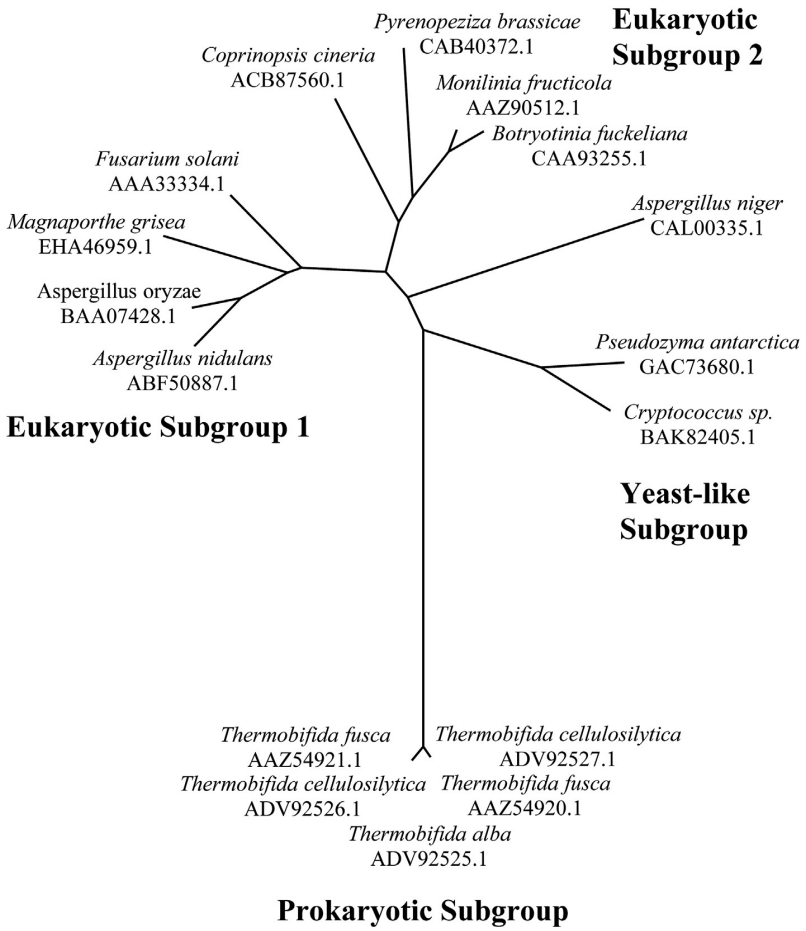

Fig. 1-3 Phylogenetic analysis of cutinase genes. Species and Genbank accession numbers of true cutinases from Table 1-1 arranged on a phylogenetic tree (Chen *et al.*, 2013).

1.3 Overall structure of fungal and bacterial cutinases

The first X-ray crystal structure of a cutinase was determined in 1992 from *F. solani* (PDB ID: 1CUS; Martinez *et al*., 1992). The structure revealed that *F. solani* cutinase adopts an α/β fold that exposes a catalytic serine residue (Ser120) to the solvent, instead of burying the active site with a hydrophobic loop. In 2009, the X-ray crystal structures of *Glomerella cingulata* cutinase (PDB ID: 3DCN; Nyon *et al*., 2009), *A. oryzae* cutinase (PDB ID: 3GBS; Liu *et al*., 2009), and *Cryptococcus* sp. cutinase (PDB ID: 2CZQ; Kodama *et al.*, 2009) were determined. These were followed in 2012

by the structural determination of bacterial cutinase from *T. alba* (PDB ID: 3VIS; Kitadokoro *et al.*, 2012) (Fig 1-4).

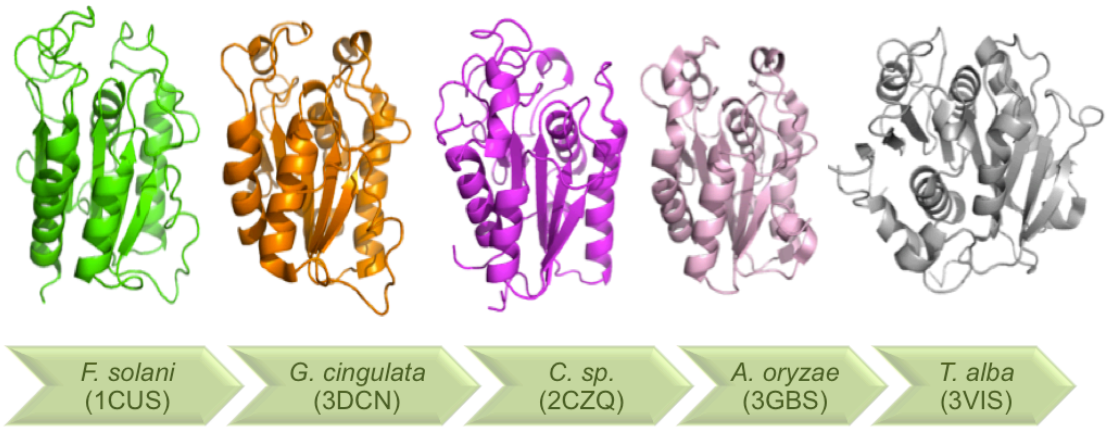

Fig. 1-4 Cutinase X-ray crystal structures from various organisms. PDB IDs of cutinase structures indicated in parentheses. *F. solani*, *G. cingulata*, *Cryptococcus* sp., *A. oryzae,* and *T. alba* cutinases rendered in green, orange, magenta, pink, and grey ribbons, respectively.

Fungal cutinase from *F. solani* consists of 197 amino acid residues as an α/β-protein with a hydrophobic core comprising a slightly twisted five-parallel-stranded β-sheet surrounded by four α-helices (Fig. 1-5). The active site consists of Ser120, Asp175, and His188, and an oxyanion hole consists of Ser42 and Gln121. The amino acid sequence encompassing Ser120 (Gly-Tyr-Ser-Gln-Gly) matches the consensus sequence Gly-His(Tyr)-Ser-X-Gly commonly present in lipases. Unlike most lipases, the catalytic serine residue is not buried under an amphipathic loop but is accessible to the solvent (Longhi and Cambillau, 1999). The two disulfide bonds in this cutinase are Cys31-Cys109, which links the N-terminal end to a β-turn and participates in stabilization of the global molecular folding, and Cys171-Cys178, which can be

assumed to play an important role in stabilization of two consecutive β-turns on which is located one of the catalytic residues, Asp175.

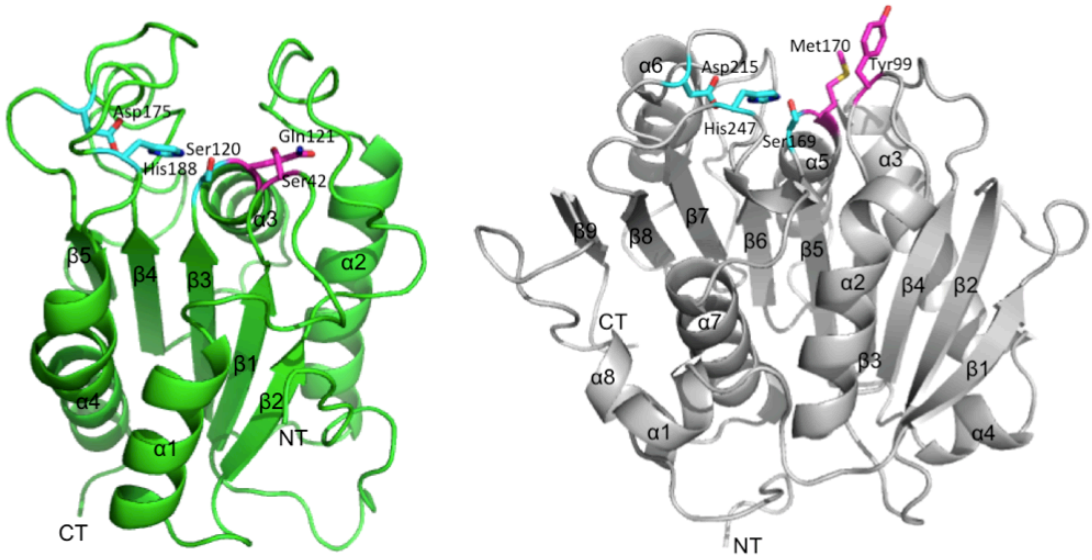

Fig. 1-5 Overall structure of fungal cutinase, *F. solani* cutinase (green) and bacterial cutinase from *T. alba* (grey) rendered as ribbon diagrams. Side chains of catalytic triads depicted as cyan sticks. Side chains of putative anion hole residues Ser42 and Gln121 of *F. solani* cutinase rendered as magenta sticks, as are putative anion hole-forming residues Tyr99 and Met170 of *T. alba* cutinase.

T. alba cutinase adopts an α/β hydrolase fold similar to fungal cutinase, but the fold is larger than those in fungal cutinases. The crystal structure of *T. alba* cutinase exhibits an α/β-hydrolase fold consisting of a central twisted β-sheet, two of which are antiparallel, rather than the five-parallel-stranded β-sheet present in fungal forms. The central β-sheet is flanked on both sides by α-helices, and the nine β-strands assemble in the order of 1-2-4-3-5-6-7-8-9 into a central parallel β-sheet, which is surrounded by eight helices. As in fungal cutinase, *T. alba* cutinase contains a Ser-Asp-His catalytic triad, and the catalytic serine residue is solvent accessible. Here, Ser169, Asp215, and His 247 form the catalytic triad, which is located on loops between the β-sheet and

helices. The oxyanion hole is formed by the main chain amides of Tyr99 and Met170. The disulfide bond is formed between Cys280 and Cys298 in the C-terminal region of the structure.

In addition to the catalytic triad, all these cutinases contain at least one disulfide bond, which is assumed to play an important role in structure stabilization. The main characteristics of these cutinases are presented in Table 1-2. However, the thermostability is not dependent on the number of disulfide bonds. For example, *T. alba* cutinase, which contains only one disulfide bond, is more thermostable than either of the *F. solani* or *A. oryzae* cutinases, which have two and three disulfide bonds, respectively (Liu *et al*., 2009).

Table 1-2. Characteristics of available cutinase structures

Organism	PDB ID	Catalytic triad	Oxyanion binding residues	Disulfide bonds	Resolution (Å)	References
F. solani	1CUS	Ser120/Asp175/His188	Ser42/Gln121	Cys31-Cys109 Cys171-Cys178	1.25	Martinez *et al*., 1992
G. cingulata	3DCN	Ser136/Asp191/His204	Ser57/Gln137	Cys46-Cys124	1.9	Nyon *et al*., 2009
A. oryzae	2CZQ	Ser126/Asp181/His194	Ser48/Gln127	Cys63-Cys76 Cys37-Cys115 Cys177-Cys184	1.75	Liu *et al*., 2009
C. sp.	3GBS	Ser85/Asp165/His180	Thr17/Gln86	Cys6-Cys78 Cys161-Cys168	1.05	Kodama *et al.*, 2009
T. alba	3VIS	Ser169/Asp215/His247	Met170/Tyr99	Cys280-Cys298	1.76	Kitadokoro *et al.*, 2012

1.4 Catalytic mechanism of cutinase

Cutinase catalyzes hydrolysis of ester bonds using the catalytic triad involving histidine, aspartic acid, and "active" serine (Fig. 1-6). A serine residue is hydrogen-bonded to a histidine residue, and a carboxylate-residue of aspartic acid hydrogen-bonded to this same histidine residue.

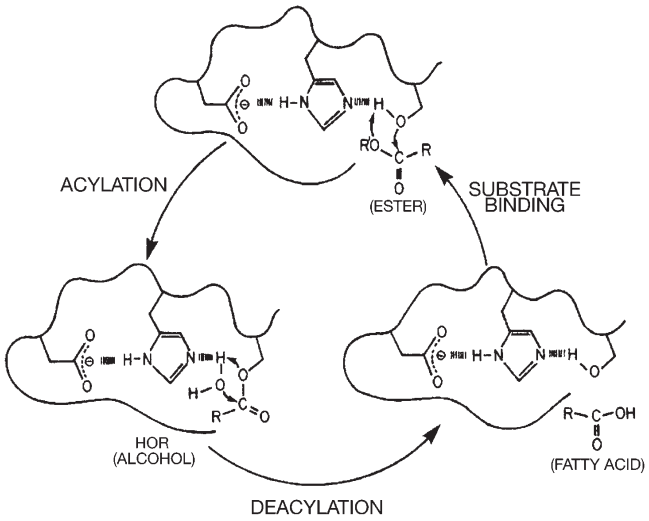

Fig. 1-6 Mechanism of cutinase catalysis. The substrate enters the catalytic pocket and generates a covalent intermediate that links the catalytic serine residue to the carbonyl group of the ester being hydrolyzed. Transition states in the enzyme mechanism's acylation/deacylation steps are stabilized by interaction of key residues forming an oxyanion hole (Kollatukudy, 2001).

Cutinases perform their catalysis in two discrete steps. First, a nucleophilic attack of the serine side chain oxygen on the ester bond's carbonyl carbon atom leads to the formation of a tetrahedral intermediate; the histidine assists in increasing the serine hydroxyl group's nucleophilicity. The histidine imidazole ring then becomes protonated and positively charged, with the positive charge stabilized by the acid residue's negative charge. The tetrahedral intermediate is stabilized by two hydrogen bonds formed with

amide bonds of residues belonging to the oxyanion hole. Finally, an alcohol is liberated, leaving behind the acyl-enzyme complex. Nucleophilic attack by a hydroxyl ion then liberates the fatty acid and the enzyme is regenerated (Jaeger *et al*., 1994).

After the first structure of *F. solani* cutinase was published (PDB ID: 1CUS; Martinez *et al*., 1992), a second structure (PDB ID: 2CUT; Martinez *et al*., 1994) was determined that contained the covalent intermediate from diethyl-*p*-nitrophenyl phosphate hydrolysis. This structure helped to identify the catalytic triad and key residues in the oxyanion hole (Ser42 and Gln121) that are important for transition state stabilization in the acylation/deacylation steps of the enzyme mechanism. Structural alignment of cutinases from *F. solani* and *A. oryzae* (PDB ID: 3GBS; Liu *et al*., 2009) reveals that these two structures are extremely similar, sharing 50% identity, and that their alpha carbons display a root mean square deviation (RMSD) of 0.83 Å. Additionally, overlay of two structures from *F. solani* and *Cryptococcus* sp. cutinases (PDB IDs: 1CUS and 2CZQ; Kodama *et al*., 2009; Fig. 1-7A) demonstrates that the catalytic triad of the *Cryptococcus* sp. enzyme (Ser85, His180 and Asp165) overlays very closely with that of the *F. solani* enzyme, as do the oxyanion hole's key residues (Thr17 and Gln86). Note that the main-chain amides of serine and threonine stabilize this negative charge through hydrogen bonding. In addition, point mutations that selectively disrupt the oxyanion hole have been designed to assess the potential function of the Ser42 side chain as part of the *F. solani* cutinase oxyanion hole. The extent of tetrahedral intermediate stabilization provided by Ser42 Oγ was evaluated by mutating Ser42 to alanine. The S42A mutation resulted in a drastic decrease in enzyme activity (450-fold) without significantly perturbing the three-dimensional structure and active site geometry. Kinetic experiments and structural analysis of this mutant provides

evidence supporting the conclusion that Ser42 Oγ is an extra component of the cutinase oxyanion hole, acting in combination with two main-chain nitrogen atoms of residues Ser42 and Gln121 (Nicolas *et al*., 1996). Furthermore, the residues found in *T. alba* cutinase's oxyanion hole (Met and Tyr) are quite different from those found in fungal cutinases (Ser/Thr and Gln; Fig. 1-7B). As with *F. solani* cutinase, the main-chain amides are thought to be responsible for stabilizing the oxyanion hole (Kitadokoro *et al.*, 2012).

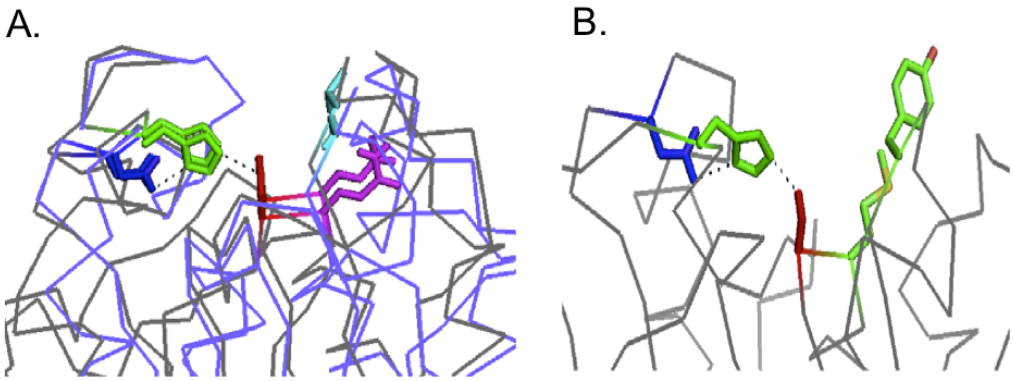

Fig. 1-7 Cutinase active sites. (A) Overlay of the structures of *F. solani* (slate blue ribbon; PDB ID: 1CUS; Martinez *et al*., 1992) and *Cryptococcus* sp. cutinase (gray ribbon; PDB ID: 2CZQ; Kodama *et al*., 2009). Side chains of catalytic Ser, Asp, and His (red, blue, and green, respectively), as well as the oxyanion hole residues Ser (1CUS) or Thr (2CZQ; cyan) and Gln (magenta) rendered as sticks. Putative hydrogen bonds shown as black dashed lines. (B) Active site of *T. alba* cutinase (PDB ID: 3VIS; Kitadokoro *et al*., 2012). Side chains of catalytic Ser, Asp, and His (red, blue, and green, respectively) rendered as sticks, as are side chains of putative anion hole residues Met and Tyr (green stick on right). Putative hydrogen bonds shown as dashed black lines (Chen *et al*., 2013).

1.5 Substrate specificity

Cutinase is able to hydrolyze both soluble esters and insoluble triglycerides, and thus, are considered as being intermediate between lipases and esterases. The simplest cutinase assay measures esterase activity by monitoring *p*-nitrophenyl ester hydrolysis. The reaction is followed by measuring the 405–412 nm absorbance of released *p*-nitrophenol. Bacterial cutinases catalyze hydrolysis of *p*-nitrophenyl esters of C_4–C_{16} fatty acids. All these substrates exhibit typical Michaelis–Menten type kinetics from which linear double-reciprocal plots K_m values and V_{max} have been calculated. There is a general trend of increasing K_m and decreasing V_{max} as the acyl group chain length increases (Sebastian and Kolattukudy, 1988). However, these changes are not as large as those observed with some fungal cutinases. With many fungal enzymes, as the acyl moiety chain length increased from C_2 to C_{12}, V_{max} decreased 200- to 1,000-fold (Purdy and Kolattukudy, 1975). The hydrolysis activity of *F. solani* cutinase toward *p*-nitrophenyl ester substrates has been examined, and overall, the highest substrate preference is for short chain *p*NP-acetate. The kinetics of *p*-nitrophenyl acetate, butyrate, valerate, and hexanoate hydrolysis by *F. solani* and *A. oryzae* cutinases shows that *F. solani* cutinase prefers *p*-nitrophenyl acetate (k_{cat}/K_m = 42,200 $M^{-1}s^{-1}$) over others by about an order of magnitude, while *A. oryzae* cutinase prefers *p*-nitrophenyl butyrate (k_{cat}/K_m = 59,200 $M^{-1}s^{-1}$) or valerate (k_{cat}/K_m = 55,300 $M^{-1}s^{-1}$; Liu *et al*., 2009). Thermophilic fungal cutinase from *Thielavia terrestris* prefers to hydrolyze *p*-nitrophenyl butyrate (k_{cat}/K_m = 620 $M^{-1}s^{-1}$; Yang *et al*., 2013), and yeast cutinase from *Cryptococcus* sp. efficiently hydrolyzes *p*NP-butyrate as its most preferred substrate (Kodama *et al*., 2009). For bacterial cutinases, including *T. cellulosilytica* (Thc_Cut1 and Thc_Cut2), *T. fusca* DSM44342 (Thf42_Cut1), and *T. alba* cutinases, all prefer *p*-

nitrophenyl acetate, with K_m values of 127, 200, 167, and 213 μM and k_{cat} values of 211.9, 2.4, 39.5, and 2.72 s^{-1}, respectively (Herrero Acero *et al*., 2011, 2013; Ribitsch *et al*., 2012b).

Additionally, triacylglycerols have been used as substrates for assessment of cutinase lipase activity. Tributyrin (glycerol tributyrate) is hydrolyzed by cutinase to produce butyric acid and a diacylglycerol. Analysis of *F. solani* cutinase hydrolytic activity toward insoluble triglyceride has revealed that this fungal cutinase prefers substrates with short acyl groups. The specific activity of *F. solani* cutinase with tributyrin, for example, has been reported to be twice its specific activity with trioctanoin (Kwon *et al*., 2009; Rogalska *et al.*, 1993). Cutinase effectively hydrolyzes tributyrin below its critical micelle concentration (CMC, 1280 U/mg) compared with that of *Rhizomucor miehei* lipase, reported as 53 U/mg (Longhi and Cambillau, 1999). Cutinase activity in this case is accounted for by its active site accessibility and by potentially deep embedding of tributyrin in the hydrophobic catalytic crevice, which reduces unfavorable interactions between the tributyrin acyl chains and surrounding bulk water.

Hydrolysis products of cutin mainly consist of C_{16} and C_{18} hydroxyl fatty acids, major components of cutin (Fig. 1-8). The most common C_{16} components are 16-hydroxyhexadecanoic acid and 9,16- or 10,16-dihydroxyhexadecanoic acid. The most common C_{18} members include 18-hydroxyoctadec-9-enoic acid, 18-hydroxyoctadec-9,12-dienoic acid, 18-hydroxy-9,10-epoxyoctadecanoic acid, 18-hydroxy-9,10-epoxy octadec-12-enoic acid, 9,12,18-trihydoxyoctadecanoic acid, and 9,10,18-trihydroxyoctadec-12-enoic acid (Kolattukudy, 2005).

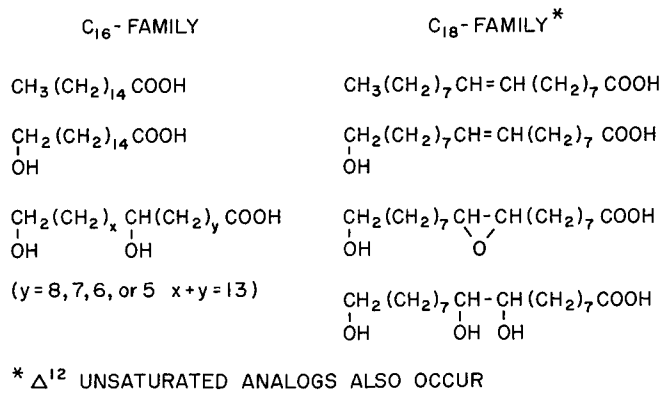

Fig. 1-8 Structures of most common fatty acids of cutin (Kolattukudy, 2005).

Cutin hydrolysis activity by cutinases from *T. fusca*, *T. alba*, *H. insolens*, and *F. solani*, lipases from *Thermomyces languinosus* and *Candida antarctica*, and PHA-depolymerase from *Pseudomonas fluorescens* GK13 have been examined. Released products, analyzed by GC-MS, reveals that two lipases clearly released lower amounts of the hydroxyl fatty acids compared with cutinases from *H. insolens*, *F. solani*, and *Thermobifida* sp. enzymes (Fig. 1-9; Korpecka *et al*., 2010). The fatty acid-releasing activities for tetradecanoic, hexadecanoic, and octadecanoic acids by lipases from *T. lanuginosus* and *C. antarctica* show the highest activities. Some fatty acids found in enzymatic reaction products could be hydrolyzed products from lipids present in cutin preparations, which are particularly difficult to obtain free of lipid contamination.

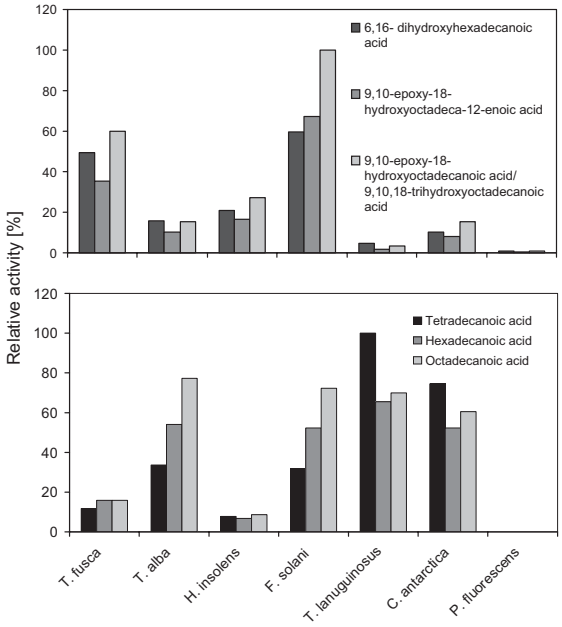

Fig. 1-9 Relative activities of various cutinases and lipases in terms of cutin hydrolysis products (Korpecka *et al*., 2010).

1.6 Synthetic polyester degradation by cutinase

Besides hydrolytic activity toward soluble esters and insoluble long-chain triglycerides, *F. solani* cutinase is also capable of hydrolyzing insoluble polymer films of poly(**ε**-caprolactone) (PCL; Murphy *et al*., 1996) and poly(ethylene terephthalate) (PET; Ronkvist *et al*., 2009; Fig. 1-10). An example of polyesters, PCL is a hydrophobic, semicrystalline polymer that can be prepared by either ring-opening polymerization of ε-caprolactone, using a variety of anionic, cationic, or coordination catalysts, or via free radical ring-opening polymerization of 2-methylene-1-3-dioxepane. PCL's good solubility, low melting point (59–64 °C), and exceptional blend-compatibility have stimulated extensive research into its potential applications in the biomedical field (Woodruff and Hutmacher, 2010).

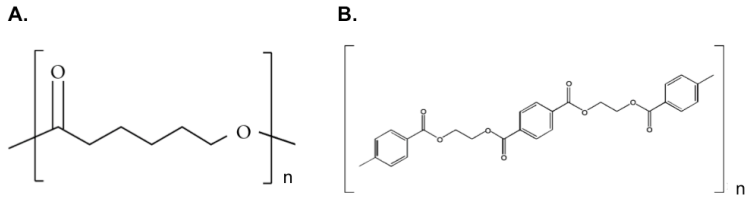

Fig. 1-10 Chemical structures of PCL (A) and PET (B).

PET, a synthetic polyester composed of terephthalic acid (TPA) and ethylene glycol, is a thermoplastic polymer widely used to produce fibers, films, and resins. Most PET produced worldwide is used for textile fiber production, while another large part constitutes PET resins for beverage containers and food packaging. Additionally, PET films are utilized in electronics and packaging industries. By hydrophilization of their surfaces, PET material properties and performance can be enhanced, such as improved dye uptake in hydrophilic PET fabrics. For such modifications, PET surface hydrolysis can be achieved by treatment with the enzymes summarized in Table 1-3. These modifications introduce polar groups to the polymer surface, resulting in PET surface functionalization (Zimmermann and Billing 2010).

Table 1-3. PET hydrolysis enzymes

Enzyme	Source	Effect on PET
Cutinase	*F. solani*	Hydrolysis and increase hydrophilicity
	F. oxysporum	Release terephthalic acid and increase hydrophilicity
	Penicillium citrinum	Release oligomers and increase hydrophilicity
	T. fusca	Hydrolysis and increase hydrophilicity

Table 1-3. (Continued) PET hydrolysis enzymes

Enzyme	Source	Effect on PET
Cutinase	*T. alba*	Hydrolysis
	P. mendocina	Hydrolysis and increase hydrophilicity
	T. terrestris	Hydrolysis
Lipase	*T. lanuginosus*	Hydrolysis and increase hydrophilicity
	H. insolens	Hydrolysis and increase hydrophilicity
	Aspergillus sp.	Hydrolysis and increase hydrophilicity

PET enzymatic hydrolysis has been described for a variety of enzymes, mostly for cutinases and lipases. PET hydrolysis products by cutinases from *T. fusca*, *T. alba*, *H. insolens*, and *F. solani*, lipases from *T. lanuginosus* and *C. antarctica*, and PHA-depolymerase from *P. fluorescens* have been detected by HPLC analysis (Fig. 1-11). The released products are TPA, mono-(2-hydroxyethyl) terephthalate (MHET), and benzoic acid (BA).

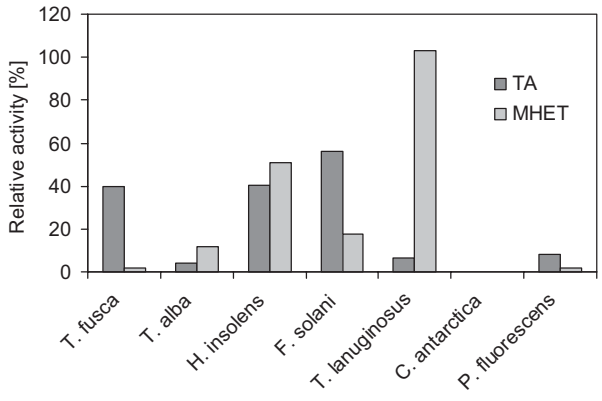

Fig. 1-11 Relative activity of various enzymes for PET-film hydrolysis. TA and MHET determined by Korpecka *et al*. (2010).

Higher rates of MHET release have been measured for *T. lanuginosus* lipase, which indicates a higher degree of endo-type hydrolysis. In contrast, *T. fusca* and *F. solani* cutinases appear to be more exo-type hydrolases, as indicated by higher rates of TA release (Korpecka *et al*., 2010).

The versatile catalytic ability of cutinases has led to recognition that these enzymes are potentially useful in many industrial applications. Therefore, much effort has been allocated to investigating their structure-activity-stability relationships. Additional research has been undertaken to improve enzymatic activity, substrate specificity, and stability of these enzymes. For example, *F. solani* and *T. fusca* cutinases have been modified by substituting residues near the active site with smaller residues to enlarge the catalytic pocket, resulting in enhanced PET enzymatic activity. This strategy has been successfully employed to enhance enzymatic activity toward PET 2–5-fold (Araújo *et al*., 2007; Silva *et al*., 2011). The substitution of a positively charged residue located on the enzyme surface with an uncharged hydrophilic or hydrophobic amino acid has been successful in improving *T. cellulosilytica* cutinase activity (Herrero Acero *et al*., 2013). Additionally, the S54D mutation of *F. solani* cutinase improves approximately 9-fold the anionic surfactant dioctyl sulfosuccinate sodium salt (AOT) tolerance while maintaining the enzymatic activity in the absence of surfactant (Brissos *et al*., 2008).

1.7 The objective of the study

Because of the variety of cutinases that have received attention for potential industrial applications, particularly for PET surface modifications, there are several reports of novel enzyme screening and subsequent study of the biochemical

characteristics of selected enzymes. Isolation of a novel cutinase, its biochemical characterization and structural determination, and thermodynamic/kinetic analyses of its stability will lead to increase our knowledge on the structure-activity-stability relationships of this enzyme type and thus allow to improve its enzymatic activity and stability for many industrial purposes.

A vast amount of biochemical characterization knowledge has been obtained for mesophilic fungal cutinases, such as *F. solani*, *A. oryzae*, *A. brassicicola*, and *F. oxysporum* cutinases. These cutinases are able to hydrolyze PET but are thermolabile. Recently, thermophilic fungal cutinases that exhibit PET hydrolysis activity have been identified. They include *H. insolens* cutinase. The catalytic efficiency of PET hydrolysis by *H. insolens* is comparable to those by thermolabile *P. mendocina* and *F. solani* cutinases at 50°C (Ronkvist *et al*., 2009). Screening of thermophilic organisms has resulted in the isolation of thermostable cutinases from a thermophilic fungus, *T. terrestris*, and two thermophilic bacteria, *T. fusca* and *T. alba*. These enzymes have been extensively characterized and the PET hydrolytic activity of *T. terrestris* cutinase is determined to be 1.1 mg/h/mg of enzyme, which is higher than that of *T. fusca* cutinase (0.05 mg/h/mg of enzyme; Yang *et al*., 2013). Thus far, the requirement of thermophilic enzymes for biotechnological applications generates considerable interest in the development of enzyme variants with effective and robust features.

The goal of this study is to isolate a novel thermophilic cutinase that is useful for industrial applications and to functionally and structurally characterize it at the molecular level. This study provides a wealth of biochemical and structural knowledge of the structure-activity-stability relationships of thermophilic cutinase, which will be useful for rational optimization and engineering of cutinase.

This thesis consists of six chapters. Chapter 1 is a general introduction, which describes the investigative history of cutinases, their characteristics, and their diversity. The reported crystal structures of cutinase are illustrated, and the polyester degradation by various cutinases are summarized.

Chapter 2 describes the isolation and characterization of a novel cutinase, LC-cutinase (LCC), which was identified by screening a metagenomic library (size: 2.1×10^4 CFU), derived from a leaf/branch compost source, for gene encoding lipolytic/esterolytic enzymes. Of the resulting 19 clones screened on tributyrin agar plates, the three that exhibited the largest haloes at 50°C were selected, and from them, the sequence of a gene encoding cutinase was determined by the transposon mutagenesis method. Biochemical characterization of this novel cutinase revealed that this enzyme resembles bacterial cutinase. In summary, LC-cutinase possesses optimal activity for *p*NP-butyrate (C_4) at pH 8.5 and 50°C. Interestingly, the enzyme also exhibits polyester degrading ability. Therefore, this novel cutinase is presented as a potential candidate for biotechnological studies, which include extensive structure-function relationship studies.

Chapter 3 discusses the knowledge obtained by the examination of LC-cutinase's crystal structure in terms of the enzyme's structure-activity-stability relationships. The crystal structure was determined at 1.5 Å resolution and the structure is found to closely resemble the structure of *T. alba* cutinase. LC-cutinase possesses an α/β-hydrolase fold structure with a catalytic triad consisting of Ser-His-Asp. The structure also reveales that this enzyme contains one conserved disulfide bond, similar to *T. alba* cutinase, at the C-terminus. Furthermore, the structural comparison of LC-

cutinase and *T. alba* cutinase illustrates the hydrophobic patch surrounding the active site, which raises the possibility of a long chain substrate-binding pocket.

Chapter 4 emphasizes the role of hydrophobic residues in contributing to the hydrophobic patch. Tyr95 was chosen as a representative residue for this study. To enlarge the catalytic pocket, the mutant LCC-Y95A was constructed, and LCC-Y95F was constructed as well to increase the hydrophobicity of this region. The results of this study clearly indicate that Tyr95 is important for the enzyme's catalytic activity and stability. Indeed, the hydrophobic property of this region is essential for maintaining a favorable catalytic configuration and for stabilizing enzyme structure. Additional experiments were performed in order to elucidate the heat-local conformational change of the enzyme's catalytic region, which is possibly protected by long chain substrate binding in the groove extending from the hydrophobic patch.

Chapter 5 describes investigations of the role of LC-cutinase's disulfide bond formed between Cys275 and Cys292 on enzymatic activity and structural stability. Double mutations at these cysteine residues (Cys to Ala) resulted in disruption of the disulfide bridge. Subsequent biochemical characterization and thermodynamic and kinetic studies on its stability revealed that the disulfide bond plays a crucial role for enzyme stabilization in terms of both thermodynamic and kinetic stabilities. Additionally, this disulfide bond-disruption mutant exhibited an optimal temperature for activity of 30°C, a downward shift of the optimal temperature by 20°C without significantly affecting the enzyme's maximal *p*NP-butyrate hydrolytic activity.

Finally, in Chapter 6, the novel findings from this study are summarized and future remarks are described.

CHAPTER 2

Isolation and characterization of metagenome-derived LC-cutinase

2.1 Introduction

As described in Chapter 1, cutinase (EC 3.1.1.74) is a lipolytic/esterolytic enzyme that hydrolyzes not only cutin, which is a major component of plant cuticle (Walton and Kolattukudy, 1972), but also water-soluble esters and insoluble triglycerides (Dutta *et al*., 2009). It hydrolyzes these substrates to carboxylic acids and alcohols through the formation of an acyl enzyme intermediate, in which the active-site serine residue is acylated by the substrate. This serine residue is located within a GXSXG sequence motif and forms a catalytic triad with His and Asp. Cutinase has been found in both fungi and bacteria. However, cutinase, like esterase, does not have a lid structure, which is responsible for interfacial activation of lipase (Cambillau *et al*., 1996). Therefore, cutinase does not show interfacial activation, like esterase (Eberl *et al*., 2009). Cutinase has recently received much attention because of its potential application for surface modification and degradation of aliphatic and aromatic polyesters (Guebitz and Cavaco-Paulo, 2008), especially polyethylene terephthalate (PET), which is a synthetic aromatic polyester composed of terephthalic acid (TPA) and ethylene glycol (Donelli *et al*., 2009; Guebitz and Cavaco-Paulo, 2008, Vertommen *et al*., 2005, Zimmermann and Billig, 2010). However, the number of cutinases, which have been studied regarding PET modification, is still limited, and this limitation may result in the delay of the research toward the practical use of cutinases. Therefore, isolation of a novel cutinase with PET-degrading activity is needed.

Metagenomics is the study of genetic material recovered directly from

environmental sources (Handelsman *et al*., 1998; Schmeisser *et al*., 2007). Because more than 99% of microorganisms in nature cannot be cultivated by the conventional method (Aman *et al*., 1995), metagenomics has attracted many researchers, who intend not only to increase our knowledge on protein sequence space in nature but also to isolate novel enzymes with potentially useful application. By using this approach, a variety of novel enzymes, including lipases/esterases, cellulases, and proteases, have been isolated and characterized (Steele *et al*., 2009; Tuffin *et al*. 2009; Uchiyama and Miyazaki, 2009).

Microorganisms that can degrade plant cell wall produce a variety of plant cell wall-degrading enzymes, which include not only carbohydrate-degrading enzymes but also lipolytic/esterolytic enzymes. For example, the plant pathogenic bacterium *Xanthomonas oryzae* secrets an esterase, LipA, which is involved in degradation of cell walls in a synergetic manner with other cell wall-degrading enzymes (Aparna *et al*., 2009). In EXPO Park, Japan, leaves and branches cut from the trees are collected periodically, mixed with urea, and agitated for composting. The temperature increases up to ≈70°C inside this compost (leaf-branch compost) and then decreases to ≈50°C roughly 1 year later upon completion of composting. This compost is expected to be rich in various plant cell wall-degrading microorganisms and therefore is a promising source of the genes encoding novel enzymes with cutinase activity.

In the present study, I constructed a DNA library for metagenomic study from leaf-branch compost and performed function-based screening for the genes encoding lipolytic/esterolytic enzymes using an agar medium containing tributyrin. I identified the gene encoding a novel cutinase homolog, termed LC-cutinase, which shows the amino acid sequence identity of 56.8% to cutinase from *T. fusca*, overexpressed it in

Escherichia coli, and purified and characterized the recombinant protein. I show that LC-cutinase exhibits a PET-degrading activity and is a potent candidate for applications in various industrial fields, especially in the textile industries.

2.2 Materials and methods

2.2.1 Cells, plasmids, and enzymes. *E. coli* BL21-CodonPlus(DE3)-RP [F^- *ompT* *hsdS*(r_B^- m_B^-) *dcm*$^+$ Tet^r *gal* λ (DE3) *endA* Hte (*argU proL* Cam^r)] was obtained from Stratagene (La Jolla, CA). Plasmid pET25b was purchased from Novagen (Madison, WI). *E. coli* BL21-CodonPlus(DE3)-RP transformants were grown in lysogeny broth (LB) medium (10 g of tryptone, 5 g of yeast extract, and 10 g of NaCl in 1 liter of H_2O) supplemented with 50 mg L^{-1} of ampicillin. *Burkholderia cepacia* lipase (Bc-Lip) and *Candida rugosa* lipase (Cr-Lip) were kindly donated from Amano Enzyme, Inc. (Nagoya, Japan). The specific esterase and lipase activities of these enzymes determined at pH 8.0 and 50°C using *p*NP-butyrate and olive oil as a substrate, respectively, are 0.5 and 30 units mg^{-1} for Bc-Lip, and 0.8 and 30 units mg^{-1} for Cr-Lip.

2.2.2 Construction of DNA library and screening. The compost sample was taken from the core (1 meter below the surface) of the 4-month-old compost made from leaves and branches in EXPO Park, Japan. The temperature and pH of this leaf-branch compost are 67°C and pH 7.5. DNA for metagenomic study was extracted from this compost sample using ISOIL from Nippon Gene (Toyama, Japan). DNA library for metagenomic study was constructed by using a CopyControl fosmid library production kit (Epicentre Biotechnologies, Madison, WI), according to the procedures recommended by the

supplier. This DNA library was spread on LB-agar plates containing 12.5 μg of chloramphenicol/ml, 1% tributyrin, 0.1% Tween 80, and 0.01% L-arabinose, and the resultant plates were incubated at 37°C for several days. Plasmids were extracted from colonies, which form halos around them due to hydrolysis of tributyrin. Genes encoding lipolytic/esterolytic enzymes were identified by transposon mutagenesis using EZ-Tn*5*<T7/KAN-2>Promoter insertion kit (Epicentre Biotechnologies), according to the procedures recommended by the supplier. The nucleotide sequence of the gene was determined by using an ABI Prism 3100 DNA sequencer (Applied Biosystems, Tokyo, Japan). Oligonucleotides for sequencing, as well as PCR primers and mutagenic primers, were synthesized by Hokkaido System Science (Sapporo, Hokkaido, Japan).

2.2.3 Overproduction and purification. The gene encoding LC-cutinase[36-293] (residues 36 to 293 of LC-cutinase) was amplified by PCR using the fosmid vector harboring the LC-cutinase gene as a template. The sequences of the PCR primers were 5'-GCGTCGCCATGGATTCCAACCCGTACCAG-3' for the 5' primer and 5'-CAGGATCCACTACTGGCAGTGGCG-3' for the 3' primer (underlining indicates the NcoI site for 5' primer and the BamHI site for 3' primer). The resultant DNA fragment was digested with NcoI and BamHI and ligated into the NcoI-BamHI sites of pET25b to construct pET-LCC for overproduction of the pelB-LC-cutinase[36-293] fusion protein. This fusion protein was designed such that Met-Asp-LC-cutinase[36-293], in which the Met-Asp sequence is derived from the NcoI site used to insert the LC-cutinase[36-293] gene into pET25b, is secreted to the periplasm with the assistance of the pelB leader sequence. PCR was performed in 25 cycles with a GeneAmp PCR system 2400 (Applied Biosystems) using KOD DNA polymerase (Toyobo). The nucleotide sequence

was confirmed by using an ABI Prism 3100 DNA sequencer (Applied Biosystems).

E. coli BL21-CodonPlus(DE3)-RP transformants with pET-LCC were cultivated at 37°C. When the absorbance of the culture at 600 nm reached ≈1.0, IPTG (isopropyl-β-D-thiogalactopyranoside) was added to the culture medium, and cultivation was continued overnight. The LC-cutinase[36 –293] derivative, termed LC-cutinase, was purified from the culture supernatant at 4°C as described below. The culture medium was centrifuged at 8,000 × *g* for 30 min to separate the supernatant and cells. The protein in the supernatant was precipitated by the addition of ammonium sulfate to 80% of the saturated concentration and then dissolved in 10 mM Tris-HCl (pH 7.0) containing 1 mM EDTA and 1 mM dithiothreitol (DTT). The solution was dialyzed against the same buffer overnight and applied to a column (1.0 ml) of SP-Sepharose (GE Healthcare, Tokyo, Japan) equilibrated with the same buffer. The protein was eluted from the column by linearly increasing the NaCl concentration from 0 to 1.0 M at 0.2 M NaCl. The fractions containing the protein were collected and applied to a Hi-Load 16/60 Superdex 200 Prep-Grade column (GE Healthcare) equilibrated with 10 mM Tris-HCl (pH 7.0) containing 1 mM EDTA, 1 mM DTT, and 0.2 M NaCl.

The production level of the protein in *E. coli* cells and the purity of the protein were analyzed by sodium dodecyl sulfate-polyacrylamide gel electrophoresis (SDS-PAGE) (Laemmli, 1970) using a 12% polyacrylamide gel, followed by staining with Coomassie brilliant blue (CBB). The amount of the protein was estimated from the intensity of the band visualized by CBB staining using the Scion Image program. The N-terminal amino acid sequence of the protein was determined by a Procise automated sequencer model 491 (Applied Biosystems). The protein concentration was determined from the UV absorption on the basis that the absorbance of a 0.1% (1.0 mg mL^{-1})

solution at 280 nm is 1.37. This value was calculated by using ε = 1,526 M^{-1} cm^{-1} for tyrosine and 5,225 M^{-1} cm^{-1} for tryptophan at 280 nm (Goodwin and Morton, 1946).

2.2.4 Construction of mutant protein. The pET25b derivative for overproduction of S165A-cutinase, in which the active-site serine residue, Ser165, of LC-cutinase is replaced by Ala, was constructed by PCR using the QuikChange II site-directed mutagenesis kit (Stratagene). The mutagenic primers were designed such that the TCG codon for Ser165 is changed to GCG for Ala. The mutant protein was overproduced and purified as described above for LC-cutinase.

2.2.5 Enzyme assays. The enzymatic activity was determined at the temperature indicated in 1 ml of 25 mM Tri-HCl (pH 8.0) containing 2% acetonitrile and 1 mM *p*-nitrophenyl butyrate (C_4). The amount of *p*-nitrophenol (*p*NP) released from the substrate was determined from the absorption at 405 nm with an absorption coefficient of 18,600 M^{-1} cm^{-1} by automatic spectrophotometer (Hitachi spectrophotometer U-2810; Hitachi High-Technologies, Tokyo, Japan). One unit of activity was defined as the amount of enzyme that produced 1 μmol of *p*NP per min. The specific activity was defined as the enzymatic activity per milligram of protein.

For determination of substrate specificity, *p*NP monoesters of fatty acids with acyl chain lengths of 2 (*p*NP-acetate), 4 (*p*NP-butyrate), 6 (*p*NP-hexanoate), 8 (*p*NP-caprylate), 12 (*p*NP-laurate), 14 (*p*NP-myristate), 16 (*p*NP-palmitate), and 18 (*p*NP-stearate) (Sigma) and olive oil were used as a substrate. Measurement of the enzymatic activities for hydrolyses of *p*NP monoesters of fatty acids was performed as described

above for hydrolysis of *p*NP-butyrate, except that the reaction mixture contained 25 mM Tris-HCl (pH 8.0), 10% acetonitrile, and 1 mM substrate. One unit of activity was defined as the amount of enzyme that produced 1 μmol of *p*NP per min. Measurement of the enzymatic activity for hydrolysis of olive oil was performed at the temperature indicated by titrating the liberated fatty acid with 10 mM NaOH as described previously (Amada *et al*., 2000), except that the reaction was carried out in 25 mM Tris-HCl (pH 8.0). One unit of activity was defined as the amount of enzyme that produced 1 μmol of fatty acid per min.

2.2.6 Inhibition with E600. LC-cutinase (1.0 nmol) was incubated at 50°C for 30 min in 100 μl of 10 mM Tris-HCl (pH 7.6) containing 5 mM diethyl *p*NP phosphate (E600; Sigma). The residual activity was determined at 30°C using *p*NP-butyrate as a substrate.

2.2.7 Detection of cutin-degrading activity. Cutin fibers were prepared from tomato peels as described previously (Macedo and Pio, 2005). These fibers (10 mg) were added into 1 ml of 20 mM Tris-HCl (pH 8.0) and preincubated at 50°C for 5 min. The reaction was initiated by the addition of enzyme (50 μg for LC-cutinase and 100 μg for Bc-Lip and Cr-Lip) and continued at 50°C with gentle shaking. At appropriate intervals, an aliquot of the reaction mixture was withdrawn, and the fatty acids released upon hydrolysis of cutin were quantified by titration with 20 mM NaOH.

2.2.8 Detection of PCL-degrading activity. Poly(ε-caprolactone) (PCL)-degrading activity was determined by measuring the weight loss of a PCL film after incubation with the enzyme. For preparation of PCL film, 20 to 30 mg of PCL (Wako Pure

Chemical, Osaka, Japan) was melted at 80°C and pressed into a thin film with ≈5 mm in diameter at room temperature. This PCL film was added into 1 ml of 500 mM Tris-HCl (pH 8.0) and preincubated at 50°C for 5 min. The reaction was initiated by the addition of enzyme (5 μg for LC-cutinase and 50 μg for Bc-Lip and Cr-Lip) and continued at 50°C for 6 h. After incubation, the films were washed with water and ethanol and dried for measurement of the weight loss.

2.2.9 Detection of PET-degrading activity. PET-degrading activity was determined by measuring the weight loss of a PET film after incubation with the enzyme. For preparation of PET film, a plastic package made of PET was cut into ≈5-mm^2 pieces (20 to 25 mg per piece). This PET film was added into 1 ml of 500 mM Tris-HCl (pH 8.0) and preincubated at 50°C for 5 min. The reaction was initiated by the addition of enzyme (5 μg for LC-cutinase and 50 μg for Bc-Lip and Cr-Lip) and continued at 50°C with gentle shaking for 24 h. After incubation, the films were washed with water and ethanol and dried for measurement of the weight loss. PET-degrading activity was also determined by quantifying the fatty acids released upon hydrolysis of PET with 50 mM NaOH. A PET film was incubated with the enzyme as mentioned above, except that the concentration of the reaction buffer was reduced to 100 mM and the incubation time was changed to 12 and 30 h.

2.2.10 Nucleotide sequence accession number. The nucleotide sequence of the LC-cutinase gene has been deposited in GenBank under accession number HQ704839.

2.3 Results and discussion

2.3.1 Gene cloning of lipolytic/esterolytic enzymes from DNA library for metagenomic study. Extraction of DNA from 4-month-old leaf-branch compost (2.5 g) yielded 11 μg of high-molecular-weight DNA for metagenomic study. Ligation of sheared DNA into fosmid vector (pCC1FOS), followed by transformation of *E. coli* cells (*E. coli* EPI300-T1^{R}), produced the DNA library for metagenomic study with a library size of approximately 2.1×10^{4} CFU. The restriction fragment length polymorphisms of 10 randomly selected clones using BamHI restriction enzymes showed nonredundant patterns and an average insert size of 35 kb.

Screening of the library for genes encoding lipolytic/esterolytic enzymes was performed using tributyrin agar plates. *E. coli* transformants which gave a halo should contain these genes. Of approximately 6,000 clones screened, 19 clones gave a halo on tributyrin agar plates when they were incubated at 37°C for 3 days. Three of them, which gave the largest halo at 50°C, were chosen to determine the nucleotide sequences of the genes responsible for halo formation. Determination of the nucleotide sequences of these genes by transposon mutagenesis indicates that all three clones harbor the same gene encoding a lipolytic/esterolytic enzyme. This protein is termed LC-cutinase (cutinase homolog from leaf-branch compost). LC-cutinase is composed of 293 amino acid residues with a calculated molecular mass of 31,494 and an isoelectric point (pI) of 9.3.

2.3.2 Amino acid sequence. Similarity search using blastp program indicates that LC-cutinase shows relatively high amino acid sequence identities of 54 to 60% to lipases, which have been classified as family III lipases (Arpigny and Jaeger, 1999), and

cutinases (Table 2-1). It shows the highest amino acid sequence identity of 59.7% to *Thermomonospora curvata* lipase. The amino acid sequence of LC-cutinase is compared to those of *Thermobifida fusca* cutinase and *T.alba* cutinase in Fig. 2-1.

Fig. 2-1 Alignment of the amino acid sequences of LC-cutinase (LCC), *T. alba* cutinase (TaC) and *T. fusca* cutinase (TfC). The amino acid sequences of these proteins without a putative signal peptide are shown. The accession numbers of these sequences are HQ704839 for LCC, BAK48590 for TaC, and CBY05529 for TfC. Gaps are denoted by dashes. The active site residues that form a catalytic triad (Ser165, Asp210, and His242 for LCC) are denoted by yellow circles, and the cysteine residues (Cys275 and Cys292 for LCC) are denoted by open circles above the sequences. The ranges of the secondary structures of LCC, which are identical to those of TaC are shown above the sequences. The numbers represent the positions of the amino acid residues starting from the N-terminus of the protein.

Table 2-1. List of the proteins with high amino acid sequence identities to LC-cutinase found by the BLAST search

Enzymes	No. of residues	Source organism	Accession no.	Identity[a] (%)
triacylglycerol lipase	289	*Thermomonospora curvata*	YP_003298899	59.7
putative lipase	334	*Streptomyces ambofaciens*	CAJ88461	57.8
lipase	310	*Streptomyces coelicolor A3(2)*	AAD09315.1	57.4
cutinase	319	*Thermobifida fusca*	CBY05529	56.8
cutinase	304	*Saccharomonospora viridis*	YP_003134604	55.8
lipase	304	*Streptomyces albus*	ZP_04702335.1	55.4
cutinase	290	*Nocardiopsis dassonvillei*	ZP_04331006.1	54.7
lipase	262	*Streptomyces exfoliatus*	1JFR_A	53.9
cutinase	300	*Thermobifida alba*	BAK48590	50.7

[a] The amino acid sequence identities of proteins to LC-cutinase without putative signal peptide.

T. fusca cutinase shows the highest amino acid sequence identity of 56.8% to LC-cutinase among various cutinases and has been biochemically characterized as a representative member of bacterial cutinases (Chen *et al*., 2008). *Streptomyces exfoliatus* lipase and *T. alba* cutinase are the only proteins listed in Table 2-1, for which the crystal structures are available (Wei *et al*., 1998; Kitadokoro *et al.*, 2012).

Analysis of the amino acid sequence of LC-cutinase using SMART (http://smart.embl.de) (Letunic *et al*., 2009, Schultz *et al*., 1998) suggests that LC-cutinase is a secretory protein and has a 34-residue signal peptide at the N terminus. The mature region of LC-cutinase without this putative signal peptide, LC-cutinase[35-293], is composed of 259 amino acid residues with a calculated molecular mass of 27,902. This size is similar to those of *T. fusca* cutinase, which is composed of 261 amino acid residues. Three active-site residues (Ser165, Asp210, and His242) that form a catalytic triad and two residues (Tyr95 and Met166) whose main-chain amide groups form an oxyanion hole are fully conserved in the LC-cutinase sequence. A typical pentapeptide GxSxG sequence motif is also fully conserved in the LC-cutinase sequence.

2.3.3 Overproduction of LC-cutinase. Met-Asp-LC-cutinase[36-293] was overproduced in *E. coli* as a fusion protein with the pelB leader sequence. Upon overproduction, the recombinant protein not only accumulated in the cells in a soluble form but also was released in the extracellular medium. With the release of this recombinant protein, a variety of the proteins, presumably periplasmic proteins, were released in the extracellular medium, suggesting that the recombinant protein is released in the extracellular medium due to a leakage. The production level of the recombinant protein accumulated in the cells and that released in the extracellular medium are

estimated to be 6 and 8 mg L^{-1} of culture, respectively, from the intensities of the bands visualized by CBB staining following SDS-PAGE. The molecular masses of these proteins estimated from SDS-PAGE are identical to each other (29 kDa). This value is slightly higher than but comparable to the calculated one of Met-Asp-LC-cutinase[36-293] (28,063 Da). These results suggest that Met-Asp-LC-cutinase[36-293] is translocated across the cytoplasmic membrane by the Sec transport system with the assistance of the pelB leader sequence, accumulated in the periplasmic space, and more than 50% of it was released in the extracellular medium due to a leakage of the outer membrane. This leakage mechanism of LC-cutinase remains to be elucidated.

It should be noted that LC-cutinase with its own signal peptide accumulated in *E. coli* cells in inclusion bodies without cleavage of signal peptide upon overproduction. This result suggests that this signal peptide cannot work properly in *E. coli* cells.

2.3.4 Purification of LC-cutinase. Because of the ease of the purification procedures, the recombinant protein was purified from the extracellular medium to give a single band on SDS-PAGE (Fig. 2-2). The amount of the protein purified from 1-liter culture was roughly 6 mg. The N-terminal amino acid sequence of the purified protein was determined to be Gln-Pro-Ala-Met, indicating that the C-terminal five residues of the pelB leader sequence and the subsequent Met-Asp sequence are kept attaching to the N terminus of LC-cutinase[36-293].

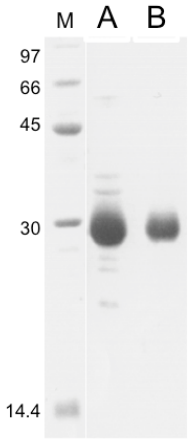

Fig. 2-2 SDS-PAGE analysis for the purified protein of LC-cutinase. Lane M is low-molecular-weight marker kit (Pharmacia Biotech). Lane A is the purified LC-cutinase after SP-Sepharose column and lane B indicates the purified LC-cutinase derived from purification by size exclusion column chromatography.

This result indicates that the 22-residue pelB leader sequence is cleaved by signal peptidase at the peptide bond between the fifth and sixth residues from the C terminus, when Met-Asp-LC-cutinase[36-293] is translocated across the cytoplasmic membrane. This incomplete processing of signal peptide has also been reported for *T. fusca* cutinase (Dresler *et al*., 2006). Upon overproduction of the OmpA-cutinase fusion protein in *E. coli* cells, this protein is transported to the periplasm after cleavage of the OmpA sequence. However, the OmpA sequence is not uniformly cleaved by signal peptidase. It is cleaved at multiple sites, mainly at the peptide bond between the ninth and tenth residues from the C terminus. It has been suggested that overload of Sec-transportation pathway forces cleavage of signal peptide at incorrect sites (Dresler *et al*., 2006). The recombinant protein of LC-cutinase was purified from the extracellular medium of *E. coli* cells as QPAMAMD-LC-cutinase, in which a seven-residue peptide, Gln-Pro-Ala-Met-Ala-Met-Asp, is attached to the N-terminus of LC-cutinase[36-293].

This seven-residue peptide is mostly derived from the pelB-leader sequence and LC-cutinase[36-293] represents LC-cutinase without a putative N-terminal signal peptide (Met1-Ala34) and Gln35. This protein will be simply designated as LC-cutinase hereafter. LC-cutinase is composed of 265 amino acid residues with a calculated molecular mass of 28,517 Da.

2.3.5 Enzymatic activity of LC-cutinase. The pH dependence of LC-cutinase was analyzed at various pH ranging from 5.5 to 9.5 and 30°C using *p*NP-butyrate as a substrate. LC-cutinase exhibited the highest activity at pH 8.5 (specific activity of 200 ± 27 units mg^{-1}) and roughly 70% of the maximal activity at pH 7.0 (sodium phosphate) and pH 9.5 (Fig. 2-3A). The temperature dependence of LC-cutinase was analyzed at various temperatures ranging from 30 to 80°C and pH 7.0 (sodium phosphate) using *p*NP-butyrate as a substrate. LC-cutinase exhibited the highest activity at 50°C (specific activity of 190 ± 21 units mg^{-1}) and roughly 70% of the maximal activity at 30 and 70°C (Fig. 2-3B). These results indicate that the optimum pH and temperature for enzymatic activity of LC-cutinase are pH 8.5 and 50°C. The specific activity of LC-cutinase at the optimum condition was 270 ± 31 units mg^{-1}.

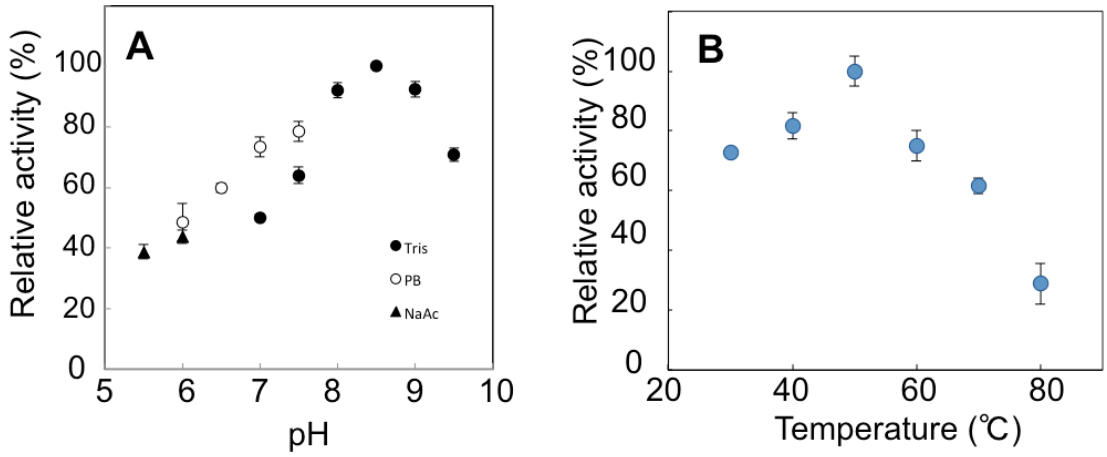

Fig. 2-3 pH and temperature dependencies of LC-cutinase. (**A**) pH dependency of LC-cutinase. The enzymatic activity was determined at 30°C using *p*NP-butyrate as a substrate in 10 mM sodium acetate (pH 5.5, 6.0) (solid triangle), 10 mM sodium phosphate (pH 6.0-7.5) (open circle), or 10 mM Tris-HCl (pH 7.0-9.5) (solid circle) containing 2% acetonitrile. The activity relative to that determined at pH 8.5 is shown as a function of pH. (**B**) Temperature dependency of LC-cutinase. The enzymatic activity was determined in 10 mM sodium phosphate (pH 7.0) containing 2% acetonitrile at various temperatures using *p*NP-butyrate as a substrate. The activity relative to that determined at 50°C is shown as a function of temperature. The experiment was carried out at least twice and the average values are shown together with error bars.

This activity was not changed either in the presence of 10 mM $CaCl_2$ or 10 mM EDTA, suggesting that LC-cutinase does not require divalent metal ions for activity. It has been reported that the specific activity of *T. fusca* cutinase is 360 units mg^{-1} for tributyrin (C_4) (Kleeberg *et al*., 2005) and 458 units mg^{-1} for *p*NP-butyrate (C_4) at pH 8.0 and 60°C (Chen *et al*., 2008). Thus, the specific activity of LC-cutinase for *p*NP-butyrate is slightly lower than but comparable to that of *T. fusca* cutinase.

Substrate specificity of LC-cutinase was analyzed using olive oil and various *p*NP monoesters of fatty acids with acyl chain lengths of 2 to 18 as a substrate at pH 8.0 and 37°C. The enzymatic activity was determined at this condition, instead of the optimum condition, because the stability of certain substrates, such as *p*NP-acetate, decreases as the pH and temperature increase beyond pH 8.0 and 40°C. The specific activity determined at pH 8.0 and 37°C was roughly 80% of that determined at the optimum condition. The specific activities of LC-cutinase for various *p*NP-substrates relative to that for *p*NP-butyrate are shown in Figure 2-4. LC-cutinase hydrolyzed *p*NP-butyrate (C_4) most preferably among various *p*NP substrates examined. It hydrolyzed

*p*NP-hexanoate (C_6) and *p*NP-caprylate (C_8) with comparable efficiencies. However, it hydrolyzed substrates with acyl chain lengths of ≥12 with much lower efficiencies. Its activities for these substrates decrease as the acyl chain lengths of these substrates increase. It did not hydrolyze olive oil at 30°C. Thus, LC-cutinase shows strong preference to the substrates with short acyl chain length. Preference to short-chain substrates has also been reported for *T. fusca* cutinase (Kleeberg *et al*., 2005).

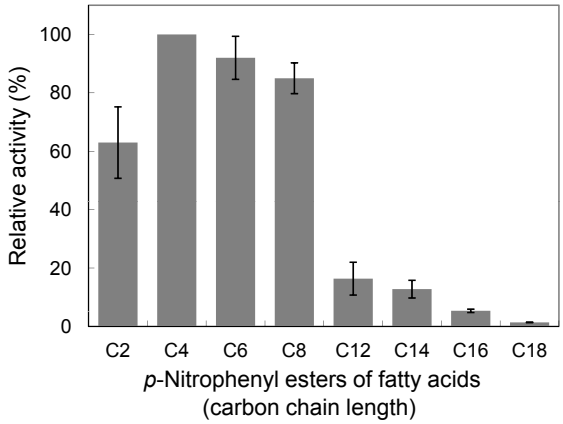

Fig. 2-4 Substrate specificity of LC-cutinase. The enzymatic activity was determined at 30°C in 25 mM Tris-HCl (pH 8.0) containing 10% acetonitrile using *p*NP-acetate (C_2), *p*NP-butyrate (C_4), *p*NP-hexanoate (C_6), *p*NP-caprylate (C_8), *p*NP-laurate (C_{12}), *p*NP-myristate (C_{14}), *p*NP-palmitate (C_{16}), or *p*NP-stearate (C_{18}) as a substrate. The specific activities relative to that determined for hydrolysis of *p*NP-butyrate are shown. The experiment was carried out at least twice and the average values are shown together with error bars.

To examine whether LC-cutinase is inhibited by diethyl *p*NP-phosphate (E600), it was incubated at pH 7.6 and 50°C for 30 min in the presence of E600. Upon incubation with E600, LC-cutinase completely lost the enzymatic activity for *p*NP-butyrate, indicating that it is inhibited by E600.

2.3.6 Stability. To analyze the stability of LC-cutinase against irreversible heat inactivation, LC-cutinase (0.1 mg ml^{-1}) was incubated in 10 mM sodium phosphate (pH 7.0) at 50, 60, 70, and 80°C. With appropriate intervals, an aliquot of the solution was withdrawn and analyzed for residual activity at 30°C using *p*NP-butyrate. As shown in Figure 2-5, LC-cutinase lost activity with half-lives of 5 h at 50°C, 80 min at 60°C, 40 min at 70°C, and 7 min at 80°C. It has been reported that *T. fusca* cutinase exhibits the highest activity at 60°C and pH 8, and high stability with residual activity of over 50% after 40 h at 60°C (Chen *et al*., 2008). Thus, LC-cutinase is slightly less stable than *T. fusca* cutinase.

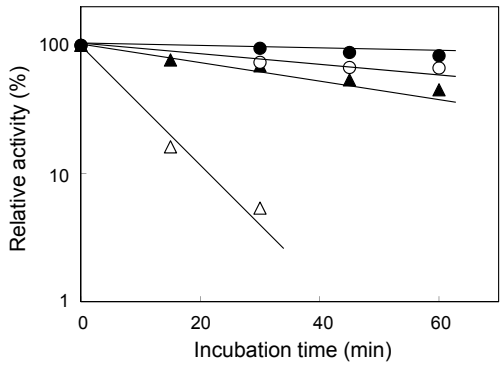

Fig. 2-5 Stability of LC-cutinase against irreversible heat inactivation. Semilog plots of the residual activity *versus* the incubation time are shown. LC-cutinase was incubated in 10 mM sodium phosphate (pH 7.0) at 50°C (solid circle), 60°C (open circle), 70°C (solid triangle), or 80°C (open triangle). Aliquots of each sample were withdrawn at the times indicated and the enzymatic activity was determined at 30°C using *p*NP-butyrate as a substrate. The line was obtained by linear regression of the data.

2.3.7 Degradation of cutin. Cutin is composed of ω-hydroxy fatty acids, dihidroxypalmitic acids, saturated and 12-monounsaturated 18-hydroxy 9,10-epoxy C_{18} acids, and saturated and 12-mono- unsaturated 9,10,18-trihydroxy C_{18} acids (Macedo and Pio, 2005). Degradation of cutin with LC-cutinase was analyzed by quantifying the

carboxylic acids produced upon hydrolysis of ester bonds in cutin with 20 mM NaOH. The results are shown in Figure 2-6. The amount of the carboxylic acids increased at 0.3 μmol h^{-1} until it reached to 2.7 μmol at pH 8.0 and 50°C. This rate is comparable to that reported for *T. fusca* cutinase (4 μmol/h/mg of enzyme at pH 8 and 60°C) (Chen *et al*., 2008), suggesting that LC-cutinase exhibits a comparable cutin-degrading activity as that of *T. fusca* cutinase.

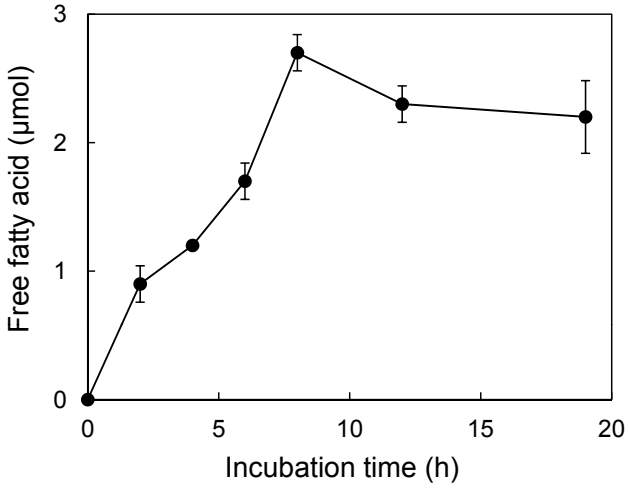

Fig. 2-6 Degradation of cutin by LC-cutinase. LC-cutinase (50 μg) was incubated with 1% (w/v) tomato cutin in 1 ml of 20 mM Tris-HCl (pH 8.0) at 50°C. The released fatty acids were quantified by titration with 50 mM NaOH. The experiment was carried out at least twice and the average values are shown together with error bars.

The carboxylic acids were not produced from cutin upon incubation with Bc-Lip, Cr-Lip, and S165A-cutinase, suggesting that these enzymes do not have an ability to degrade cutin. However, neither the purity of the cutin used as a substrate nor the species of the hydrolytic products was determined. Further studies will be necessary to show that LC-cutinase can really degrade cutin.

2.3.8 Degradation of PCL. Poly(ε-caprolactone) (PCL) is one of the synthetic aliphatic biodegradable polyesters (Amass *et al*., 1998). LC-cutinase and Bc-Lip exhibited PCL-degrading activity, whereas Cr-Lip did not exhibit it (Fig. 2-7). Bc-Lip has been reported to degrade PCL (Hiraishi *et al*. 2007). The amount of PCL degraded by LC-cutinase at pH 8.0 and 50°C was 9.5 mg after incubation for 6 h. This amount increased in proportion to the incubation time. Thus, the specific PCL-degrading activity of LC-cutinase at pH 8.0 and 50°C was determined to be 300 mg/h/mg of enzyme. S165A-cutinase did not degrade a PCL film, indicating that the hydrolytic activity of LC-cutinase is responsible for the degradation of PCL. The specific PCL-degrading activity of Bc-Lip was determined to be 8 mg/h/mg of enzyme, indicating that Bc-Lip degrades PCL with much lower efficiency than LC-cutinase does.

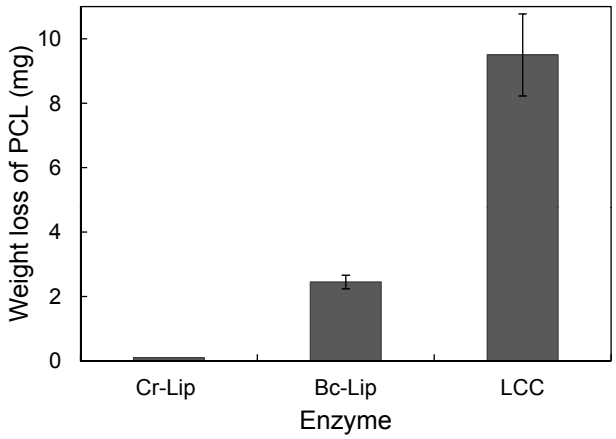

Fig. 2-7 Degradation of PCL film by LC-cutinase. A PCL film (20-30 mg) was incubated at 50°C for 6 h in 1 ml of 500 mM Tris-HCl (pH 8.0) containing 5 μg of LC-cutinase (LCC), or 50 μg of *B. cepacia* lipase (Bc-Lip) or *C. rugosa* lipase (Cr-Lip), and its weight loss after incubation was determined. The experiment was carried out at least twice and the average values are shown together with error bars.

2.3.9 Degradation of PET. LC-cutinase exhibited PET-degrading activity, while Bc-Lip and Cr-Lip did not exhibit it (Fig. 2-8). The amount of PET degraded by LC-

cutinase at pH 8.0 and 50°C was 1.45 mg after incubation for 24 h. This amount increased in proportion to the incubation time up to ≈10 mg. Thus, the specific PET-degrading activity of LC-cutinase at pH 8.0 and 50°C was determined to be 12 mg/h/mg of enzyme. These results indicate that LC-cutinase can degrade a PET film, but with much less efficiency than a PCL film.

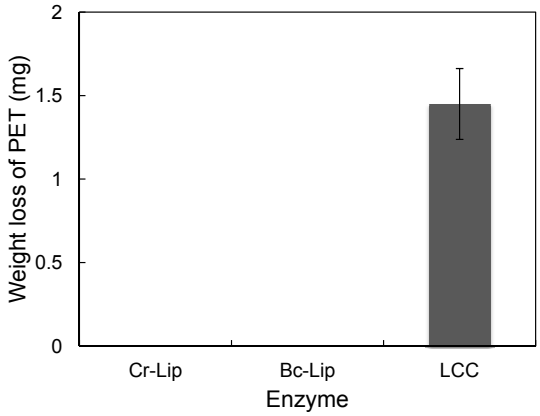

Fig. 2-8 Degradation of PET film by LC-cutinase. A PET film (20-25 mg) was incubated at 50°C for 24 h in 1 ml of 500 mM Tris-HCl (pH 8.0) containing 5 μg of LC-cutinase (LCC), or 50 μg of Bc-Lip or Cr-Lip, and its weight loss after incubation was determined. The experiment was carried out at least twice and the average values are shown together with error bars.

When the degradation products of PET with LC-cutinase were analyzed by reversed-phase high-pressure liquid chromatography, terephthalic acid (TPA) and mono(2-hydroxyethyl)terephthalate (MHET) were eluted from a column as major and minor peaks, respectively (Fig. 2-9). The peak for *bis*(2-hydroxyethyl)terephthalate (BHET) was not detected. These results indicate that LC-cutinase has an ability to completely degrade PET to TPA and ethylene glycol.

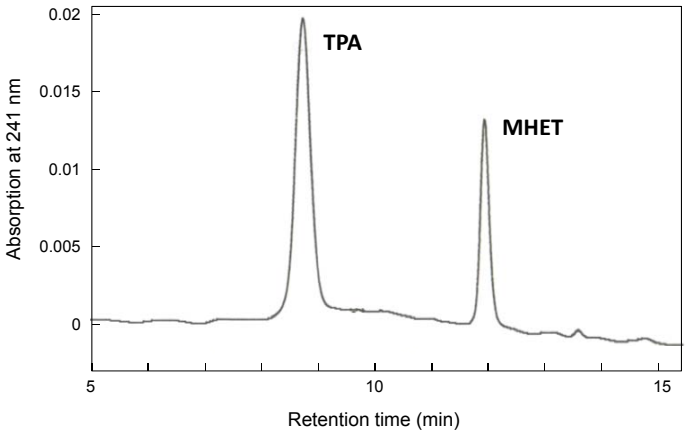

Fig. 2-9 Separation of degradation products of PET with LC-cutinase on reverse-phase HPLC. An aliquot of the degradation products of a PET film with LC-cutinase was directly loaded on a Cosmosil $5C_{18}$-AR-II column (4.6 x 250 mm, Nacalai Tesque Inc, Kyoto, Japan) equilibrated with 10% (v/v) solvent B in solvent A. Elution was performed by raising linearly the concentration of solvent B in solvent A from 10 to 40% (v/v) over 15 min. Solvent A was aq. 0.25% (v/v) trifluoroacetic acid and solvent B was acetonitrile. The flow rate was 1.0 ml min^{-1}. The degradation products of PET were detected by a UV detector set at 241 nm, at which terephthalic acid (TPA) and its esters exhibit the highest absorption coefficient (Yoon *et al*., 2002). TPA and mono (2-hydroxyethyl) terephthalate (MHET) were eluted from the column with the retention times of 9.1 and 12.3 min, respectively, both of which were identical with those of TPA commercially available (Tokyo Chemical Industry Co. Ltd., Tokyo, Japan) and MHET produced from *bis* (2-hydroxyethyl) terephthalate (BHET) (Tokyo Chemical Industry Co. Ltd., Tokyo, Japan) upon partial hydrolysis (Vertommen *et al*., 2005).

2.3.10 Possible application of LC-cutinase. PET is widely used for industrial purposes, mainly as polyester fibers, beverage containers, and food packaging (Donelli *et al*., 2009; Zimmermann and Billig, 2010). It is characterized by the high strength in chemical, physical, and mechanical properties. However, low hydrophilicity, poor wettability, and low moisture gain of polyester fibers cause various problems in manufacturing and consumer use. Hydrolysis and functionalization of polyester fibers

with lipolytic and esterolytic enzymes are thought to be an effective way to improve surface properties of polyester fibers in an environmentally friendly manner (Ribitsch *et al*., 2011; Zimmermann and Billig, 2010). Cutinase is one of these enzymes, and cutinases from *F. solani* (Araújo *et al*., 2007; Donelli *et al*., 2009; Nimchua *et al*., 2008; Vertommen *et al*., 2005), *F. oxysporum* (Nimchua *et al*., 2008), and *T. fusca* (Alisch-Mark *et al*., 2006; Eberl *et al*., 2008; Eberl *et al*. 2009; Müller *et al*., 2005; Silva *et al*., 2011) have been well studied regarding PET modification. However, the catalytic efficiencies of these enzymes are not sufficiently high to meet the requirements of the textile industry (Donelli *et al*., 2009).

I showed here that a novel cutinase homolog isolated from leaf-branch compost with metagenomic approach exhibits a PET-degrading activity. It degrades a PET film at a rate of 12 mg/h/mg of enzyme. The degradation rate of a PET film with cutinase has been reported to be 0.05 mg/h/mg of enzyme for *T. fusca* cutinase at pH 7.0 and 55°C (Müller *et al*., 2005), 0.19 μg/h/one unit of *p*NP-butyrate-degrading activity for *F. solani* PBU-RU-5B cutinase at pH 7.0 and 25°C (Nimchua *et al*., 2008), 0.047 μg/h/one unit of *p*NP-butyrate-degrading activity for *F. solani* cutinase at pH 7.0 and 30°C (Nimchua *et al*., 2007), and 0.084 μg/h/one unit of *p*NP-butyrate-degrading activity for *F. oxysporum* cutinase at pH 7.0 and 30°C (Nimchua *et al*., 2007). Thus, the degradation rate of PET with LC-cutinase is higher than the reported values for other cutinases by 230- to 970-fold. The catalytic efficiencies of *F. solani* (Araújo *et al*., 2007) and *T. fusca* (Silva *et al*., 2011) cutinases have been successfully enhanced with protein engineering technology, but by only 5-fold. Therefore, LC-cutinase might be potentially applicable for functionalization of PET fibers. In addition, detailed structural and functional analyses of LC-cutinase will facilitate understanding of the mechanism

by which LC-cutinase hydrolyzes PET fibers and thereby lead to the development of a more efficient enzyme.

2.4 Summary

The gene encoding a cutinase homolog, LC-cutinase, was cloned from a fosmid library of a leaf-branch compost metagenome by functional screening using tributyrin agar plates. LC-cutinase shows the highest amino acid sequence identity of 56.8% to *T. fusca* cutinase. It also shows the 50.7% identity to *T. alba* cutinase. When LC-cutinase without a putative signal peptide was secreted to the periplasm of *E. coli* cells with the assistance of the pelB leader sequence, more than 50% of the recombinant protein, termed LC-cutinase, was leaked into the extracellular medium. It was purified and characterized. LC-cutinase hydrolyzed various fatty acid monoesters with acyl chain lengths of 2-18 with the preference to short-chain substrates (C4 substrate at most) most optimally at pH 8.5 and 50°C, but could not hydrolyze olive oil. It lost activity with half-lives of 40 min at 70°C and 7 min at 80°C. LC-cutinase had an ability to degrade PCL and PET. The specific PET-degrading activity of LC-cutinase was determined to be 12 mg/h/mg of enzyme at pH 8.0 and 50°C. This activity is higher than those of bacterial and fungal cutinases reported thus far, suggesting that LC-cutinase not only serves as a good model for understanding the molecular mechanism of PET-degrading enzyme but also is potentially applicable for surface modification and degradation of PET.

CHAPTER 3

Crystal structure of LC-cutinase

3.1 Introduction

As described in Chapter 2, LC-cutinase isolated from leaf-branch compost is potentially applicable for industrial purposes due to its ability to hydrolyze aliphatic and aromatic polyesters, such as poly(ε-caprolactone) (PCL) and polyethylene terephthalate (PET). However, to meet the requirement of industrial applications, the enzymatic properties of LC-cutinase should be greatly improved. Protein engineering is a promising strategy to improve the enzymatic properties of LC-cutinase. However, to engineer a LC-cutinase variant with higher activity and stability in a rational manner, deep understanding of the structure-activity-stability relationships of LC-cutinase is necessary. To understand the structure-activity-stability relationships of LC-cutinase, it is necessary to determine the crystal structure of LC-cutinase.

To date, the crystal structures of two fungal cutinases from *F. solani* (Longhi *et al*., 1997) and *G. cingulata* (Nyon *et al*., 2009) and one bacterial cutinase from *T. alba* (Kitadokoro *et al*., 2012) have been determined. *F. solani* cutinase consists of 197 residues. It is an α/β-protein with a hydrophobic core comprising a slightly twisted five-parallel-stranded β-sheet, surrounded by four α-helices (Fig. 3-1). The catalytic triad of *F. solani* cutinase consists of Ser120, Asp175 and His188, and its oxyanion hole consists of Ser42 and Gln121. The amino acid sequence, Gly-Tyr-Ser-Gln-Gly, encompasses the catalytic serine residue, Ser120.

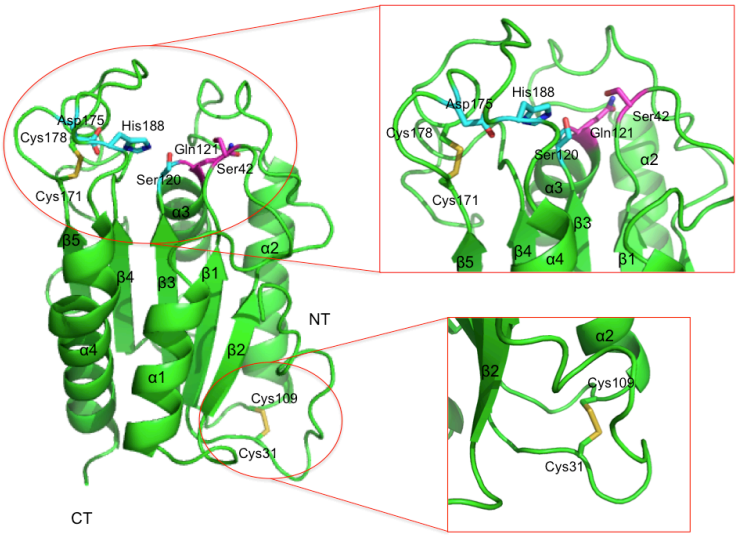

Fig. 3-1 Overall structure of *F. solani* cutinase. The main chain (green) is rendered as ribbon diagram. The catalytic triad consists of Ser120, Asp175 and His188, which are depicted as cyan sticks. The side chains of anion hole-forming residues Ser42 and Gln121 are rendered as magenta sticks. Cys31-Cys108 and Cys171-Cys178 forming disulfide bonds are rendered by a stick model, in which the sulfur atom is colored yellow. The oxygen and nitrogen atoms are colored red and blue, respectively. NT and CT represent N- and C-termini, respectively.

Unlike most lipases, the catalytic serine residue is not buried under an amphipathic loop but is accessible to the solvent (Longhi and Cambillau, 1999). Two disulfide bonds are present in this cutinase. They are Cys31-Cys109, which links the N-terminal end to a β-turn and participates in the stabilization of the global molecular folding, and Cys171-Cys178, which is assumed to play an important role in the stabilization of the two consecutive β-turns, on which one of the catalytic triad-forming residues, Asp175, is located.

T. alba cutinase has an α/β hydrolase fold structure like fungal cutinase, but it is larger than fungal cutinases in size. *T. alba* cutinase consists of 306 residues. The structure of *T. alba* cutinase consists of a central twisted β-sheet, two of which are

antiparallel, rather than a five-parallel-stranded β-sheet present in fungal cutinases (Fig. 3-2).

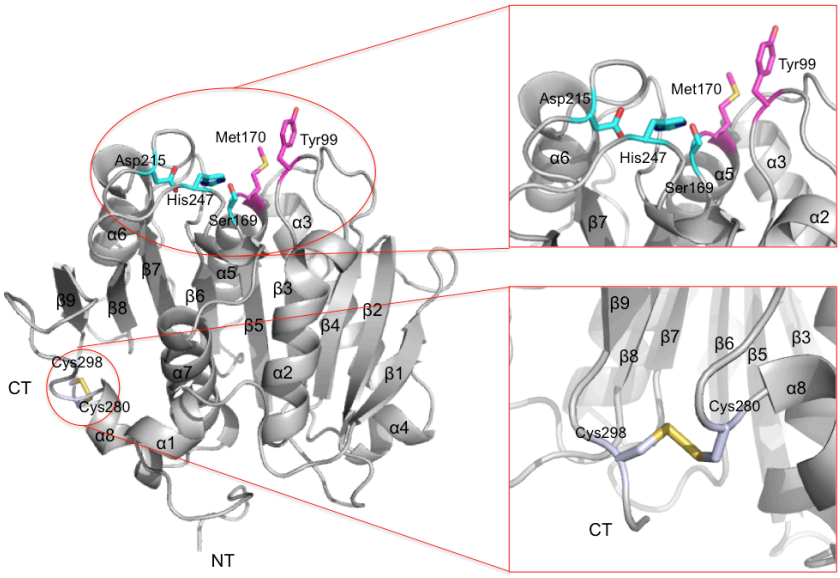

Fig. 3-2 Overall structure of *T. alba* cutinase. The main chain (grey) is rendered as ribbon diagram. The catalytic triad consists of Ser169, Asp215 and His247, which are depicted as cyan sticks. The side chains of the putative anion hole-forming residues Tyr99 and Met170 are rendered as magenta sticks. The disulfide bond formed between Cys280 and Cys298 is illustrated by a stick model, in which the sulfur atom is colored yellow. The oxygen and nitrogen atoms are colored red and blue, respectively. NT and CT represent N- and C-termini, respectively.

Like fungal cutinases, *T. alba* cutinase contains a Ser-Asp-His catalytic triad, and the catalytic serine residue is accessible to the solvent. Ser169, Asp215 and His 247 form the catalytic triad, which is located on the loops between the β-strands and α-helices. The oxyanion hole is formed by the main chain amides of Tyr99 and Met170. The disulfide bond is formed between Cys280 and Cys298 in the C-terminal region of the structure.

As described in Chapter 2, the recombinant protein of LC-cutinase, which is simply designated as LC-cutinase, is composed of 265 amino acid residues with the calculated molecular mass of 28,517 Da, because a seven-residue peptide, Gln-Pro-Ala-Met-Ala-Met-Asp, is attached to the N-terminus of LC-cutinase[36-293]. The size of LC-cutinase is more similar to that of *T. alba* cutinase than to that of *F. solani* cutinase. In addition, The LC-cutinase sequence is more similar to *T. alba* cutinsase than to *F. solani* cutinase. LC-cutinase shows the amino acid sequence identities of 50.7% to *T. alba* cutinsase and 14.9% to *F. solani* cutinsase. Therefore, the structure of LC-cutinase can be modeled based on the crystal structure of *T. alba* cutinsase. However, to understand the structure-activity-stability relationships of LC-cutinase accurately, it is necessary to determine the crystal structure of LC-cutinase.

In this study, I determined the crystal structure of LC-cutinase at 1.5Å resolution. The structure highly resembles that of *T. alba* cutinase. Ser165, Asp210, and His242 form the catalytic triad. Single disulfide bond is formed between Cys275 and Cys292.

3.2 Materials and methods

3.2.1 Protein preparation. LC-cutinases was overproduced in *E. coli* BL21-CodonPlus (DE3)-RP as a fusion protein with the pelB leader sequence and purified from the extracellular medium, as described in Chapter 2.

3.2.2 Crystallization and structure determination. Crystallization of LC-cutinase was carried out at 20℃ using sitting drop vapor diffusion method in a 96-well Corning Crystal*EX* plate (Hampton Research, Aliso Viejo, CA, USA). Drop solutions were

prepared by mixing 1 µl each of protein and reservoir solutions, and equilibrated against a 100 µl reservoir solution. LC-cutinase was concentrated to approximately 11 mg ml^{-1} before crystallization. The crystallization conditions were screened using Wizard III and IV (Emerald BioStructures, Inc. & Emerald BioSystems, Bainbridge Island, Washington, USA). Crystals of LC-cutinase were appeared in the drops containing 20% (w/v) polyethylene glycol (PEG) 3350 and 0.2 M sodium thiocyanate after incubation for two weeks. These crystals belonged to the space group $P2_12_12_1$ with cell parameters a = 40.91 Å, b = 71.08 Å, c = 72.73 Å and contained one protein molecule per asymmetric unit.

Diffraction data of LC-cutinase were collected at a wavelength of 0.9 Å with the beam line BL44XU at SPring-8, Japan. The data were indexed, integrated and scaled using the HKL2000 program suit (Otwinowski and Minor, 1997). The structure was solved by the molecular replacement method using MOLREP (Vagin and Teplyakov, 1997) in the CCP4 program suite (Collaborative computational project, Number 4, 1994). The crystal structure of *Streptomyces exfoliatus* lipase at 1.9Å resolution was used as a starting model. Automated model building was done by using ArpWarp (Langer *et al*., 2008). Structural refinement was carried out by using REFMAC (Murshudov *et al*., 1997) of the CCP4 program and the model was corrected using COOT (Emsley and Cowtan, 2004). The statistics for data collection and refinements are summarized in Table 3-1.

Table 3-1. Data collection and refinement statistics

Crystal	LC-cutinase
Wavelength (Å)	0.9
Space group	$P2_12_12_1$
Cell parameters	
a, b, c (Å)	40.91, 71.08, 72.73
α=β=γ (°)	90.0
Molecules/asymmetric unit	1
Resolution range (Å)	50.0-1.5 (1.53-1.5)[a]
Reflections measured	480,881
Unique reflections	35,110
Completeness (%)	99.9 (100)[a]
R_{merge} (%)[b]	10.6 (41.9)[a]
Average *I*/*s* (*I*)	31.7 (4.1)[a]
Refinement statistics	
Resolution limits (Å)	50.0-1.5
No. of atoms	
Protein/water/SCN	1962/315/12
R_{work} (%) / R_{free} (%)[c]	15.7/18.6
Rms deviations from ideal values	
Bond lengths (Å)	0.007
Average B factors (Å^2)	
Protein	15.5
Water/SCN	27.1/23.6
Ramachandran plot statistics	
Most favored regions (%)	97.3
Additional allowed regions (%)	2.7

[a] Numbers in parentheses are for the highest-resolution shell.

[b] $R_{merge} = \sum|I_{hkl} - \langle I_{hkl}\rangle|/\sum I_{hkl}$, where I_{hkl} is an intensity measurement for reflection with indices *hkl* and $\langle I_{hkl}\rangle$ is the mean intensity for multiply recorded reflections.

[c] Free *R*-value was calculated using 5% of the total reflections chosen randomly and omitted from refinement.

3.2.3 Protein Data Bank accession number. The coordinates and structure factors have been deposited in the RCSB Protein Data Bank under ID code 4EB0.

3.3 Results and discussion

3.3.1 Crystallization of LC-cutinase. LC-cutinase was purified from the extracellular medium of *E. coli* cells as described in Chapter 2. LC-cutinase was screened for crystallization condition using the kits available from commercial sources. Crystals suitable for X-ray crystallographic analyses were obtained in two weeks (Fig. 3-3).

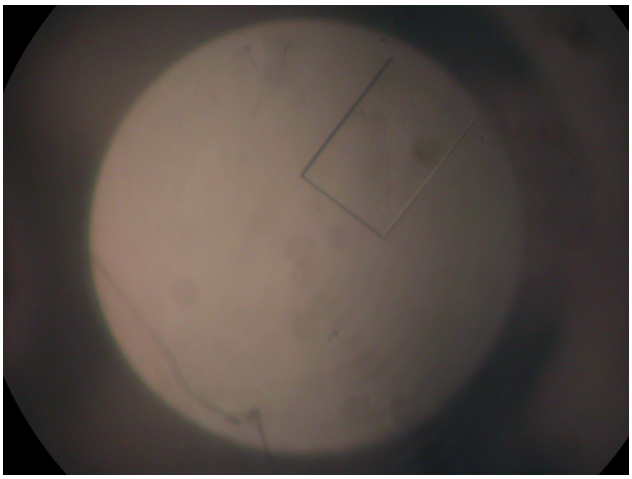

Fig. 3-3 Protein crystal of LC-cutinase after 2 weeks incubation at 20°C. The protein concentration of 11 mg ml^{-1} was combined with reservoir solution containing 0.2 M sodium thiocyanate and 20% PEG 3350 by the ratio of 1:1.

3.3.2 Overall structure of LC-cutinase. The crystal structure of LC-cutinase was determined at 1.5Å resolution. The asymmetric unit of the crystal structure consists of one molecule. The protein contains 258 of 265 residues, with the N-terminal seven residues missing. Electron density for these residues is not observed, probably due to a structural disorder. The LC-cutinase structure belongs to an α/β hydrolase fold superfamily and consists of a nine-stranded β-sheet and eight α-helices (Fig. 3-4).

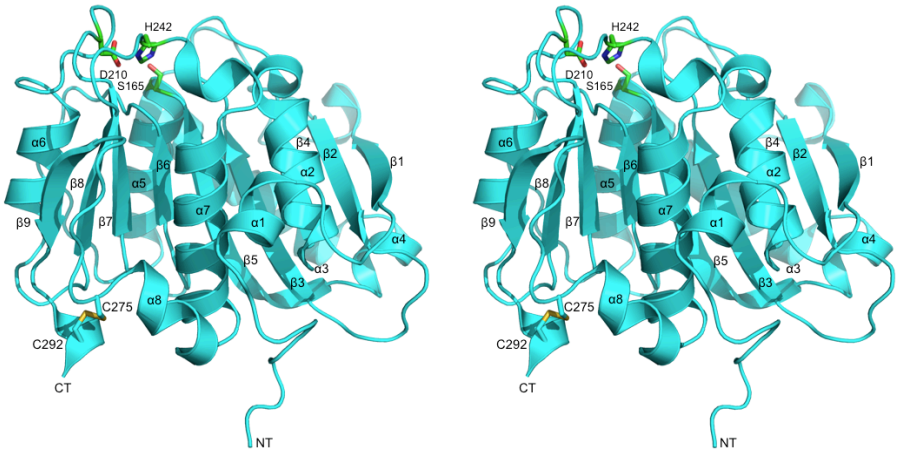

Fig. 3-4 Stereoview of the crystal structure of LC-cutinase. The main chain (cyan) is rendered as ribbon diagram. The catalytic triad consists of Ser165, Asp210 and His242, which are depicted as green sticks. The disulfide bond formed between Cys275 and Cys292 is illustrated by a stick model, in which the sulfur atom is colored yellow. The oxygen and nitrogen atoms are colored red and blue, respectively. NT and CT represent N- and C-termini, respectively.

LC-cutinase highly resembles the structures of *T. alba* cutinase (PDB code 3VIS) (Kitadokoro *et al.*, 2012) and *S. exfoliatus* lipase (PDB code 1JFR) (Wei *et al.*, 1998). The root-mean-square deviation (RMSD) value between LC-cutinase and *T. alba* cutinase is 0.77 Å for 255 Cα atoms and that between LC-cutinase and *S. exfoliatus*

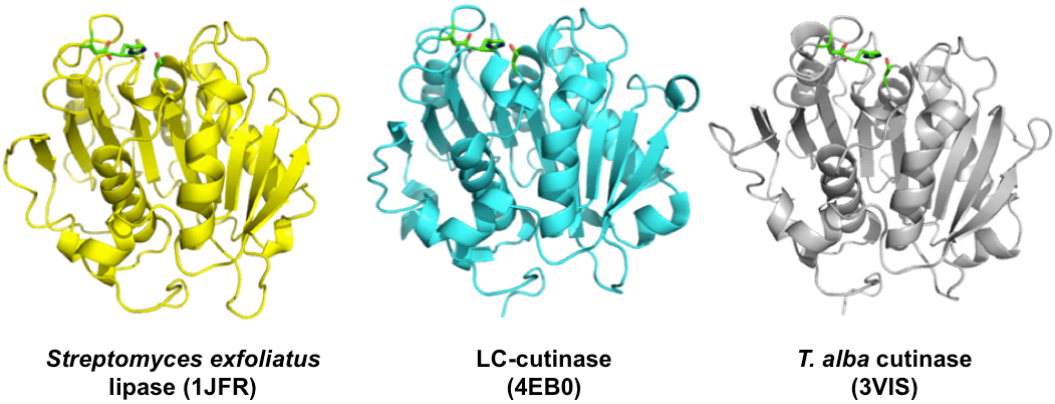

Fig. 3-5 Comparison of the structures of LC-cutinase and its homologs. The LC-cutinase structure is shown by cyan ribbon. *S. exfoliatus* lipase and *T. alba* cutinase are shown by yellow and grey ribbons.

lipase is 1.01 Å for 252 Cα atoms (Fig. 3-5). The LC-cutinase structure reveals that Ser165, Asp210, and His242 form a catalytic triad. Ser165 within a GXSXG motif (GHSMG for LC-cutinase and its homologs) is located within a sharp turn, termed nucleophilic elbow (Ollis *et al*., 1992), between β5-strand and α5-helix.

It also reveals that one disulfide bond is formed between Cys275 and Cys292. This disulfide bond apparently anchors the C-terminus to the loop between α8-helix and β9-strand as does that of *T. alba* cutinase between Cys280 and Cys298 (Fig. 3-6). In addition, Tyr95 and Met166 form a putative oxyanion hole of LC-cutinase.

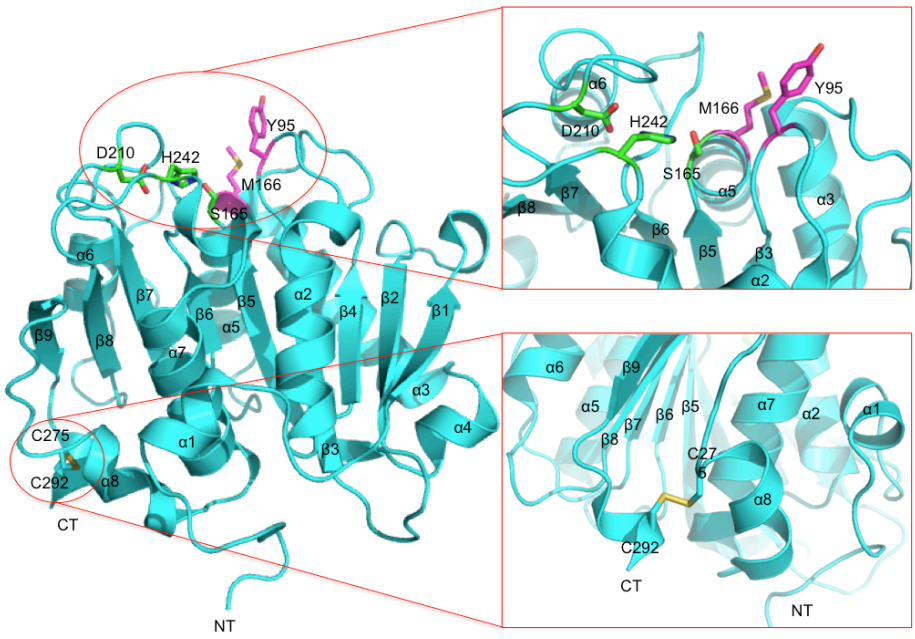

Fig. 3-6 Overall structure of LC-cutinase. The main chain (cyan) is rendered as ribbon diagram. The catalytic triad consists of Ser165, Asp210 and His242, which are depicted as green sticks. The side chains of the putative anion hole-forming residues Tyr95 and Met166 are rendered as magenta sticks. The disulfide bond formed between Cys275 and Cys292 is illustrated by a stick model, in which the sulfur atom is colored yellow. The oxygen and nitrogen atoms are colored red and blue, respectively. NT and CT represent N- and C-termini, respectively.

The structure of *F. solani* cutinase complexed with covalently-bound diethyl *p*-nitrophenyl phosphate (E600) reveals that the oxyanion hole of this enzyme is preformed in cutinase instead of being induced by ligand binding like lipase (Martinez *et al*., 1994). Overall structure of *F. solani* cutinase in complex with E600 is very similar to that of the native crystal structure, as indicated by the very low RMSD value of 0.33 Å obtained with all Cα atoms. This contrasts with what has been observed for lipases from *Rhizomucor miehei* (Brzozowski *et al*., 1991; Derewenda *at al*., 1992) and human pancreas (van Tilbeurgh *et al*., 1993), where conformational changes between the closed and open forms involve displacements of the lid covering the active site consisting of 15 and 33 residues, respectively, by a complex movement with an amplitude of 12 Å in *R. miehei* lipase and 27 Å in human pancreas lipase, leading to an "open" lipase conformation. The rearrangement of the lid results in a large increase in the lipophilic surface. The exposure of these surfaces to water would probably be thermodynamically unfavorable in the absence of a lipid-water interface and much less soluble. A second consequence of the movement of the lid of these lipases is the formation of the oxyanion hole upon substrate binding. According to this report, LC-cutinase probably contains the preformed oxyanion hole due to a lack of the lid structure and resembles geometry of catalytic triad to that of *F. solani* cutinase.

3.3.3 Substrate binding sites of LC-cutinase and T. alba cutinase. In characterizing mutants and covalently inhibited complexes of *F. solani* cutinase, 34 variant structures, crystalizing in 8 different crystal forms, have been determined. A structural comparative analysis was carried out to investigate the dynamics of cutinase (Longhi *et al*., 1996). The result reveals that surface loop is identified as the major flexible protein regions,

particularly those forming the active-site groove, whereas the elements constituting the protein scaffold were found to retain the same conformation in all cutinase variants studied. The surface loop for lipid binding site of *F. solani* cutinase consists of two loops (residues 80-87 and residues 180-188) above the active site crevice bearing hydrophobic residues Leu81, Gly82, Ala85, Leu86, Pro87, Leu182, Ile183 and Val184, in which this flexibility had been suggested to occur in order to allow a productive interaction with the substrate (Martinez *et al*., 1992) (Fig. 3-7).

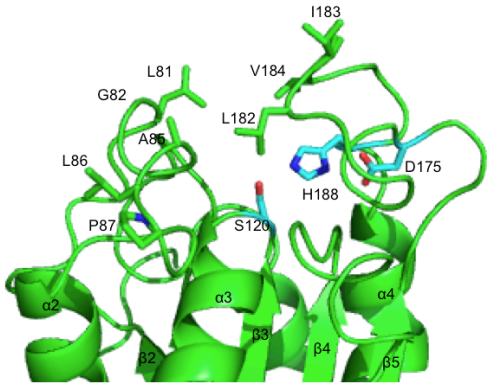

Fig. 3-7 The structure of the active site of *F. solani* cutinase with the lipid binding region. The residues forming a surface loop and three active site residues of *F. solani* cutinase are shown by stick models (cyan for active site residues) with labels. In these stick models, the oxygen and nitrogen atoms are colored red and blue, respectively.

The structure of LC-cutinase around the active site is compared with that of *T. alba* cutinase in Fig. 3-8. The *T. alba* cutinase structure shows that Tyr99, Thr100, Leu129, Met170, Trp194, Thr216, Ile217, and Phe248 form a hydrophobic patch on protein surface, to which a polyethylene glycol (PEG) partially binds (Kitadokoro *et al*., 2012). Three active site residues, Ser169, Asp215, and His247, are embedded in this hydrophobic patch. The corresponding residues of LC-cutinase are Tyr95, Thr96, Phe125, Met166, Trp190, Thr211, Val212, and Phe243.

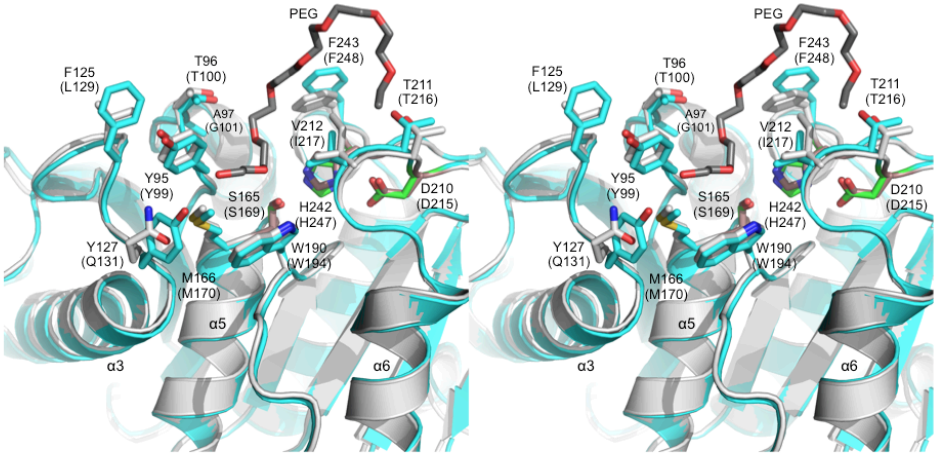

Fig. 3-8 Stereoview of the structures of LC-cutinase and *T. alba* cutinase around the active site. The structure of LC-cutinase is superimposed on that of *T. alba* cutinase (PDB code 3VIS chain A). The structures of LC-cutinase and *T. alba* cutinase are colored cyan and grey, respectively. The residues that form a hydrophobic patch on protein surface and three active site residues of LC-cutinase are shown by stick models (green ones for active site residues) with labels. The corresponding residues of *T. alba* cutinase are also shown by stick models with labels in parentheses. In these stick models, the oxygen and nitrogen atoms are colored red and blue, respectively. A part of the PEG molecule is indicated by a dark grey stick model, in which the oxygen atom is colored red.

These residues, as well as Ala97 and Tyr127, which are replaced by Gly (Gly101) and Gln (Gln131), respectively, in *T. alba* cutinase, apparently form a hydrophobic patch. A long groove is extended from the catalytic pocket in this hydrophobic patch, suggesting that this groove serves as a binding site of an amphiphilic long-chain substrate, such as PET. However, further structural studies will be necessary to understand the substrate recognition mechanism of the enzyme.

3.4 Summary

The structure of LC-cutinase was determined at 1.5Å resolution. The LC-cutinase structure has a typical α/β hydrolase fold consisting of a nine-stranded β-sheet and eight α-helices. The catalytic triad consists of Ser165, Asp210 and His242. These residues are embedded in the hydrophobic patch formed by Tyr95, Thr96, Phe125, Met166, Trp190, Thr211, Val212, and Phe243. This hydrophobic patch may serve as a binding site of an amphiphilic long-chain substrate, such as PET. One disulfide bond is formed between Cys275 and Cys292 at the C-terminal region. This disulfide bond is not conserved in fungal cutinases but is conserved in *T. alba* cutinase and apparently anchors the C-terminus to the loop between α8-helix and β9-strand.

CHAPTER 4

Effects of the mutation at Tyr95 on the activity and stability of LC-cutinase

4.1 Introduction

Determination of the LC-cutinase structure indicates a hydrophobic patch is present on protein surface (Fig. 4-1). The residues forming this hydrophobic patch are Tyr95, Thr96, Phe125, Met166, Trp190, Thr211, Val212, and Phe243. The corresponding residues of *T. alba* cutinase form a PEG binding groove, suggesting that these residues form a substrate-binding pocket. The catalytic residues are located at the bottom of this pocket. This hydrophobic patch probably facilitates binding of a long chain substrate as proposed for *T. alba* cutinase.

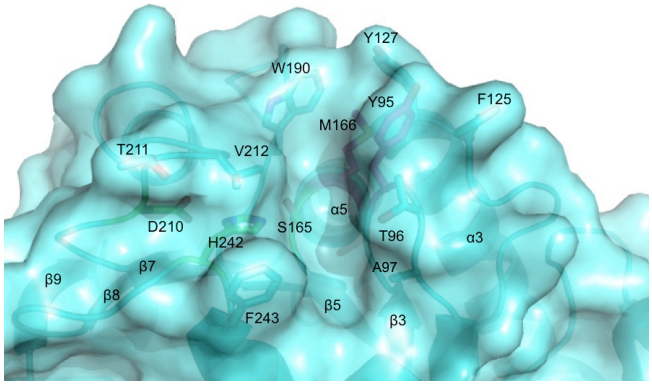

Fig. 4-1 The substrate-binding pocket of LC-cutinase. The residues forming a hydrophobic patch on protein surface and three active site residues of LC-cutinase are shown by stick models (green ones for active site residues) with labels. The transparent surface of LC-cutinase illustrates the long groove of substrate binding pocket, which surrounded by the labeled hydrophobic residues.

The lipid-binding region is also present in *F. solani* cutinase. This region includes the catalytic residues of the enzyme. This region also includes two loops consisting of residues 80-87 and 180-188 (Martinez *et al.*, 1994). The structural

comparison of *A. oryzae* and *F. solani* cutinases demonstrates the presence of the two gatekeeper residues (Leu87 and Val190 for *A. oryzae*, and Leu81 and Val184 for *F. solani* cutinase). These residues play an important role in substrate recognition. The distance between these residues is 9.87 Å (Cβ to Cβ) for *A. oryzae* cutinase and 8.74 Å for *F. solani* cutinase (Liu *et al*., 2009). This result indicates that *A. oryzae* cutinase has a wider groove region surrounding the active site than *F. solani* cutinase and therefore may allow binding of long-chain substrate more effectively than *F. solani* cutinase. The mutational studies of *F. solani* cutinase near the active site indicate that one of the mutants, L81A, exhibits a four-fold higher activity than the wild-type protein toward PET fibers, possible due to an increase in the width of the substrate binding groove (Araújo *et al*., 2007). These results encourage me to examine whether the enzymatic activity of LC-cutinase toward polymer substrate is increased by enlargement of the substrate binding cavity.

When the residues forming the hydrophobic patch of LC-cutinase are compared with those of *T. alba* cutinase, five residues are conserved in these proteins. They are Tyr95, Met166, Trp190, Thr211, and Phe243. The corresponding residues of *T. alba* cutinase are Tyr99, Met170, Trp194, Thr216 and Phe248. Sequence analysis also reveals that Tyr95 is replaced by Phe in *S. exfoliatus* lipase, to which LC-cutinase shows the highest amino acid sequence similarity. As mentioned above, the mutational studies at the substrate binding site of fungal cutinase provides a valuable information on the substrate binding mechanism of cutinase. This information may facilitate the development of the method to engineer a mutant protein with higher activity. However, none of the mutational studies at the substrate binding site of bacterial cutinase has been done.

To examine whether the mutations at the substrate binding site affects the activity and stability of LC-cutinase, I constructed the mutant proteins Y95A- and Y95F-cutinases and characterized them. I showed that Tyr95 contributes to protein stability and enzymatic activity. In addition, I showed that LC-cutinase is a thermostable protein with the $T_{1/2}$ value of 86.2°C. This temperature is higher than the optimum temperature for activity by 36°C. The temperature dependence of the activity of LC-cutinase in the presence of PEG or that toward PET suggests that the conformation of the active site is locally changed before the protein is thermally denatured and the active site is protected from this conformational change by binding of PEG or PET.

4.2 Materials and methods

4.2.1 Protein preparation. The pET25b derivatives for overproduction of Y95A- and Y95F-cutinases were constructed by KOD plus mutagenesis kit (Toyobo, Osaka, Japan). The pET25b derivative for overproduction of the pelB-LC-cutinase[36-293] fusion protein constructed in Chapter 2 was used as a template. The primers for the polymerase chain reaction (PCR) were designed such that the TAC codon for Tyr95 is changed to GCG for Ala and TTC for Phe. PCR was performed using a thermal cycler (Gene Amp PCR system 2400, Applied Biosystems, Tokyo, Japan). All DNA oligomers were synthesized by Hokkaido System Science (Sapporo, Japan). The nucleotide sequence was confirmed with a Prism 3100 DNA sequencer (Applied Biosystems).

Y95A- and Y95F-cutinases were overproduced in *E. coli* BL21-CodonPlus (DE3)-RP as a fusion protein with the pelB leader sequence and purified from the extracellular medium, as described for LC-cutinase in Chapter 2.

4.2.2 Circular dichroism (CD) spectroscopy. The far-UV (200-260 nm) CD spectrum of the protein was measured on a J-725 spectropolarimeter (Japan Spectroscopic Co., Tokyo, Japan) at 30°C. The protein was dissolved in 10 mM Tris-HCl (pH 8.0). The protein concentration and optical path length were 0.1 mg mL^{-1} and 2 mm. The mean residue ellipticity, [θ], which has the units of deg cm^2 $dmol^{-1}$, was calculated by using an average amino acid molecular mass of 110 Da.

4.2.3 Detection of PCL-degrading activity. PCL-degrading activity was determined by measuring the weight loss of a PCL film after incubation with the enzyme. PCL films were prepared as described in Chapter 2. This PCL film was added into 1 ml of 100 mM Tris-HCl (pH 8.0) and preincubated at 50°C for 5 min. The reaction was initiated by the addition of 5 μg enzyme and continued at 50°C for 6 h. After incubation, the films were washed with water and ethanol and dried for measurement of the weight loss.

4.2.4 Detection of PET-degrading activity. PET-degrading activity was determined by measuring the weight loss of a PET film after incubation with the enzyme. PET film, a plastic package made of PET, was prepared as described in Chapter 2. This PET film was added into 1 ml of 100 mM Tris-HCl (pH 8.0) and preincubated at 50, 60 and 70°C for 5 min. The reaction was initiated by the addition of 5 μg enzyme and continued at 50, 60 and 70°C with gentle shaking for 24 h. After incubation, the films were washed with water and ethanol and dried for measurement of the weight loss.

4.2.5 Determination of enzymatic activity. The enzymatic activity was determined at the temperature indicated in 25 mM Tris-HCl (pH 8.0) containing 10% (v/v) acetonitrile

and 2 mM *p*NP-butyrate. The amount of *p*NP released from the substrate was determined from the absorption at 412 nm with an absorption coefficient of 14,200 M^{-1} cm^{-1} by automatic spectrophotometer (Hitachi spectrophotometer U2810, Hitachi High-Technologies, Tokyo, Japan). One unit of activity was defined as the amount of enzyme that produced 1 μmol of *p*NP per min. For determination of the kinetic parameters, the substrate concentration was varied from 0.05 to 5 mM. The enzymatic reaction followed Michaelis-Menten kinetics and the kinetic parameters were determined from the Lineweaver-Burk plot.

4.2.6 Thermal denaturation. Thermal denaturation curves of the proteins were obtained by monitoring the change in CD values at 222 nm as the temperature was increased. The proteins were dissolved in 10 mM Tris-HCl (pH 8.0). The protein concentration and optical path length were 0.1 mg mL^{-1} and 2 mm, respectively. The rate of temperature increase was 1.0°C min^{-1}. The temperature of the midpoint of the transition, $T_{1/2}$, was calculated by curve fitting of the resultant CD values versus temperature data on the basis of a least-square analysis.

4.3 Results and discussion

4.3.1 Preparation of Y95A- and Y95F-cutinases. Tyr95 is one of the residues forming the hydrophobic patch of LC-cutinase and is located at the center of this patch. To examine whether the mutations of Tyr95 to Ala and Phe affect the activity and stability of LC-cutinase, two single mutant proteins, Y95A- and Y95F-cutinases, in which Tyr95 is replaced by Ala and Phe, respectively, were constructed. The mutation of Tyr95 to Ala is expected to enlarge the substrate-binding pocket, whereas that to Phe is expected

to increase the hydrophobicity of this pocket. Y95A- and Y95F-cutinases were purified to give a single band on SDS-PAGE. The purified recombinant proteins, in which a seven-residue peptide is attached to Y95A- and Y95F-cutinase[36-293], will be simply designated as Y95A- and Y95F-cutinases hereafter. The production levels and purification yields of these two proteins were comparable to those of LC-cutinase.

The far-UV CD spectra of Y95A- and Y95F-cutinases are compared with that of LC-cutinase in Fig. 4-2. The spectrum of Y95A-cutinase is similar to that of LC-cutinase, suggesting that the structure of LC-cutinase is not markedly changed by the mutation of Tyr95 to Ala. In contrast, the far-UV CD spectrum of Y95F-cutinase is slightly different from that of LC-cutinase, suggesting that the structure of LC-cutinase is slightly changed by the mutation of Tyr95 to Phe.

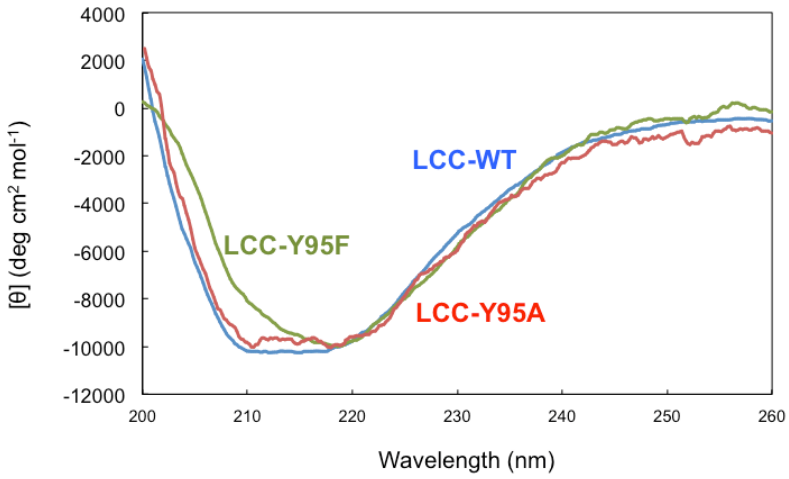

Fig. 4-2 CD spectra of LC-cutinase and its derivatives. The far-UV spectra of LC-, Y95A- and Y95F-cutinases are shown by blue, red and green lines, respectively. These spectra were measured at 30°C as described in Materials and methods.

4.3.2 PCL-degrading activity. To examine whether the mutations of Tyr95 to Ala and Phe affect the PCL-degrading activity of LC-cutinase, the PCL-degrading activities of

LC-, Y95A- and Y95F-cutinases were determined in 100 mM Tris-HCl (pH 8.0) at 50°C using a PCL film as a substrate. The amount of PCL degraded by the enzyme upon incubation for 6 h was 4.73 mg for LC-cutinase, 2.83 mg for Y95A-cutinase, and 4.70 mg for Y95F-cutinase (Fig. 4-3A). Thus, the specific PCL-degrading activity of the enzyme was calculated to be 157.6 mg/h/mg of enzyme for LC-cutinase, 94.4 mg/h/mg of enzyme for Y95A-cutinase, and 156.6 mg/h/mg of enzyme for Y95F-cutinase. This result indicates that Y95A-cutinase degrades PCL with lower efficiency than LC- and Y95A-cutinases, which exhibit comparable activities to each other.

It is noted that the specific PCL-degrading activity of LC-cutinase reported in this chapter is lower than that reported in Chapter 2 (300 mg/h/mg of enzyme), probably because 100 mM Tris-HCl (pH 8.0), instead of 500 mM Tris-HCl (pH 8.0), was used as a buffer for assay in this chapter.

4.3.3 PET-degrading activity. To examine whether the mutations of Tyr95 to Ala and Phe affect the PET-degrading activity of LC-cutinase, the PET-degrading activities of LC-, Y95A- and Y95F-cutinases were determined in 100 mM Tris-HCl (pH 8.0) at 50°C using a PET film as a substrate. The amount of PET degraded by the enzyme upon incubation for 24 h was 0.43 mg for LC-cutinase, 0.1 mg for Y95A-cutinase, and 0.43 mg for Y95F-cutinase (Fig. 4-3A). Thus, the specific PCL-degrading activity of the enzyme was calculated to be 3.6 mg/h/mg of enzyme for LC-cutinase, 0.86 mg/h/mg of enzyme for Y95A-cutinase, and 3.6 mg/h/mg of enzyme for Y95F-cutinase. This result indicates that Y95A-cutinase degrades PET with much lower efficiency than that of LC-cutinase, whereas Y95F-cutinase degrades PET with equal efficiency to that of LC-cutinase.

It is noted that the specific PCL-degrading activity of LC-cutinase reported in this chapter is lower than that reported in Chapter 2 (12 mg/h/mg of enzyme), probably because 100 mM Tris-HCl (pH 8.0), instead of 500 mM Tris-HCl (pH 8.0), was used as a buffer for assay in this chapter.

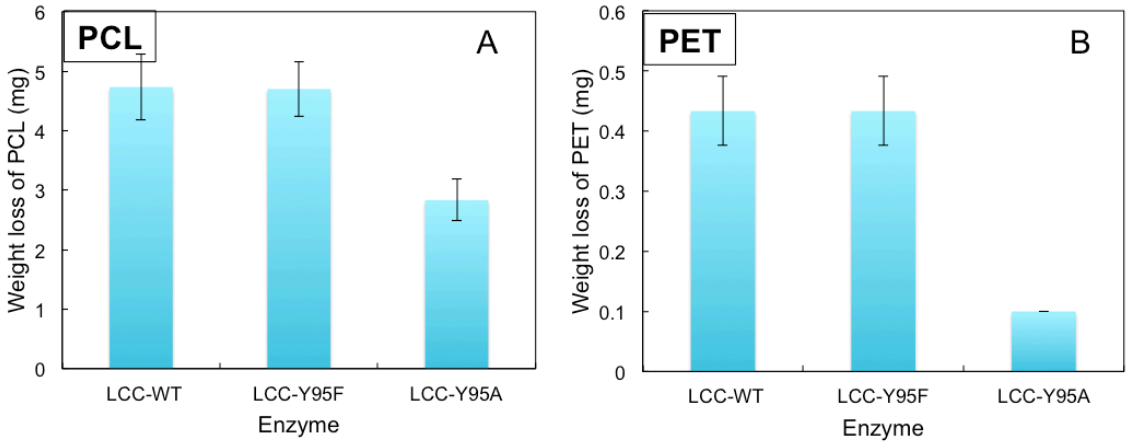

Fig. 4-3 Degradation of PCL and PET by LC-cutinase and its variants. **(A)** A PCL film (20-30 mg) was incubated at 50°C for 6 h in 1 ml of 100 mM Tris-HCl (pH 8.0) containing 5 μg of LC-cutinase (LCC-WT), Y95F-cutinase (LCC-Y95F) and Y95A-cutinase (LCC-Y95A) and its weight loss after incubation was determined. **(B)** A PET film (20-25 mg) was incubated at 50°C for 24 h in 1 ml of 100 mM Tris-HCl (pH 8.0) containing 5 μg of LC-cutinase (LCC-WT), Y95F-cutinase (LCC-Y95F) and Y95A-cutinase (LCC-Y95A) and its weight loss after incubation was determined. The experiment was carried out at least twice and the average values are shown together with error bars.

The mutational studies at Tyr95 thus indicate that Tyr95 is important for PET- and PCL-degrading activities of LC-cutinase. Y95A-cutinase exhibits lower PCL- and PET-degrading activities than LC-cutinase, whereas Y95F-cutinase fully retains these activities. This result suggests that the aromatic side chain of residue 95 is necessary for efficient binding and catalysis of polymer substrate, as suggested for chitinases A and B of *Serratia marcescens* (Zakariassen *et al*., 2009).

4.3.4 Temperature dependencies of activities of Y95A- and Y95F-cutinases. To examine whether the mutations of Tyr95 to Ala and Phe affect the optimum temperature for activity of LC-cutinase, the temperature dependencies of the activities of LC-, Y95A- and Y95F-cutinases were analyzed by using *p*NP-butyrate as a substrate. All proteins exhibited the highest activity at 50°C (Fig. 4-4). However, the activity of Y95F-cutinase was slightly lower than that of LC-cutinase at 50°C, but is slightly higher than that of LC-cutinase at 70°C, suggesting that the optimum temperature for activity of Y95F-cutinase is slightly higher than that of LC-cutinase by a few degrees. Likewise the activity of Y95A-cutinase at 40°C relative to that at 50°C is higher than that of LC-cutinase, suggesting that the optimum temperature for activity of Y95A-cutinase is slightly lower than that of LC-cutinase by a few degrees. These results suggest that the mutation of Tyr95 to Phe stabilizes the protein, whereas that to Ala destabilizes the protein. Like the PCL- and PET-degrading activities of LC-cutinase, the activity of LC-cutinase toward *p*NP-butyrat was greatly decreased by the mutation of Tyr95 to Ala, but was not significantly changed by the mutation of Tyr95 to Phe. This result indicates that the aromatic side chain of residue 95 is important for the activity of LC-cutinase toward this substrate as well.

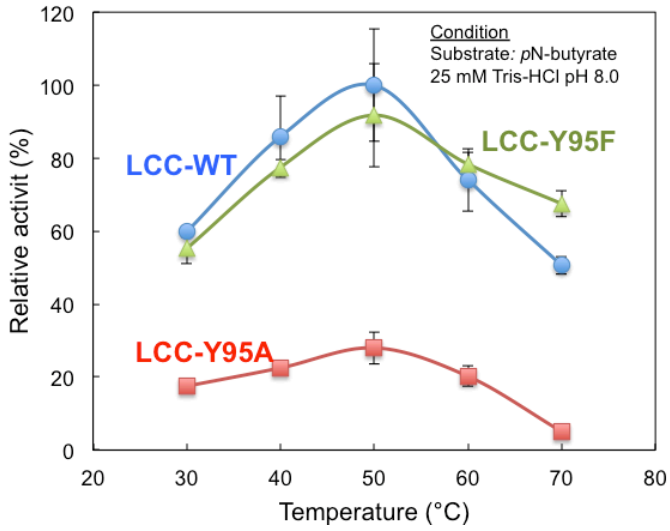

Fig. 4-4 Temperature dependencies of enzymatic activities of LC-cutinase and its variants. The enzymatic activities of LC-cutinase (blue circle and line), Y95F-cutinase (green triangle and line) and Y95A-cutinase (red rectangle and line) were determined in 25 mM Tris-HCl (pH 8.0) containing 10% (v/v) acetonitrile and 0.5 mM *p*NP-butyrate at the temperatures indicated.

4.3.5 Kinetic parameters for enzymatic activities of LC-cutinase and its variants. To examine whether a reduction of activity at the temperatures higher than the optimum temperature for activity is due to a decrease in substrate binding affinity or turnover number, the kinetic parameters for the activities of LC-cutinase and its variants were determined at various temperatures using *p*NP-butyrate as a substrate. At any substrate concentration and temperature examined, the amount of the product increases in proportion to the incubation time for at least 10 min (data not shown), suggesting that the proteins are not thermally denatured during assay.

The K_m values of LC-cutinase determined at 30, 50 and 70°C were similar with one another (0.21-0.24 mM), whereas its k_{cat} values determined at these temperatures varied in proportion to its specific activities (Table 4-1). These results indicate that a reduction of the activity of LC-cutinase at 60-70°C as compared to the maximal one is

not due to a decrease in substrate binding affinity but due to a decrease in turnover number. The steric configurations of the active site residues are probably changed at these temperatures, such that they are not optimum for activity.

In contrast, the K_m value of Y95F-cutinase determined at 70°C was 3-fold higher than that determined at 50°C, whereas the k_{cat} value of Y95F-cutinase determined at 70°C was only slightly lower than that determined at 50°C (Table 4-1). Likewise, the K_m value of Y95A-cutinase determined at 70°C was 4-fold higher than that determined at 50°C, whereas the k_{cat} value of Y95A-cutinase determined at 70°C was comparable to that determined at 50°C (Table 4-1). These results suggest that a reduction of the activities of Y95F- and Y95A-cutinases at 70°C is not due to a decrease in turnover number but due to a decrease in substrate binding affinity. Further studies will be required to understand the reason why the mechanism by which these mutant proteins exhibit lower activities at 60-70°C as compared to the maximal one is different from that by which LC-cutinase exhibits lower activities at these temperatures.

Table 4-1. Kinetic parameters of enzymatic activities of LC-, Y95F- and Y95A-cutinases

Enzyme	LC-cutinase		Y95F-cutinase		Y95A-cutinase	
Temperature (°C)	K_m (mM)	k_{cat} (s^{-1})	K_m (mM)	k_{cat} (s^{-1})	K_m (mM)	k_{cat} (s^{-1})
30	0.22	232	-	-	-	-
50	0.21	343	0.19	322	0.6	199
70	0.24	213	0.57	268	2.36	181

The K_m and k_{cat} values of other cutinases have been reported to be 1.93 mM and 6.03 s^{-1} for *T. alba* cutinase, at 30°C (Ribitsch *et al*., 2012), 2.1 mM and 30.9 s^{-1} for *T. fusca* cutinase at 25°C (Herrero Acero *et al*., 2011), 0.51 mM and 742 s^{-1} for *T. fusca* cutinase at 60°C (Chen *et al*., 2010), and 0.27 mM and 837 s^{-1} for *F. solani* cutinase at 40°C (Chen *et al*., 2010). The K_m and k_{cat} values of LC-cutinase are 0.22 mM and 232 s^{-1} at 30°C, and 0.21 mM and 343 s^{-1} at 50°C (Table 4-1). These results indicate that both the substrate binding affinity and turnover number of LC-cutinase are considerably higher than those of *T. alba* and *T. fusca* cutinases at 30°C, whereas they are comparable to those of *T. fusca* and *F. solani* cutinases at 50°C.

4.3.6 Thermal stability of LC-, Y95A- and Y95F-cutinases. To examine whether the mutations of Tyr95 to Ala and Phe affect the stability of LC-cutinase, thermal denaturation of LC-, Y95A- and Y95F-cutinases was analyzed at pH 8.0 by monitoring the change in CD values at 222 nm. Thermal denaturation of these proteins was irreversible at the condition examined. However, the thermal denaturation curves of these proteins were reproducible unless the protein concentration, pH, and the rate of the temperature increase (scan rate) were significantly changed. The thermal denaturation curves of LC-, Y95A- and Y95F-cutinases measured in 10 mM Tris-HCl (pH 8.0) are shown in Figure 4-5. The $T_{1/2}$ values of LC-cutinase and its variants are summarized in Table 4-2. The midpoints of the transition of these curves, $T_{1/2}$, are 86.2°C for LC-cutinase, 82.0°C for Y95A-cutinase, and 94.8°C for Y95F-cutinase. This result indicates that the mutation of Tyr to Ala decreases the thermal stability of LC-cutinase by 4.2°C, whereas that to Phe increases it by 8.6°C. The mutation of Tyr95 to Phe increases the stability of LC-cutinase, probably due to the removal of the hydroxyl

group of Tyr95. The hydroxyl group of Tyr95 probably causes a steric hindrance at the hydrophobic pocket, which may result in a decreased conformational stability, as reported for chloramphenicol acetyltransferase (Chirakkal and Moir, 2001). On the other hand, the mutation of Tyr95 to Ala destabilizes the protein, probably because the aromatic side chain was removed. Because hydrophobic interaction is one of the major stabilizing factors of proteins (Kyte and Doolittle, 1982), this mutation probably reduce hydrophobic interaction between residue 95 and a surrounding residue at the hydrophobic patch, which contributes to the stabilization of the protein.

The melting temperatures (T_m) of cutinases have been reported to be 60°C for *T. alba* cutinase (Kawai *et al*., 2013), 56°C for *F. solani* cutinase (Liu *et al*., 2009) and 59°C for *A. oryzae* cutinase (Liu *et al*., 2009). These results indicate that LC-cutinase is thermally highly robust protein.

Table 4-2. $T_{1/2}$ values of LC-, Y95F- and Y95A-cutinase at pH 8.0

Enzyme	$T_{1/2}$ (°C)	Δ $T_{1/2}$ (°C)
LC-cutinase	86.2	-
Y95F-cutinase	94.8	+8.6
Y95A-cutinase	82	-4.2

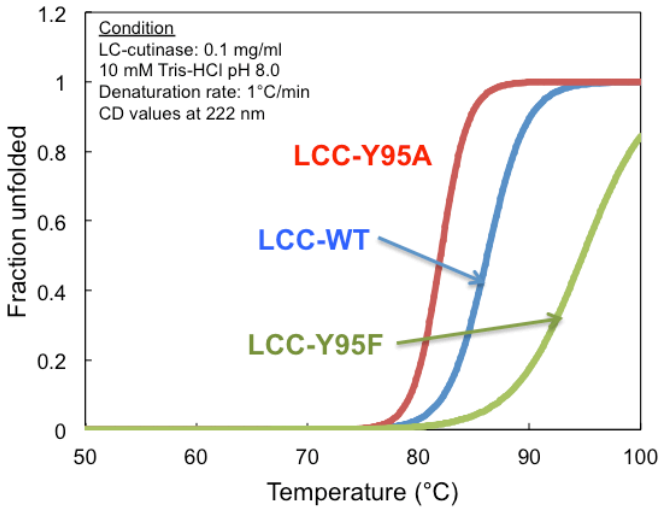

Fig. 4-5 Thermal denaturation curves of LC-cutinase and its variants. The thermal denaturation curves of LC-cutinase (blue line), Y95A-cutinase (red line) and Y95F-cutinase (green line) are shown. The thermal denaturation curves were obtained in 10 mM Tris-HCl (pH 8.0). The rate of temperature increase was 1°C/min.

Determination of the thermal stability of LC-cutinase indicates that LC-cutinase is a thermostable enzyme with the $T_{1/2}$ value of 86.2°C. This means that LC-cutinase is not thermally denatured up to 75°C. However, the optimum temperature for activity of LC-cutinase toward *p*NP-butyrate is 50°C. This temperature is lower than the $T_{1/2}$ value by 36.2°C. This means that the activity of LC-cutinase decreases as the temperature increases beyond 50°C, before the protein is thermally denatured. Determination of the kinetic parameters for the activity of LC-cutinase at these temperatures indicates that the enzymatic activity decreases at high temperatures due to a decrease in turnover number. This result strongly suggests that the reduction of activity of LC-cutinase at 60-70°C is caused by a heat-induced local conformation change of the active site. A similar result that low concentrations of GdnHCl cause local unfolding of the active site region and thereby cause a reduction in enzymatic activity has been reported for *F. solani*

cutinase (Ternström *et al*., 2005). As described in Chapter 3, the hydrophobic patch of LC-cutinase may function as a binding pocket for amphiphilic long chain substrate, such as PEG. It would be therefore informative to examine whether binding of a long chain amphiphilic substrate to the substrate binding site prevents a heat-induced conformational change at the active site and thereby increases the optimum temperature for activity of LC-cutinase.

4.3.7 Protection of active site from heat-induced local conformational change by PEG and PET. To examine whether the active site is protected from a heat-induced local conformational change by PEG, the enzymatic activity of LC-cutinase was determined in the presence of 1% PEG 1000 at various temperatures. The results are shown in Figure 4-6. The enzymatic activities of LC-cutinase in the presence and absence of 1% PEG 1000 in the reaction mixture clearly shows that the optimum temperature for activity of LC-cutinase toward *p*NP-butyrate was shifted upward by 10°C in the presence of PEG. The specific activities of LC-cutinase determined in the presence of PEG at 10-50°C are slightly higher than, but comparable to those determined in the absence of PEG. This result suggests that PEG partially prevents a heat-induced local conformational change around the active by binding to this region.

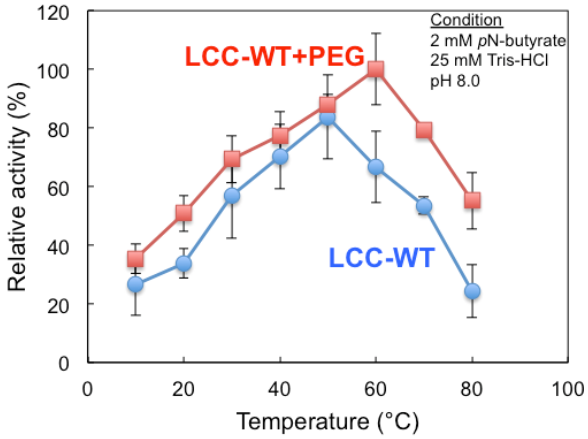

Fig. 4-6 Temperature dependencies of enzymatic activities of LC-cutinase in the presence and absence of 1% PEG 1000. The enzymatic activities of LC-cutinase in the absence of PEG (blue circle) and in the presence of 1% PEG (red aquares) are shown. The reactions were carried out in 25 mM Tris-HCl (pH 8.0) containing 10% (v/v) acetonitrile and 2 mM *p*NP-butyrate at the temperatures indicated.

The optimum temperature for activity of LC-cutinase increases by 10°C in the presence of PEG, suggesting that PEG increases the stability of the local structure around the active site by binding to this region. However, the stability of the overall structure is rather decreased by 3.0°C in the presence of 1% PEG (data not shown). LC-cutinase is slightly destabilized in the presence of PEG probably due to a change in protein solvation, as reported for hen egg-white lysozyme (Zielenkiewicz *et al*., 2006). This result may suggest that PEG stabilizes the overall structure by binding to the region near the active site, but this stabilization effect is cancelled by the destabilization effect of PEG for the overall structure. Alternatively, PEG stabilizes the local structure around the active site by binding to this region without significantly affecting the stability of the overall structure. The reason why binding of PEG to the region near the active site stabilizes this region without significantly affecting the stability of the overall structure remains to be understood.

To examine whether the active site of LC-cutinase is protected from a heat-induced local conformational change by a long-chain substrate as well, the activity of LC-cutinase toward PET was analyzed by measuring the weight loss of a PET film at various temperatures. As mentioned above, the activity of LC-cutinase decreases at 60-70°C as compared to the maximal one due to a heat-induced local conformational change and PEG partially prevents this conformational change by binding to the region near the active sire. Therefore, the PET degrading activity of LC-cutinase was analyzed at 50, 60 and 70°C. The results are shown in Figure 4-7, together with the temperature dependencies of the activities of LC-cutinase toward *p*NP-butyrate in the presence and absence of 1% PEG.

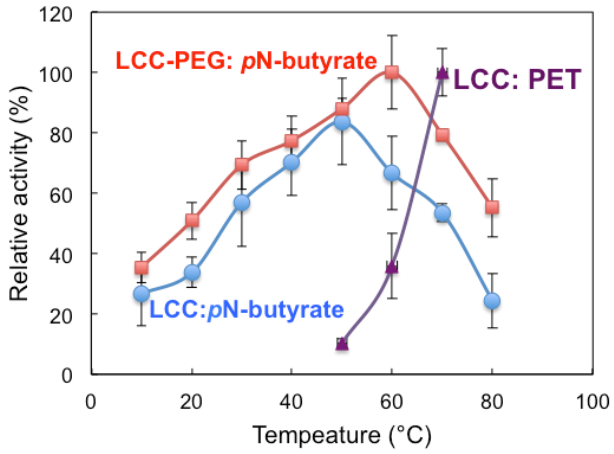

Fig. 4-7 Comparison of temperature dependencies of enzymatic activities of LC-cutinase toward *p*NP-butyrate in the presence (red square) and absence (blue circle) of 1% PEG 1000, and toward PET film (magenta triangl). The activity toward *p*NP-butyrate was determined in 25 mM Tris-HCl (pH 8.0) containing 10% (v/v) acetonitrile and 2 mM *p*NP-butyrate. The PET-degrading activity was determined by incubating a PET film in 1 ml of 100 mM Tris-HCl (pH 8.0) containing 5 μg of LC-cutinase for 24 h at the temperatures indicated.

The activity of LC-cutinase toward PET increased as the temperature increased up to 70°C (Fig. 4-7), indicating that the optimum temperature for activity of LC-cutinase toward PET increases by at least 20°C as compared to that toward *p*NP-butyrate. These results suggest that a heat-induced local conformational change of the active site is well prevented by binding of a long-chain substrate. The activity of LC-cutinase toward PET was not analyzed at the temperatures higher than 80°C, because the surface of a PET film used for assay became turbid upon incubation at these temperatures and could not be degraded by the enzyme even at 50°C.

4.4 Summary

Y95A-cutinase is much less active than LC-cutinase toward *p*NP-butyrate, PCL, and PET, whereas Y95F-cutinase is as active as LC-cutinase toward these substrates. This result suggests that the aromatic side chain of Tyr95 is important for activity of LC-cutinase. In addition, Y95A-cutinase is less stable than LC-cutinase, whereas Y95F-cutinase is more stable than LC-cutinase. This result suggests that the aromatic side chain of Tyr95 is important for stability as well. Thermal denaturation of these proteins analyzed by CD spectroscopy indicates that LC-cutinase is a highly thermostable protein with the $T_{1/2}$ value of 86.2°C. This value is higher than the T_m values of *T. alba*, *F. solani* and *A. oryzae* cutinases by 26-30°C. Nevertheless, LC-cutinase exhibits the highest activity at 50°C. Its activity decreases at 60-70°C due to a decrease in turnover number. The optimum temperature for activity of LC-cutinase increases by 10°C when the activity toward *p*NP-butyrate is determined in the presence of 1% PEG or by 20°C when the substrate is changed from *p*NP-butyrate to PET. This result suggests that the activity of LC-cutinase decreases at 60-70°C as compared to the maximal one due to a

heat-induced local conformational change and the active site of LC-cutinase is at least partially protected from this heat-induced local conformational change by binding of PEG or PET.

CHAPTER 5

Effects of the removal of the disulfide bond on the activity and stability of LC-cutinase

5.1 Introduction

Determination of the LC-cutinase structure reveals that this protein contains one disulfide bond between Cys275 and Cys292. This disulfide bond is conserved in bacterial cutinases, such as *T. alba* cutinase, but is not conserved in fungal cutinases, such as *F. solani* and *A. oryzae* cutinases. *T. alba* cutinase contains one disulfide bond as does LC-cutinase, whereas *F. solani* and *A. oryzae* cutinases contain two and three disulfide bonds, respectively. However, the number of the disulfide bond and stability are apparently not correlated with each other for these cutinases, because the melting temperatures, T_m, of these cutinases are 56°C for *F. solani* cutinase (Liu *et al*., 2009), 59°C for *A. oryzae* cutinase (Liu *et al*., 2009) and 60°C for *T. alba* cutinase (Est1) (Kawai *et al*., 2013). Therefore, it would be informative to examine whether the disulfide bond of LC-cutinase contributes to the protein stability.

Disulfide bond is one of the stabilizing factors of protein. Proteins are usually destabilized by removal of a native disulfide bond (Pace *et al*., 1988; Piatek *et al*., 2010; Schulenburg *et al.,* 2010; Mason *et al.*, 2012) and stabilized by introduction of a non-native disulfide bond (Matsumura *et al.*, 1989; Kanaya *et al.*, 1991; Boone *et al.*, 2013; Vinther *et al.*, 2013; Wozniak-Knopp and Rüker, 2012). Therefore, the C-terminal disulfide bond of bacterial cutinase is probably important for protein stability. However, disulfide bond does not always show a stabilizing effect (Schmidt *et al.*, 2006; Fernandes *et al.*, 2011).

The thermodynamic and kinetic stability of several fungal cutinases has been analyzed. For example, the free energy change of unfolding in the absence of GdnHCl, $\Delta G(H_2O)$, has been reported to be 47.0 kJ mol^{-1} for *F. solani* cutinase and 49.4 kJ mol^{-1} for *H. insolens* cutinase (Ternström *et al*., 2005). The unfolding rate, $k_u(H_2O)$, has been reported to be 2.57 s^{-1} for *F. solani* cutinase and 0.83 s^{-1} for *H. insolens* cutinase (Ternström *et al*., 2005). However, none of the parameters characterizing GdnHCl-induced unfolding of bacterial cutinases has been reported.

In this study, I constructed the LC-cutinase derivative without the disulfide bond, C275/292A-cutinase, in which both Cys275 and Cys292 are replaced by Ala, and analyzed its stability. I showed that the disulfide bond of LC-cutinase contributes to the thermodynamic and kinetic stability of LC-cutinase. I also showed that LC-cutinase is a kinetically robust protein.

5.2 Materials and methods

5.2.1 Protein preparation. The pET25b derivative for overproduction of C275/292A-cutinase was constructed by KOD plus mutagenesis kit (Toyobo, Osaka, Japan). The pET25b derivative for overproduction of the pelB-LC-cutinase[36-293] fusion protein constructed in Chapter 2 was used as a template. The primers for the polymerase chain reaction (PCR) were designed such that both TGC codons for Cys275 and Cys292 are changed to GCC for Ala. PCR was performed using a thermal cycler (Gene Amp PCR system 2400, Applied Biosystems, Tokyo, Japan). All DNA oligomers were synthesized by Hokkaido System Science (Sapporo, Japan). The nucleotide sequence was confirmed with a Prism 3100 DNA sequencer (Applied Biosystems).

LC- and C275/292A-cutinases were overproduced in *E. coli* BL21-CodonPlus

(DE3)-RP as a fusion protein with the pelB leader sequence and purified from the extracellular medium, as described in Chapter 2. The protein concentration was determined from the UV absorption on the basis that the absorbance of a 0.1% (1.0 mg mL^{-1}) solution at 280 nm is 1.37. This value was calculated by using ε = 1,526 M^{-1} cm^{-1} for tyrosine and 5,225 M^{-1} cm^{-1} for tryptophan at 280 nm (Goodwin and Morton, 1946).

5.2.2 Circular dichroism (CD) spectroscopy. The far-UV (200-260 nm) and near-UV (250-320 nm) CD spectra of the protein were measured on a J-725 spectropolarimeter (Japan Spectroscopic Co., Tokyo, Japan) at 20°C. The protein was dissolved in 10 mM Tris-HCl (pH 8.0). The protein concentration and optical path length were 0.1 mg mL^{-1} and 2 mm for far-UV CD spectra and 1.0 mg mL^{-1} and 1 cm for near-UV CD spectra, respectively. The mean residue ellipticity, [θ], which has the units of deg cm^2 $dmol^{-1}$, was calculated by using an average amino acid molecular mass of 110 Da.

5.2.3 Determination of enzymatic activity. The enzymatic activity was determined at the temperature indicated in 10 mM Tris-HCl (pH 8.0) containing 10% (v/v) acetonitrile and 0.5 or 2 mM *p*-nitrophenyl butyrate (*p*NP-butyrate), as described in Chapter 2. The amount of *p*-nitrophenol (*p*NP) released from the substrate was determined from the absorption at 412 nm with an absorption coefficient of 14,200 M^{-1} cm^{-1} by automatic spectrophotometer (Hitachi spectrophotometer U2810, Hitachi High-Technologies, Tokyo, Japan). One unit of activity was defined as the amount of enzyme that produced 1 μmol of *p*NP per min. For determination of the kinetic parameters, the substrate concentration was varied from 0.05 to 5 mM. The enzymatic reaction followed Michaelis-Menten kinetics and the kinetic parameters were determined from the

Lineweaver-Burk plot.

5.2.4 Thermal denaturation. Thermal denaturation curves of the proteins were obtained by monitoring the change in CD values at 222 nm as the temperature was increased. The proteins were dissolved in 10 mM sodium phosphate (pH 8.0) or the same buffer containing 10 mM dithiothreitol (DTT). The protein concentration and optical path length were 0.1 mg mL^{-1} and 2 mm, respectively. The rate of temperature increase was 1.0°C min^{-1}. The temperature of the midpoint of the transition, $T_{1/2}$, was calculated by curve fitting of the resultant CD values versus temperature data on the basis of a least-square analysis.

5.2.5 Equilibrium experiments on GdnHCl-induced unfolding. GdnHCl-induced unfolding of the protein was analyzed by monitoring the change in CD values at 222 nm, as described previously (Mukaiyama *et al*., 2004). The protein concentration and optical path length were 0.1 mg mL^{-1} and 2 mm, respectively. The protein was incubated in 10 mM Tris-HCl (pH 8.0) containing various concentrations of guanidine hydrochloride (GdnHCl) at 30°C for 48 h for LC-cutinase and 24 h for C275/292A-cutinase prior to the measurement of the CD values. The GdnHCl–induced unfolding curves were determined and the nonlinear least-squares analysis (Pace, 1990) was used to fit the data to

$$y = \frac{((b_n^0 + a_n [D]) + (b_u^0 + a_u [D]) \exp((\frac{\Delta G(H_2O) - m[D]}{RT}))}{(1 + \exp((\frac{\Delta G(H_2O) - m[D]}{RT}))} \quad (1)$$

$$C_m = \frac{\Delta G(\mathrm{H_2O})}{m} \quad (2)$$

where y is the observed CD signal at a given concentration of GdnHCl, $[D]$ is the concentration of GdnHCl, b_n^0 and b_u^0 are the CD signals for the native and unfolded states, a_n and a_u are the slopes of the pretransition and posttransition of the baseline, $\Delta G(\mathrm{H_2O})$ is the Gibbs energy change (ΔG) of unfolding in the absence of GdnHCl, m is the slope of the linear correlation between ΔG and the GdnHCl concentration $[D]$, and C_m is the GdnHCl concentration at the midpoint of the curve. The raw experimental data were directly fitted to Eq. (1) using SigmaPlot. Two replicates were measured for each condition.

5.2.6 Kinetic experiments on GdnHCl-induced unfolding. The unfolding reactions of the proteins were performed at 50°C in 10 mM Tris-HCl (pH 8.0) and followed by a CD spectra measurement at 222 nm, as described previously (Mukaiyama *et al*., 2004). The unfolding reaction was initiated by mixing the protein solution and GdnHCl solution, such that the final protein and GdnHCl concentrations become 0.1 mg mL^{-1} and 5-6 M for LC-cutinase or 3-4 M for C275/292A-cutinase, respectively. The kinetic data were analyzed using Eq. (3):

$$A(t) - A(\infty) = \sum A_i \, e^{-k_i t} \quad (3)$$

where $A(t)$ is the value of the CD signal at a given time t, $A(\infty)$ is the value when no further change is observed, k_i is the apparent rate constant of the ith kinetic phase, and

A_i is the amplitude of the *i*th phase. The GdnHCl concentration dependence of the logarithms of the apparent rate constant (k_{app}) for unfolding was also examined. The rate constant for unfolding in the absence of GdnHCl ($k_{\mathrm{u}}(\mathrm{H_2O})$) was calculated by fitting to Eq. (4):

$$\ln k_{\mathrm{app}} = \ln k_{\mathrm{u}}(\mathrm{H_2O}) + m_{\mathrm{u}}[D] \quad (4)$$

where $[D]$ is the concentration of GdnHCl and m_{u} is the slope of the linear correlation of ln k_{u} with the GdnHCl concentration.

5.3 Results and discussion

5.3.1 Preparation of C275/292A-cutinase. To examine whether the disulfide bond of LC-cutinase contributes to the stability of LC-cutinase, the double mutant protein C275/292A-cutinase, in which both Cys275 and Cys292 are replaced by Ala, was constructed and purified. The purified recombinant protein, in which a seven-residue peptide is attached to C275/292A-cutinase[36-293], will be simply designated as C275/292A-cutinase hereafter. The production level and purification yield of C275/292A-cutinase were comparable to those of LC-cutinase. The far-UV (Fig. 5-1A) and near-UV (Fig. 5-1B) CD spectra of C275/292A-cutinase were similar to those of LC-cutinase, suggesting that the structure of LC-cutinase is not markedly changed by the mutations.

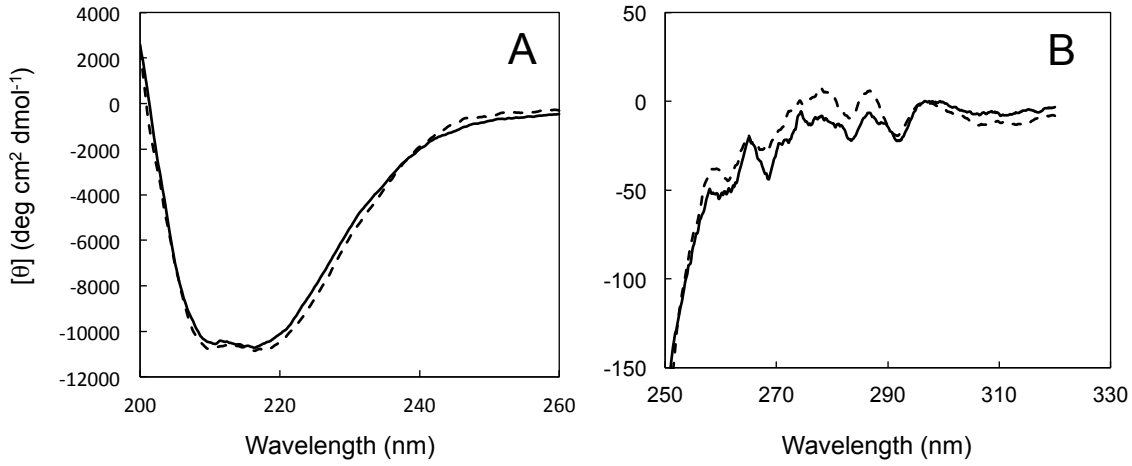

Fig. 5-1 CD spectra LC-cutinase and C275/292A-cutinase. The far-UV **(A)** and near-UV **(B)** CD spectra of LC-cutinase (solid line) and C275/292A-cutinase (broken line) are shown. These spectra were measured at 20°C as described in Materials and Methods.

5.3.2 Temperature dependence of activity of C275/292A-cutinase. The optimum temperature for activity of LC-cutinase toward *p*NP-butyrate was determined to be 50°C in Chapter 4. To examine whether removal of the disulfide bond affects the optimum temperature for activity of LC-cutinase, the temperature dependence of the activity of C275/292A-cutinase was analyzed by using *p*NP-butyrate as a substrate. The result is shown in Figure 5-2 in comparison with that of LC-cutinase. C275/292A-cutinase exhibited the highest activity at 30°C. The activity of C275/292A-cutinase at 30°C was comparable to that of LC-cutinase at 50°C. These results indicate that removal of the disulfide bond shifts the optimum temperature for activity of LC-cutinase downward by 20°C without significantly affecting the maximal activity.

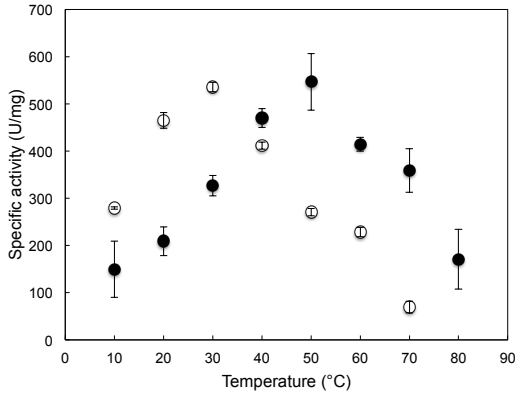

Fig. 5-2 Temperature dependencies of enzymatic activities of LC-cutinase and C275/292A-cutinase. The enzymatic activities of LC-cutinase (closed circle) and C275/292A-cutinase (open circle) were determined in 10 mM Tris-HCl (pH 8.0) containing 10% (v/v) acetonitrile and 0.5 mM *p*NP-butyrate at the temperatures indicated.

To examine whether a reduction of activity of C275/292A-cutinase at ≥40°C is due to a decrease in substrate binding affinity or turnover number of this protein, the kinetic parameters for the activity of C275/292A-cutinase were determined at 30, 50 and 70°C using *p*NP-butyrate as a substrate. At any substrate concentration and temperature examined, the amount of the product increases in proportion to the incubation time for at least 10 min (data not shown), suggesting that the protein is not thermally denatured during assay. The kinetic parameters for the activity of 275/292A-cutinase determined at various temperatures are compared with those of LC-cutinase determined in Chapter 4 in Table 5-1. The K_m values of LC- and C275/292A-cutinases determined at 30, 50, and 70°C are similar with one another (0.18-0.25 mM), whereas their k_{cat} values determined at these temperatures vary in proportion to their specific activities. These results indicate that a reduction of the activity of C275/292A-cutinase at ≥40°C as compared to the maximal one is not due to a decrease in substrate binding affinity but due to a decrease in turnover number. The steric configurations of the active

site residues are probably changed at these temperatures, such that they are not optimum for activity. Thus, the activity of C275/292A-cutinase is reduced at ≥40°C probably due to a heat-induced local conformational change of the active site.

Table 5-1. Kinetic parameters of LC-cutinase and C275/292A-cutinase

Enzyme	LC-cutinase		C275/292A-cutinase	
Temperature (°C)	K_m (mM)	k_{cat} (s^{-1})	K_m (mM)	k_{cat} (s^{-1})
30	0.22	232	0.25	342
50	0.21	343	0.18	196
70	0.24	213	0.19	49

5.3.3 Thermal stability of C275/292A-cutinase.

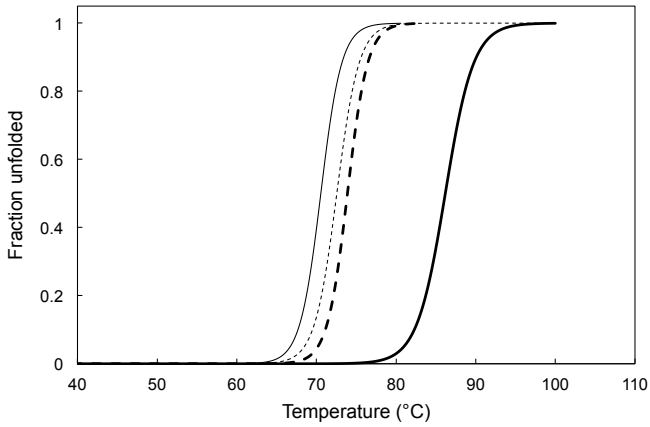

Fig. 5-2 Thermal denaturation curves of LC-cutinase and C275/292A-cutinas. The thermal denaturation curves of LC-cutinase obtained in the absence of DTT (thick solid line), and in the presence of 10 mM DTT (thick dashed line), and those of C275/292A-cutinase obtained in the absence of DTT (thin solid line) and in the presence of 10 mM DTT (thin dashed line) are shown. The rate of temperature increase was 1°C/min.

To examine whether removal of the disulfide bond affects thermal stability of LC-cutinase, the stability of LC- and C275/292A-cutinases was analyzed at pH 8.0 either in the presence or absence of 10 mM DTT by monitoring the change in CD values at 222 nm. Thermal denaturation of these proteins was irreversible at the condition examined. However, the thermal denaturation curves of these proteins were reproducible unless the protein concentration, pH, and the rate of the temperature increase (scan rate) were significantly changed. The thermal denaturation curves of LC-cutinase and C275/292A-cutinase are shown in Figure 5-2. The $T_{1/2}$ values determined from these curves are summarized in Table 5-2. The $T_{1/2}$ value of C275/292A-cutinase measured in the absence of DTT is lower than that of LC-cutinase by 15.6°C, whereas the $T_{1/2}$ value of LC-cutinase measured in the presence of DTT is lower than that measured in the absence of DTT by 12.3°C. However, the $T_{1/2}$ value of C275/292A-cutinase measured in the presence of DTT is higher than that measured in the absence of DTT by 2.0°C, suggesting that the difference between the $T_{1/2}$ values of oxidized and reduced forms of LC-cutinase is 14.3°C, instead of 12.3°C. The mechanism by which C275/292A-cutinase is slightly stabilized in the presence of DTT remains to be understood. These results indicate that LC-cutinase is destabilized by approximately 15°C, regardless of whether the disulfide bond is removed by reduction or by double mutations at Cys275 and Cys292.

Table 5-2. $T_{1/2}$ values of LC-cutinase and C275/292A-cutinase at pH 8.0

Protein	$T_{1/2}$ (°C)	$\Delta T_{1/2}$ (°C)
LC-cutinase	86.2	-
LC-cutinase: 10mM DTT	73.9	-12.3
LCC-C275/292A-cutinase	70.6	-15.6
LCC-C275/292A-cutinase: 10mM DTT	72.6	-13.6

5.3.4 Equilibrium unfolding of LC-cutinase C275/292A-cutinase *in GdnHCl.*

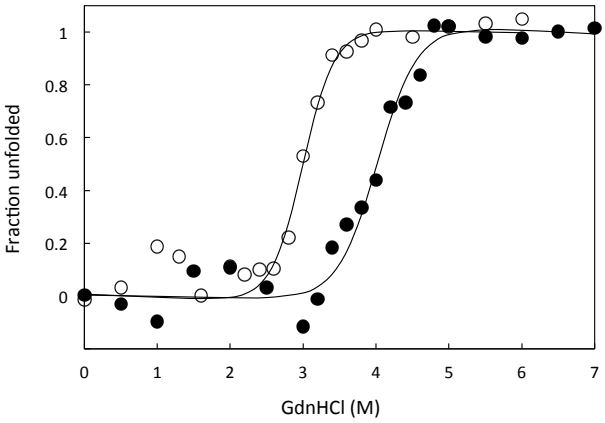

Fig. 5-3 GdnHCl-induced unfolding curves of LC-cutinase and C275/292A-cutinas at 30°C. The apparent fraction of unfolded protein is shown as a function of GdnHCl concentration. LC-cutinase was incubated for 48 h (solid circle) at pH 8.0 and 30°C prior to the measurement of the CD value at 222 nm. C275/292A-cutinase (open circle) was incubated at the same condition for 24 h prior to the measurement of the CD value at 222 nm. The lines represent the fit to Eq. (1).

Table 5-3. Thermodynamic parameters at 30°C and kinetic parameters at 50°C for GdnHCl-induced unfolding of LC- and C275/292A-cutinases

Protein	C_m (M)	m_{av}[a] (kJ mol^{-1} M^{-1})	$\Delta G(H_2O)$ (kJ mol^{-1})	$\Delta\Delta G(H_2O)$[a] (kJ mol^{-1})	$k_u(H_2O)$ (s^{-1})
LC-cutinase	4.02±0.03	10.4	41.8±0.3	-	(3.28±0.60) ×10^{-6}
C275/292A-cutinase	3.00±0.10	10.4	31.2±1.0	-10.6	(1.83±0.14) ×10^{-5}

[a] The average of the *m* values of LC-cutinase (9.2±1.4 kJ mol^{-1} M^{-1}) and C275/292A-cutinase (11.7±1.6 kJ mol^{-1} M^{-1}).

[b] $\Delta\Delta G(H_2O) = \Delta G(H_2O)$ (C275/292A-cutinase) $-\Delta G(H_2O)$ (LC-cutinase).

To examine whether removal of the disulfide bond affects equilibrium unfolding of LC-cutinase in GdnHCl, GdnHCl-induced unfolding of LC- and C275/292A-cutinases was analyzed at 30°C by monitoring the CD values at 222 nm. GdnHCl-induced unfolding of these proteins was fully reversible and followed a two-state mechanism. The protein unfolded by GdnHCl was fully refolded by removal of GdnHCl by dialysis. The GdnHCl-induced unfolding curves of LC-cutinase and C275/292A-cutinase are shown in Fig. 5-3. To obtain these curves, the protein was incubated in the presence of various concentrations of GdnHCl for two days for LC-cutinase and one day for C275/292A-cutinase. These curves were not obtained when the incubation time was short. The GdnHCl-induced unfolding curves of LC- and C275/292A-cutinases obtained after two-day and one-day incubations, respectively, were not significantly changed upon further incubation. This result suggests that unfolding of LC- and C275/292A-cutinases is slow and it takes at least two and one days for the unfolding reactions of LC- and C275/292A-cutinases, respectively, to attain the equilibrium. This result also suggests that C275/292A-cutinase unfolds more rapidly than LC-cutinase. Thermodynamic parameters for GdnHCl-induced unfolding of LC- and C275/292A-cutinases are summarized in Table 5-3. The C_m and $\Delta G(H_2O)$ values of C275/292A-cutinase are lower than those of LC-cutinase by 1.02 M and 10.6 kJ mol^{-1}, respectively. We used the average of the *m* values of LC- and C275/292A-cutinases for the calculation of the $\Delta G(H_2O)$ values of these proteins. If we use the *m* values of LC- and C275/292A-cutinases, which were determined to be 9.2 and 11.7 kJ mol^{-1} M^{-1}, respectively, for calculation of the $\Delta G(H_2O)$ values, the $\Delta G(H_2O)$ value of C275/292A-cutinase is lower than that of LC-cutinase only by 2.0 kJ mol^{-1}. Despite this observed difference, the results indicate that the thermodynamic stability of LC-cutinase is

significantly decreased by removal of the disulfide bond.

The C_m values of *F. solani* and *H. insolens* cutinases for GdnHCl-induced unfolding have been reported to be 1.35 and 1.94 M, respectively (Ternström *et al*., 2005). These values are considerably lower than that of LC-cutinase, suggesting that LC-cutinase is more stable than these fungal cutinases. However, the $\Delta G(H_2O)$ values of these proteins (47-49 kJ mol^{-1}) are rather higher than that of LC-cutinase due to their high *m* values.

5.3.5 GdnHCl-induced unfolding kinetics of LC-cutinase and C275/292A-cutinase.

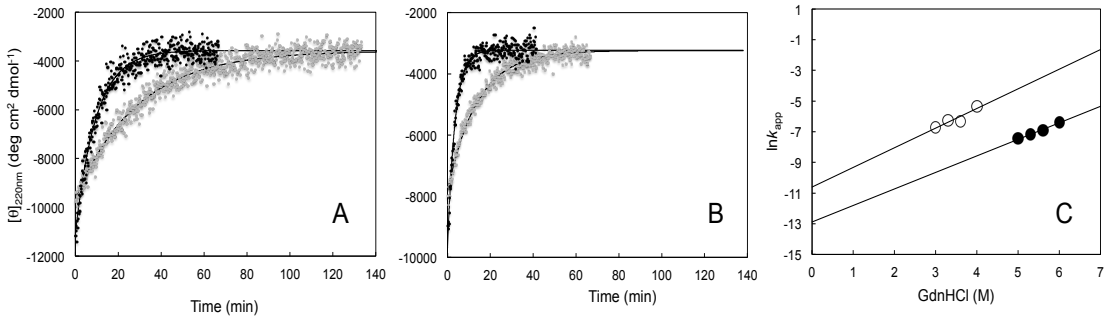

Fig. 5-4 Unfolding kinetics of LC-cutinase and C275/292A-cutinase at 50°C. **(A)** Kinetic traces of GdnHCl-induced unfolding of LC-cutinase to a final concentration of 5.0 M (grey scatter) and 6.0 M (black scatter) GdnHCl are shown. The lines represent the fit of Eq. (3). **(B)** Unfolding kinetics of C275/292A-cutinase at 50°C. Kinetic traces of GdnHCl-induced unfolding of C275/292A-cutinase to a final concentration of 3.0 M (grey scatter) and 4.0 M (black scatter) GdnHCl are shown. The lines represent the fit of Eq. (3). **(C)** GdnHCl concentration dependence of the apparent rate constant (k_{app}) of unfolding kinetics of LC-cutinase (solid circle) and C275/292A-cutinase (open circle). The lines represent the fit of Eq. (4).

The equilibrium studies on GdnHCl-induced unfolding of LC- and C275-292A-cutinases suggest that these proteins unfold very slowly, but C275/292A-cutinase-cutinase unfolds more rapidly than LC-cutinase. To determine the unfolding rates of these proteins, GdnHCl-induced unfolding kinetics of these proteins were analyzed at 50°C by monitoring the CD values at 222nm. These analyses were performed at 50°C, instead of 30°C, because unfolding of LC-cutinase was too slow to be completed within several hours at 30°C. All unfolding reactions gave monophasic kinetics. Typical kinetic traces for unfolding of LC- and C275/292A-cutinases are shown in Fig. 5-4A and Fig. 5-5A, respectively. The dependence of the logarithm of the apparent rate constant of unfolding, k_{app}, on the GdnHCl concentration is shown in Fig. 5-4C. From this dependence, the rate constants of unfolding of LC- and C275/292A-cutinases in the absence of GdnHCl, $k_u(H_2O)$, were calculated to be 3.28×10^{-6} and 1.83×10^{-5} s^{-1}, respectively (Table 5-3). Thus, the unfolding rate of C275/292A-cutinase is one order of magnitude higher than that of LC-cutinase, indicating that the disulfide bond of LC-cutinase contributes not only to the thermodynamic stability but also to the kinetic stability of the protein.

The refolding experiments were also performed at 30°C using LC-cutinase fully unfolded in the presence of 5 M GdnHCl. However, this protein was not refolded by reducing the GdnHCl concentration by dilution, and therefore the kinetic refolding curves of this protein were not obtained. This protein was kept soluble upon dilution, but was kept unfolded even after 5-day incubation at 30°C. In contrast, this protein was fully refolded when the GdnHCl concentration was reduced by dialysis, instead of dilution, suggesting that this protein is refolded only when the GdnHCl concentration is gradually decreased. This protein may be trapped in an unfolded state when the GdnHCl

concentration is rapidly decreased.

The unfolding rates of *F. solani* and *H. insolens* cutinase have been reported to be 2.57 and 0.829 s^{-1}, respectively, at 25°C (Ternström *et al*., 2005). These unfolding rates are at least six orders of magnitude higher than that of LC-cutinase, indicating that LC-cutinase is a kinetically robust protein. However, LC-cutinase is still less stable than hyperthermophilic archaeal proteins, which are characterized by the extremely slow unfolding rate (Okada *et al*., 2010). For example, the unfolding rate of LC-cutinase is two orders of magnitude higher than that of RNase H2 from hyperthermophilic archaeon *Thermococcus kodakarensis* (5.0×10^{-8} s^{-1} at 50°C) (Mukaiyama *et al*., 2004).

5.4 Summary

Thermal denaturation and guanidine hydrochloride (GdnHCl)-induced unfolding of LC-cutinase were analyzed at pH 8.0 by CD spectroscopy. The midpoint of the transition of the thermal denaturation curve, $T_{1/2}$, and that of the GdnHCl-induced unfolding curve, C_m, at 30°C were 86.2°C and 4.02 M, respectively. The free energy change of unfolding in the absence of GdnHCl, $\Delta G(H_2O)$, was 41.8 kJ mol^{-1} at 30°C. LC-cutinase unfolded very slowly in GdnHCl with the unfolding rate, $k_u(H_2O)$, of 3.28 x 10^{-6} s^{-1} at 50°C. These results indicate that LC-cutinase is a kinetically robust protein. LC-cutinase contains one disulfide bond at Cys275-Cys292. To examine whether this disulfide bond contributes to the thermodynamic and kinetic stability of LC-cutinase, C275/292A-cutinase without this disulfide bond was constructed. Thermal denaturation studies and equilibrium and kinetic studies on GdnHCl-induced unfolding of C275/292A-cutinase indicate that this disulfide bond contributes not only to the thermodynamic stability but also to the kinetic stability of LC-cutinase.

CHAPTER 6

General discussion and future remarks

6.1 General discussion

This study focuses on the structure, activity, and stability of LC-cutinase, the first metagemone-derived cutinase. The metagenomic approach has been shown to be effective to isolate novel lipases, esterases, cellulases, and proteases (Steele *et al*., 2009; Tuffin *et al*. 2009; Uchiyama and Miyazaki, 2009). However, none of cutinases has so far been isolated by this approach. Isolation of LC-cutinase with PET-degrading activity and high thermodynamic and kinetic stability from leaf-branch compost by this approach indicates that this approach is useful to isolate a novel cutinase as well. Because of its high PET-degrading activity and stability, LC-cutinase serves not only as a good model to understand the molecular mechanism of PET-degrading enzyme, but also as a potential candidate for industrial applications.

In Chapter 2, I showed that the recombinant LC-cutinase is easily purified from the extracellular medium of the culture of *E. coli* cells as a fusion protein with the pelB leader sequence. LC-cutinase exhibits strong preference to the substrates (*p*-nitrophenyl acy esters) with short acyl chain length as do fungal and bacterial cutinases (Kleeberg *et al*., 2005; Kwon *et al*., 2009; Ribitsch *et al*., 2012; Yang *et al*., 2013). This substrate specificity discriminates cutinase from true lipase. The optimum pH and temperature for activity of LC-cutinase toward the *p*NP-butyrate are pH 8.0 and 50°C. The optimum temperature for activity of LC-cutinase is compared with those of other cutinases in Table 6-1. The optimum temperature of LC-cutinase is identical to that of *T. alba* and *T. terrestris* cutinases. It is higher than that of *F. solani* cutinase by 10°C and lower than that of *T. fusca* cutinase by 10°C. These cutinases

have an ability to degrade PET. LC-cutinase degrades PET with the rate of 12 mg/h/mg of enzyme, whereas *T. fusca* and *F. solani* cutinases degrade it with the rates of 0.05 and 0.25 mg/h/mg of enzyme, respectively, at their optimum conditions. Thus, LC-cutinase degrades PET 240-fold and 48-fold more efficiently than *T. fusca* and *F. solani* cutinases, respectively.

Table 6-1. Optimum condition for cutinase activity toward *p*NP-monoesters

Protein	pH	Temperature (°C)
LC-cutinase	8.0	50
T. alba cutinase	6.0	50
T. fusca cutinase	8.0	60
F. solani cutinase	8.0	40
T. terrestris cutinase	4.0	50

In Chapter 3, I showed that LC-cutinase is more similar to *T. alba* cutinase in size and tertiary structure than to fungal cutinase. Although these cutinases have similar substrate specificities toward soluble substrates, the structural analysis indicates that the shape and size of the substrate binding pocket of bacterial cutinase is different from that of fungal cutinase (Fig. 6-1). The rate of LC-cutinase for cutin degradation (6 μmol/h/mg of enzyme) is comparable to those of *T. fusca* and *F. solani* cutinases (6-7.5 μmol/h/mg of enzyme). However, the content of the C_{16} and C_{18} fatty acid monomers in the products released from cutin after 18 h incubation with *F. solani* cutinase (57.54%) is higher than that with *T. fusca* cutinase (50.14%) (Chen *et al*., 2008).

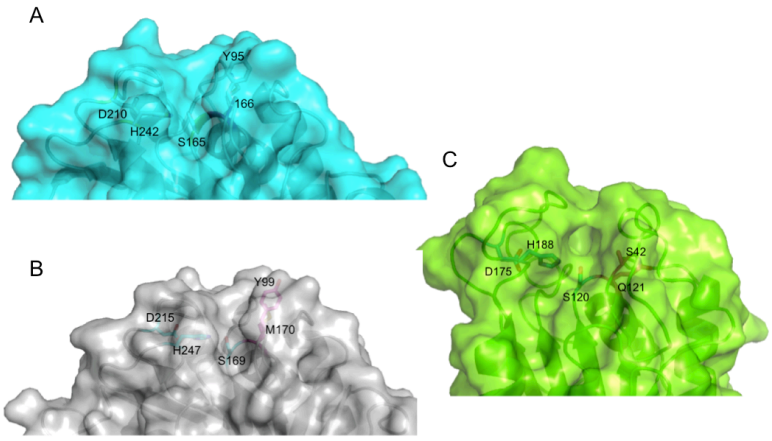

Fig. 6-1 The substrate-binding pockets of LC-, *T. alba* and *F. solani* cutinase. The transparent surfaces of LC-cutinase (A), *T. alba* cutinase (B), and *F. solani* cutinase (C) around the long groove of substrate binding pocket are illustrated by cyan, grey and green surfaces, respectively. The active site residues of these cutinases are shown by green stick models with labels. The side chains of anion hole-forming residues are rendered as magenta sticks.

This result may suggest that the substrate binding pocket of *F. solani* cutinase is deeper and longer than that of bacterial cutinase and is more suitable for accommodation of a long chain and compact substrate, such as cutin.

It has been reported that the enzyme surface located around the first β-strand of *T. cellulosilytica* cutinases is crucial for hydrolysis of PET because this region is essential for binding to the polymer (Herrero Acero *et al*., 2011). The mutation of positively charged Arg29 of *T. cellulosilytica* cutinase to the non-charged asparagine residue greatly increases the PET-degrading activity of this enzyme (Herrero Acero *et al*., 2013). Therefore, the neutral electrostatic potential on the surface of this region is more favorable for PET binding and therefore PET hydrolysis. Arg67 and Arg70 are presented in the corresponding region of *T. alba* cutinase. Likewise, Arg17 and Arg20 are presented in the corresponding region of *F. solani* cutinase. However, one of these positively charged redidues is replaced by the non-charged residue, Thr62, in LC-

cutinase. The electrostatic surface potential of LC-cutinase around this region is compared with those of *T. alba* and *F. solani* cutinases in Figure 6-2. Therefore, the effective PET degrading ability of LC-cutinase is probably due to the presence of a non-charged residue at the position where a positively charged residue of *T. alba* or *F. solani* cutinase is present.

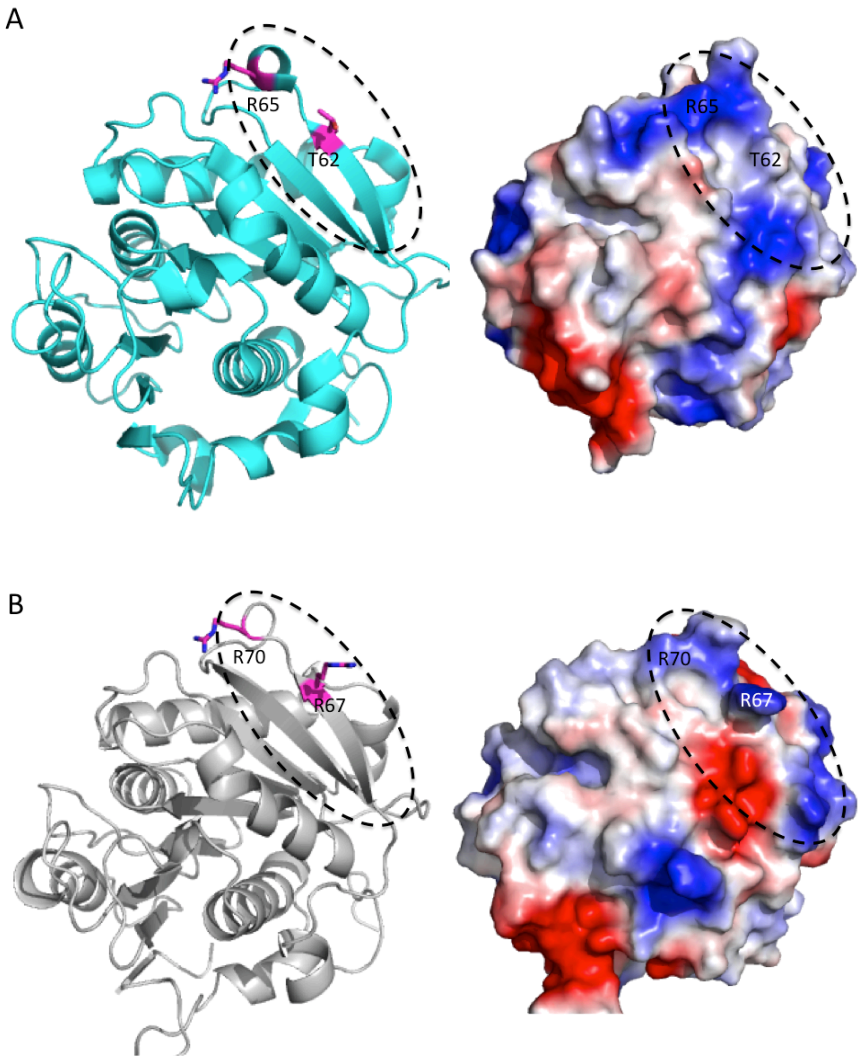

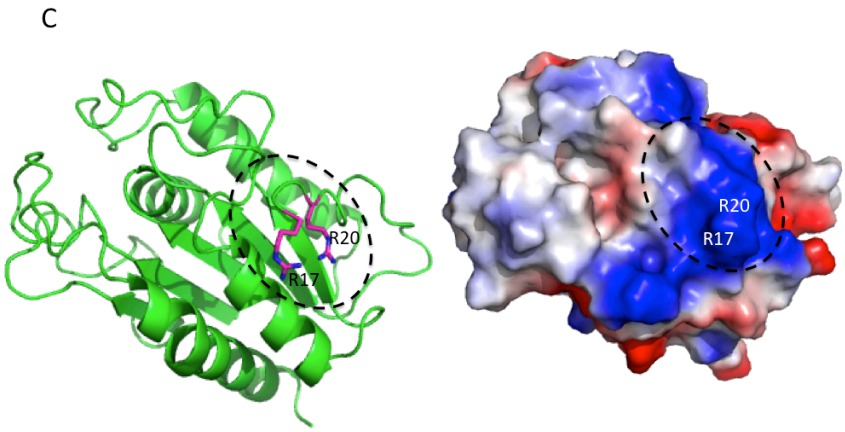

Fig. 6-2 Electrostatic surface potentials of of LC-, *T. alba* and *F. solani* cutinases. The backbone structures and electrostatic surface potentials of LC-cuitnase (A), *T. alba* cutinase (B), and *F. solani* cutinase (C) are shown in the left and right panels, respectively. For electrostatic surface potential, negatively and positively charged surfaces are rendered by red and blue surfaces, respectively. The broken circle and labeled magenta sticks indicate the region and amino acid residues that are involved in PET hydrolysis.

In Chapter 4, I showed that the hydrophobicity of the substrate binding pocket is important not only for the activity but also for the stability. I also showed that the active site of LC-cutinase is locally destabilized and its structure is changed before the overall structure is changed upon thermal denaturation. This heat-induced local conformational change around the active site of LC-cutinase is at least partially prevented by binding of PEG or PET. Like the optimum temperature for activity of LC-cutinase, which is lower than the stability of the overall structure by 36.2°C, the optimum temperature for activity of *T. alba* cutinase, which is identical to that of LC-cutinase (50°C), is lower than the stability of the overall structure, but by only 10°C, suggesting that a heat-induced local conformational change of the active site of *T. alba* cutinase is less significant than that of LC-cutinase.

In Chapter 5, I showed that LC-cuitnase is a thermodynamically and kinetically robust protein. I also showed that the single disulfide bond located at the

C-terminal region of LC-cutinase contributes not only to the thermodynamic stability but also to the kinetic stability. Despite the high similarity in tertiary structure between LC-cutinase and *T. alba* cutinase, LC-cutinase is more stable than *T. alba* cutinase by approximately 26°C. Proteins are stabilized by the combination of various factors, such as increased number of ion pairs (ion pair networks) (Karshikoff and Ladenstein, 2001), reduced cavity volume (Nguyen *et al.,* 2012), anchoring of C-terminal tail (You *et al.,* 2007), increased interior hydrophobicity (Pace *et al.,* 2011), increased number of proline residues in loop regions (Watanabe *et al.,* 1991), and increased number of disulfide bonds (Boutz *et al.,* 2007). Comparison of these factors between LC-cutinase and *T. alba* cutinase indicates that the number of ion pairs and interior hydrophobicity of LC-cutinase are higher than those of *T. alba* cutinase, although the difference is not so significant (Table 5).

Table 5. Structural features of LC-cutinase and *T. alba* cutinase

	LC-cutinase	*T. alba* cutinase
No. of amino acids	259	263
T_m (°C)	86.2[a]	60[b]
Opt. Temp. for activity (°C)	50[c]	50[d]
Content of the residues (%)		
Buried polar	19.4	23.4
Buried apolar	40.7	38.3
Buried apolar/buried total	67.7	62.1
No. of ion pairs (≤4.0 Å)	8	6
No. of disulfide bond	1	1
No. of Pro in loop	10	11

[a] $T_{1/2}$ value.

[b] Data from (Kawai *et al*., 2013)

[c] Data from Chapter 2

[d] Data from (Hu *et al*., 2010)

The number of ion pairs is eight for LC-cutinase and six for *T. alba* cutinase, and only two of them are conserved in these proteins. The ratio of interior apolar residues to total interior residues is 68% for LC-cutinase and 62% for *T. alba* cutinase. In contrast, the number of proline residues in loop regions of LC-cutinase (ten) is lower than that of *T. alba* cutinase (eleven), and seven of them are conserved in these proteins. Likewise, the disulfide bond of LC-cutinase is conserved in *T. alba* cutinase and this disulfide bond anchors the C-termini of these proteins to the central regions equally. Furthermore, no clear cavity exists in the LC-cutinase and *T. alba* cutinase structures. These results suggest that the difference in the number of ion pairs and interior hydrophobicity may at least partly account for the difference in stability between LC-cutinase and *T. alba* cutinase.

6.2 Future remarks

6.2.1 Mechanism of LC-cutinase secretion. As mentioned in Chapter 2, LC-cutinase is partly secreted to the extracellular medium, when it is overproduced in *E. coli* cells as a fusion protein with the pelB leader sequence. The pelB leader sequence directs tranlocation of various synthetic peptides to the periplasmic space of *E. coli* cells (Choi and Lee, 2004). Because LC-cutinase accumulates in the cells mostly in an insoluble form when LC-cutinase without the pelB leader sequence is overproduced in *E. coli* cells, the pelB-LC-cutinase fusion protein is probably secreted through the

type 2 secretion system (T2SS), in which the protein is translocated across the inner membrane by the Sec system at first and then translocated across the outer membrane by the T2SS (Fronzes *et al*., 2009; Pugsley, 1993). Because LC-cutinase purified from the extracellular medium lacks a large part of the pelB leader sequence, the fusion protein is probably secreted to the periplasmic space of *E. coli* cells with the assistance of the pelB-leader sequence. However, the mechanism by which LC-cutinase is translocated across the outer membrane remains to be clarified.

In order to identify the region of LC-cutinase, which is responsible for secretion of LC-cutinase, I have constructed a series of the mutant proteins of LC-cutinase with N-terminal truncations. Secretion of the resultant mutant proteins was analyzed by SDS-PAGE. These proteins were detected by CBB staining and Western blotting analysis. So far, I have found that truncation of the N-terminal 22 residues (residues 36-57) greatly reduces the secretion level of LC-cutinase and that of the N-terminal 32 residues (residues 36-67) reduces it to the background level. I have also found that deletion of the residues 41-46 does not significantly affect the secretion level of LC-cutinase, whereas deletion of the residues 47-57, 57-67, and 47-67 reduces it to the background level. Further studies will be required to understand the mechanism by which truncation of the limited N-terminal region greatly reduces the secretion level of LC-cutinase. Identification of the region responsible for secretion of LC-cutinase may facilitate understanding of the secretion mechanism of LC-cutinase.

6.2.2 Calcium ion binding site of LC-cutinase. Determination of the *T. alba* cutinase structure reveals that this protein contains two Ca^{2+} binding sites (Kawai *et al*., 2013). Binding of these Ca^{2+} ions stabilizes *T. alba* cutinase by approximately 13°C. The dissociation constants of these Ca^{2+} ions are apparently high, because considerably

high concentration of Ca^{2+} ions (200 mM) is required to maximize the stability of *T. alba* cutinase. To examine whether LC-cutinase is stabilized by Ca^{2+} ions, I have analyzed the thermal stability of LC-cutinase in the presence of various concentrations of Ca^{2+} ions. The results suggest that LC-cutinase is stabilized by a single calcium ion and its dissociation constant is 2.50 mM. According to the *T. alba* cutinase structure, one of the calcium ions is apparently coordinated with Asp243, Asp290, and Glu292, while the other is apparently coordinated with Asp236 and the C-terminal carboxyl group. Asp243 and Asp290 are conserved as Asp238 and Asp283, respectively, in LC-cutinase. However, these residues are not located within the distance that allows coordination of Ca^{2+} ion. The distance between these residues is 11.1 Å, whereas that between Asp243 and Asp290 of *T. alba* cutinase is 6.2 Å. In addition, Glu292 is replaced by Arg (Arg286) in LC-cutinase (Fig. 2-1). Likewise, Asp236 is replaced by Pro (Pro231) in LC-cutinase (Fig. 2-1). These results suggest that a single Ca^{2+} ion does not bind to the site, which is corresponding to either one of the Ca^{2+} binding sites of *T. alba* cutinase, but binds to the unique site in LC-cutinase. Further mutational and structural studies will be required to identify this Ca^{2+} binding.

6.2.3 Improvement of enzymatic function by random mutagenesis. As described in Chapter 1, the mutations that enlarge the substrate binding pocket (Araújo *et al*., 2007; Silva *et al*., 2011) and those that decrease polarity and increase hydrophobicity of the substrate binding pocket (Thumarat *et al*., 2012; Herrero Acero *et al*., 2013) are effective to increase PET-degrading activity of cutinase. In fact, the mutations at Tyr95 significantly affect the activity and stability of LC-cutinase. Therefore, it would be informative to examine whether the activity and/or stability of LC-cutinase

increrease by introducing random and site-directd mutagenesis into the substrate binding pocket.

References

Alisch-Mark, M., Herrmann, A., and Zimmermann, W. (2006) Increase of the hydrophilicity of polyethylene terephthalate fibres by hydrolases from *Thermomonospora fusca* and *Fusarium solani* f. sp. *pisi*. *Biotechnol. Lett. 28*, 681-685.

Amada, K., Haruki, M., Imanaka, T., Morikawa, M., and Kanaya, S. (2000) Overproduction in *Escherichia coli*, purification and characterization of a family I.3 lipase from *Pseudomonas sp.* MIS38. *Biochim. Biophys. Acta - Protein Struct. Mol. Enzymol. 1478*, 201-210.

Amann, R. I., Ludwig, W., and Schleifer, K. H. (1995) Phylogenetic identification and in situ detection of individual microbial cells without cultivation. *Microbiol. Rev. 59*, 143-169.

Amass, W., Amass, A., and Tighe, B. (1998) A review of biodegradable polymers: Uses, current developments in the synthesis and characterization of biodegradable polyesters, blends of biodegradable polymers and recent advances in biodegradation studies. *Polym. Int. 47*, 89-144.

Aparna, G., Chatterjee, A., Sonti, R. V, and Sankaranarayanan, R. (2009) A cell wall-degrading esterase of *Xanthomonas oryzae* requires a unique substrate recognition module for pathogenesis on rice. *Plant Cell 21*, 1860-1873.

Araújo, R., Silva, C., O'Neill, A., Micaelo, N., Guebitz, G., Soares, C. M., Casal, M., and Cavaco-Paulo, A. (2007) Tailoring cutinase activity towards polyethylene terephthalate and polyamide 6,6 fibers. *J. Biotechnol. 128*, 849-857.

Arpigny, J. L., and Jaeger, K. E. (1999) Bacterial lipolytic enzymes: classification and properties. *Biochem. J. 343*, 177-183.

Belbahri, L., Calmin, G., Mauch, F., and Andersson, J. O. (2008) Evolution of the cutinase gene family: Evidence for lateral gene transfer of a candidate Phytophthora virulence factor. *Gene 408*, 1-8.

Boone, C. D., Habibzadegan, A., Tu, C., Silverman, D. N., and McKenna, R. (2013) Structural and catalytic characterization of a thermally stable and acid-stable variant of human carbonic anhydrase II containing an engineered disulfide bond. *Acta Crystallogr. D. Biol. Crystallogr. 69*, 1414-22.

Boutz, D. R., Cascio, D., Whitelegge, J., Perry, L. J., and Yeates, T. O. (2007) Discovery of a thermophilic protein complex stabilized by topologically interlinked chains. *J. Mol. Biol. 368*, 1332-1344.

Brissos, V., Eggert, T., Cabral, J. M. S., and Jaeger, K.-E. (2008) Improving activity and stability of cutinase towards the anionic detergent AOT by complete saturation mutagenesis. *Protein Eng. Des. Sel. 21*, 387-393.

Brzozowski, A. M., Derewenda, U., Derewenda, Z. S., Dodson, G. G., Lawson, D. M., Turkenburg, J. P., Bjorkling, F., Huge-Jensen, B., Patkar, S. A., and Thim, L. (1991) A model for interfacial activation in lipases from the structure of a fungal lipase-inhibitor complex. *Nature 351*, 491-494.

Cambillau, C., Longhi, S., Nicolas, A., and Martinez, C. (1996) Acyl glycerol hydrolases: Inhibitors, interface and catalysis. *Curr. Opin. Struct. Biol. 6,* 449-455.

Castro-Ochoa, D., Peña-Montes, C., González-Canto, A., Alva-Gasca, A., Esquivel-Bautista, R., Navarro-Ocaña, A., and Farrés, A. (2012) ANCUT2, an Extracellular cutinase from *Aspergillus nidulans* induced by olive oil. *Appl. Biochem. Biotechnol. 166,* 1275-1290.

Chen, S., Su, L., Billig, S., Zimmermann, W., Chen, J., and Wu, J. (2010) Biochemical characterization of the cutinases from *Thermobifida fusca*. *J. Mol. Catal. B Enzym. 63*, 121-127.

Chen, S., Su, L., Chen, J., and Wu, J. (2013) Cutinase: Characteristics, preparation, and application. *Biotechnol. Adv. 31,* 1754-1767.

Chen, S., Tong, X., Woodard, R. W., Du, G., Wu, J., and Chen, J. (2008) Identification and Characterization of Bacterial Cutinase. *J. Biol. Chem. 283*, 25854-25862.

Chen, Z., Franco, C. F., Baptista, R. P., Cabral, J. M. S., Coelho, A. V, Rodrigues, C. J., and Melo, E. P. (2007) Purification and identification of cutinases from *Colletotrichum kahawae* and *Colletotrichum gloeosporioides*. *Appl. Microbiol. Biotechnol. 73*, 1306-1313.

Chirakkal, H., Ford, G. C., and Moir, A. (2001) Analysis of a conserved hydrophobic pocket important for the thermostability of *Bacillus pumilus* chloramphenicol acetyltransferase (CAT-86). *Protein Eng. 14*, 161-166.

Choi, J. H., and Lee, S. Y. (2004) Secretory and extracellular production of recombinant proteins using *Escherichia coli*. *Appl. Microbiol. Biotechnol. 64*, 625-635.

Collaborative Computational Project, N. (1994) The CCP4 suite: programs for protein crystallography. *Acta Crystallogr. Sect. D Biol. Crystallogr. 50*, 760-763.

Davies, K. a., De Lorono, I., Foster, S. J., Li, D., Johnstone, K., and Ashby, a. M. (2000) Evidence for a role of cutinase in pathogenicity of *Pyrenopeziza brassicae* on brassicas. *Physiol. Mol. Plant Pathol. Physiol. Mol. Plant Pathol. 57*, 63-75.

Degani, O., Salman, H., Gepstein, S., and Dosoretz, C. G. (2006) Synthesis and characterization of a new cutinase substrate, 4-nitrophenyl (16-methyl sulfone ester) hexadecanoate. *J. Biotechnol. 121*, 346-350.

Deng, J., Carbone, I., and Dean, R. A. (2007) The evolutionary history of cytochrome P450 genes in four filamentous Ascomycetes. *BMC Evol. Biol. 7*, 30.

Derewenda, Z. S., Derewenda, U., and Dodson, G. G. (1992) The crystal and molecular structure of the *Rhizomucor miehei* triacylglyceride lipase at 1.9 Å resolution. *J. Mol. Biol. 227*, 818-839.

Donelli, I., Taddei, P., Smet, P. F., Poelman, D., Nierstrasz, V. A., and Freddi, G. (2009) Enzymatic surface modification and functionalization of PET: a water contact angle, FTIR, and fluorescence spectroscopy study. *Biotechnol. Bioeng. 103*, 845-856.

Dresler, K., van den Heuvel, J., Müller, R.-J., and Deckwer, W.-D. (2006) Production of a recombinant polyester-cleaving hydrolase from *Thermobifida fusca* in *Escherichia coli*. *Bioprocess Biosyst. Eng. 29*, 169-183.

Dutta, K., Sen, S., and Veeranki, V. D. (2009) Production, characterization and applications of microbial cutinases. *Process Biochem., 44,* 127-134.

Eberl, A., Heumann, S., Brückner, T., Araujo, R., Cavaco-Paulo, A., Kaufmann, F., Kroutil, W., and Guebitz, G. M. (2009) Enzymatic surface hydrolysis of poly(ethylene terephthalate) and bis(benzoyloxyethyl) terephthalate by lipase and cutinase in the presence of surface active molecules. *J. Biotechnol. 143*, 207-212.

Eberl, A., Heumann, S., Kotek, R., Kaufmann, F., Mitsche, S., Cavaco-Paulo, A., and Gübitz, G. M. (2008) Enzymatic hydrolysis of PTT polymers and oligomers. *J. Biotechnol. 135*, 45-51.

Egmond, M. R., and Bemmel van, C. J. (1997) Impact of structural information on understanding lipolytic function. *Methods Enzymol. 284*, 119-129.

Emsley, P., and Cowtan, K. (2004) Coot: model-building tools for molecular graphics. *Acta Crystallogr. Sect. D Biol. Crystallogr. 60*, 2126-2132.

Fan, C., and Köller, W. (1998) Diversity of cutinases from plant pathogenic fungi: differential and sequential expression of cutinolytic esterases by *Alternaria brassicicola*. *FEMS Microbiol. Lett. 158*, 33-38.

Fernandes, A. T., Pereira, M. M., Silva, C. S., Lindley, P. F., Bento, I., Melo, E. P., and Martins, L. O. (2011) The removal of a disulfide bridge in CotA-laccase changes the slower motion dynamics involved in copper binding but has no effect on the thermodynamic stability. *J. Biol. Inorg. Chem. 16*, 641-651.

Fett, W. F., Gerard, H. C., Moreau, R. A., Osman, S. F., and Jones, L. E. (1992) Screening of nonfilamentous bacteria for production of cutin-degrading enzymes. *Appl. Environ. Microbiol. 58*, 2123-2130.

Fett, W. F., Gérard, H. C., Moreau, R. A., Osman, S. F., and Jones, L. E. (1992) Cutinase production by *Streptomyces spp. Curr. Microbiol. 25,* 165-171.

Fett, W. F., Wijey, C., Moreau, R. A., and Osman, S. F. (2000) Production of cutinolytic esterase by filamentous bacteria. *Lett. Appl. Microbiol. 31*, 25-29.

Fronzes, R., Christie, P. J., and Waksman, G (2009) The structural biology of type IV secretion systems. *Nature Rev. Microbiol.* 7, 703-714.

Goodwin, T. W., and Morton, R. A. (1946) The spectrophotometric determination of tyrosine and tryptophan in proteins. *Biochem. J. 40*, 628-632.

Guebitz, G. M., and Cavaco-Paulo, A. (2008) Enzymes go big: surface hydrolysis and functionalisation of synthetic polymers. *Trends Biotechnol. 26,* 32-38.

Handelsman, J., Rondon, M. R., Brady, S. F., Clardy, J., and Goodman, R. M. (1998) Molecular biological access to the chemistry of unknown soil microbes: a new frontier for natural products. *Chem. Biol. 5*, R245-R249.

Herrero Acero, E., Ribitsch, D., Dellacher, A., Zitzenbacher, S., Marold, A., Steinkellner, G., Gruber, K., Schwab, H., and Guebitz, G. M. (2013) Surface engineering of a cutinase from *Thermobifida cellulosilytica* for improved polyester hydrolysis. *Biotechnol. Bioeng. 110*, 2581-2590.

Herrero Acero, E., Ribitsch, D., Steinkellner, G., Gruber, K., Greimel, K., Eiteljoerg, I., Trotscha, E., Wei, R., Zimmermann, W., Zinn, M., Cavaco-Paulo, A., Freddi, G., Schwab, H., and Guebitz, G. (2011) Enzymatic Surface Hydrolysis of PET: Effect of

Structural Diversity on Kinetic Properties of Cutinases from *Thermobifida*. *Macromolecules 44*, 4632-4640.

Hijden, V., Marugg, HTJD, Warr, J.F., Klugkist, J., Musters, W., Hondmann, D. Enzyme-containing surfactants compositions. Unilever Patent. WO 9403578.

Hiraishi, N., Yau, J. Y. Y., Loushine, R. J., Armstrong, S. R., Weller, R. N., King, N. M., Pashley, D. H., and Tay, F. R. (2007) Susceptibility of a polycaprolactone-based root canal-filling material to degradation. III. turbidimetric evaluation of enzymatic hydrolysis. *J. Endod. 33*, 952-956.

Hu, X., Thumarat, U., Zhang, X., Tang, M., and Kawai, F. (2010) Diversity of polyester-degrading bacteria in compost and molecular analysis of a thermoactive esterase from *Thermobifida alba* AHK119. *Appl. Microbiol. Biotechnol. 87*, 771-779.

Jaeger, K. E., Ransac, S., Dijkstra, B. W., Colson, C., van Heuvel, M., and Misset, O. (1994) Bacterial lipases. *FEMS Microbiol. Rev. 15*, 29-63.

Kanaya, S., Katsuda-Nakai, C., and Ikehara, M. (1991) Importance of the positive charge cluster in *Escherichia coli* ribonuclease HI for the effective binding of the substrate. *J. Biol. Chem. 266*, 11621-11627.

Karshikoff, A., and Ladenstein, R. (2001) Ion pairs and the thermotolerance of proteins from hyperthermophiles: a “traffic rule” for hot roads. *Trends Biochem. Sci. 26*, 550-556.

Kawai, F., Thumarat, U., Kitadokoro, K., Waku, T., Tada, T., Tanaka, N., and Kawabata, T. (2013) Comparison of Polyester-Degrading Cutinases from Genus *Thermobifida*. *ACS Symp. Ser. 1144*, 111-120.

Kitadokoro, K., Thumarat, U., Nakamura, R., Nishimura, K., Karatani, H., Suzuki, H., and Kawai, F. (2012) Crystal structure of cutinase Est119 from *Thermobifida alba* AHK119 that can degrade modified polyethylene terephthalate at 1.76Å resolution. *Polym. Degrad. Stab. 97*, 771-775.

Kleeberg, I., Hetz, C., Kroppenstedt, R. M., Müller, R. J., and Deckwer, W. D. (1998) Biodegradation of aliphatic-aromatic copolyesters by *Thermomonospora fusca* and other thermophilic compost isolates. *Appl. Environ. Microbiol. 64*, 1731-1735.

Kleeberg, I., Welzel, K., Vandenheuvel, J., Müller, R.-J., and Deckwer, W.-D. (2005) Characterization of a new extracellular hydrolase from *Thermobifida fusca* degrading aliphatic-aromatic copolyesters. *Biomacromolecules 6*, 262-270.

Kodama, Y., Masaki, K., Kondo, H., Suzuki, M., Tsuda, S., Nagura, T., Shimba, N., Suzuki, E., and Iefuji, H. (2009) Crystal structure and enhanced activity of a cutinase-like enzyme from *Cryptococcus sp.* strain S-2. *Proteins 77*, 710-717.

Kolattukudy, P. (2005) Cutin from plants. *Biopolym. Online* 1-12.

Kolattukudy, P. E. (1980) Biopolyester membranes of plants: cutin and suberin. *Science 208*, 990-1000.

Kolattukudy, P. E. (1981) Structure, Biosynthesis, and Biodegradation of Cutin and Suberin. *Annu. Rev. Plant Physiol. 32*, 539-567.

Kolattukudy, P. E. (2001) Polyesters in higher plants. *Adv. Biochem. Eng. Biotechnol. 71*, 1-49.

Köller, W., Parker, D. M. (1989) Purification and Characterization of Cutinase from *Venturia inaequalis*. *Physiol. Biochem.* 278-283.

Kontkanen, H., Westerholm-Parvinen, A., Saloheimo, M., Bailey, M., Rättö, M., Mattila, I., Mohsina, M., Kalkkinen, N., Nakari-Setälä, T., and Buchert, J. (2009) Novel *Coprinopsis cinerea* polyesterase that hydrolyzes cutin and suberin. *Appl. Environ. Microbiol. 75*, 2148-2157.

Korpecka, J., Heumann, S., Billig, S., Zimmermann, W., Zinn, M., Ihssen, J., Cavaco-Paulo, A., and Guebitz, G. M. (2010) Hydrolysis of Cutin by PET-Hydrolases. *Macromol. Symp. 296*, 342-346.

Kwon, M.-A., Kim, H. S., Yang, T. H., Song, B. K., and Song, J. K. (2009) High-level expression and characterization of Fusarium solani cutinase in *Pichia pastoris*. *Protein Expr. Purif. 68*, 104-109.

Kyte, J., and Doolittle, R. F. (1982) A simple method for displaying the hydropathic character of a protein. *J. Mol. Biol. 157*, 105-132.

Laemmli, U. K. (1970) Cleavage of structural proteins during the assembly of the head of bacteriophage T4. *Nature 227*, 680-685.

Langer, G., Cohen, S. X., Lamzin, V. S., and Perrakis, A. (2008) Automated macromolecular model building for X-ray crystallography using ARP/wARP version 7. *Nat. Protoc. 3*, 1171-1179.

Letunic, I., Doerks, T., and Bork, P. (2009) SMART 6: recent updates and new developments. *Nucleic Acids Res. 37*, D229-D232.

Liebminger, S., Eberl, A., Sousa, F., Heumann, S., Fischer-Colbrie, G., Cavaco-Paulo, A., and Guebitz, G. M. (2007) Hydrolysis of PET and bis-(benzoyloxyethyl) terephthalate with a new polyesterase from *Penicillium citrinum*. *Biocatal. Biotransformation 25*, 171-177.

Lin, T. S., and Kolattukudy, P. E. (1980) Isolation and characterization of a cuticular polyester (cutin) hydrolyzing enzyme from phytopathogenic fungi. *Physiol. Plant Pathol. 17*, 1-15.

Liu, Z., Gosser, Y., Baker, P. J., Ravee, Y., Lu, Z., Alemu, G., Li, H., Butterfoss, G. L., Kong, X.-P., Gross, R., and Montclare, J. K. (2009) Structural and functional studies of *Aspergillus oryzae* cutinase: enhanced thermostability and hydrolytic activity of synthetic ester and polyester degradation. *J. Am. Chem. Soc. 131*, 15711-15716.

Longhi, S., and Cambillau, C. (1999) Structure-activity of cutinase, a small lipolytic enzyme. *Biochim. Biophys. Acta 1441*, 185-196.

Longhi, S., Czjzek, M., Lamzin, V., Nicolas, A., Cambillau, C., and Aiguier, J. (1997) Atomic resolution (1.0 Å) crystal structure of *Fusarium solani* cutinase: stereochemical analysis. *J. Mol. Biol. 268*, 779-799.

Longhi, S., Nicolas, a, Creveld, L., Egmond, M., Verrips, C. T., de Vlieg, J., Martinez, C., and Cambillau, C. (1996) Dynamics of *Fusarium solani* cutinase investigated through structural comparison among different crystal forms of its variants. *Proteins 26*, 442-458.

Macedo, G. A., and Pio, T. F. (2005) a rapid screening method for cutinase producing microorganism. *Brazilian J. Microbiol. 36*, 388-394.

Maiti, I. B., Kolattukudy, P. E., and M., S. (1979) purification and characterization of a novel cutinase from nasturtium. *Arch. Biochem. Biophys. 196*, 412-423.

Martinez, C., De Geus, P., Lauwereys, M., Matthyssens, G., and Cambillau, C. (1992) *Fusarium solani* cutinase is a lipolytic enzyme with a catalytic serine accessible to solvent. *Nature 356*, 615-618.

Martinez, C., Nicolas, a, van Tilbeurgh, H., Egloff, M. P., Cudrey, C., Verger, R., and Cambillau, C. (1994) Cutinase, a lipolytic enzyme with a preformed oxyanion hole. *Biochemistry 33*, 83-89.

Masaki, K., Kamini, N. R., Ikeda, H., and Iefuji, H. (2005) Cutinase-like enzyme from the yeast *Cryptococcus sp.* strain S-2 hydrolyzes polylactic acid and other biodegradable plastics. *Appl. Environ. Microbiol. 71*, 7548-7550.

Mason, J. M., Bendall, D. S., Howe, C. J., and Worrall, J. A. (2012) The role of a disulfide bridge in the stability and folding kinetics of *Arabidopsis thaliana* cytochrome c(6A). *Biochim Biophys Acta. 1824*, 311-318.

Matsumura, M., Becktel, W. J., Levitt, M., and Matthews, B. W. (1989) Stabilization of phage T4 lysozyme by engineered disulfide bonds. *Proc. Natl. Acad. Sci. U. S. A. 86*, 6562-6566.

Mukaiyama, A., Takano, K., Haruki, M., Morikawa, M., and Kanaya, S. (2004) Kinetically robust monomeric protein from a hyperthermophile. *Biochemistry 43*, 13859-13866.

Müller, R. J., Schrader, H., Profe, J., Dresler, K., and Deckwer, W. D. (2005) Enzymatic Degradation of Poly(ethylene terephthalate): Rapid Hydrolyse using a Hydrolase from *Thermobifia fusca*. *Macromol. Rapid Commun. 26*, 1400-1405.

Murphy, C. A., Cameron, J. A., Huang, S. J., and Vinopal, R. T. (1996) Fusarium polycaprolactone depolymerase is cutinase. *Appl. Environ. Microbiol. 62*, 456-460.

Murshudov, G. N., Vagin, A. A., and Dodson, E. J. (1997) Refinement of macromolecular structures by the maximum-likelihood method. *Acta Crystallogr. Sect. D Biol. Crystallogr. 53*, 240-255.

Nguyen, T.-N., Angkawidjaja, C., Kanaya, E., Koga, Y., Takano, K., and Kanaya, S. (2012) Activity, stability, and structure of metagenome-derived LC11-RNase H1, a homolog of *Sulfolobus tokodaii* RNase H1. *Protein Sci. 21*, 553-561.

Nicolas, a, Egmond, M., Verrips, C. T., de Vlieg, J., Longhi, S., Cambillau, C., and Martinez, C. (1996) Contribution of cutinase serine 42 side chain to the stabilization of the oxyanion transition state. *Biochemistry 35*, 398-410.

Nimchua, T., Eveleigh, D. E., Sangwatanaroj, U., and Punnapayak, H. (2008) Screening of tropical fungi producing polyethylene terephthalate-hydrolyzing enzyme for fabric modification. *J. Ind. Microbiol. Biotechnol. 35*, 843-850.

Nimchua, T., Punnapayak, H., and Zimmermann, W. (2007) Comparison of the hydrolysis of polyethylene terephthalate fibers by a hydrolase from *Fusarium oxysporum* LCH I and *Fusarium solani* f. sp. *pisi*. *Biotechnol. J. 2*, 361-364.

Nyon, M. P., Rice, D. W., Berrisford, J. M., Hounslow, A. M., Moir, A. J. G., Huang, H., Nathan, S., Mahadi, N. M., Bakar, F. D. A., and Craven, C. J. (2009) Catalysis by *Glomerella cingulata* cutinase requires conformational cycling between the active and inactive states of its catalytic triad. *J. Mol. Biol. 385*, 226-235.

Nyyssölä, A., Pihlajaniemi, V., Järvinen, R., Mikander, S., Kontkanen, H., Kruus, K., Kallio, H., and Buchert, J. (2013) Screening of microbes for novel acidic cutinases and cloning and expression of an acidic cutinase from *Aspergillus niger* CBS 513.88. *Enzyme Microb. Technol. 52*, 272-278.

Ohnishi, K., Toida, J., Nakazawa, H., and Sekiguchi, J. (1995) Genome structure and nucleotide sequence of a lipolytic enzyme gene of *Aspergillus oryzae*. *FEMS Microbiol. Lett. 126*, 145-150.

Okada, J., Okamoto, T., Mukaiyama, A., Tadokoro, T., You, D.-J., Chon, H., Koga, Y., Takano, K., and Kanaya, S. (2010) Evolution and thermodynamics of the slow unfolding of hyperstable monomeric proteins. *BMC Evol. Biol. 10*, 207.

Ollis, D. L., Cheah, E., Cygler, M., Dijkstra, B., Frolow, F., Franken, S. M., Harel, M., Remington, S. J., Silman, I., and Schrag, J. (1992) The α/β hydrolase fold. *Protein Eng. 5*, 197-211.

Otwinowski, Z., and Minor, W. (1997) Processing of X-ray diffraction data collected in oscillation mode. *Methods Enzymol. 276*, 307-326.

Pace, C. N. (1990) Measuring and increasing protein stability. *Trends Biotechnol. 8*, 93-98.

Pace, C. N., Fu, H., Fryar, K. L., Landua, J., Trevino, S. R., Shirley, B. A., Hendricks, M. M., Iimura, S., Gajiwala, K., Scholtz, J. M., and Grimsley, G. R. (2011)

Contribution of hydrophobic interactions to protein stability. *J. Mol. Biol. 408*, 514-528.

Pace, C. N., Grimsley, G. R., Thomson, J. A., and Barnett, B. J. (1988) Conformational stability and activity of ribonuclease T1 with zero, one, and two intact disulfide bonds. *J. Biol. Chem. 263*, 11820-11825.

Piatek, R., Bruździak, P., Wojciechowski, M., Zalewska-Piatek, B., and Kur, J. (2010) The noncanonical disulfide bond as the important stabilizing element of the immunoglobulin fold of the Dr fimbrial DraE subunit. *Biochemistry 49*, 1460-1468.

Pugsley, A. P. (1993) The complete general secretory pathway in gram-negative bacteria. *Microbiol. Rev. 57*, 50-108.

Purdy, R. E., and Kolattukudy, P. E. (1975) Hydrolysis of plant cuticle by plant pathogens. Properties of cutinase I, cutinase II, and a nonspecific esterase isolated from *Fusarium solani pisi*. *Biochemistry 14*, 2832-2840.

Ribitsch, D., Acero, E. H., Greimel, K., Eiteljoerg, I., Trotscha, E., Freddi, G., Schwab, H., and Guebitz, G. M. (2012) Characterization of a new cutinase from *Thermobifida alba* for PET-surface hydrolysis. *Biocatal. Biotransformation 30*, 2-9.

Ribitsch, D., Heumann, S., Trotscha, E., Herrero Acero, E., Greimel, K., Leber, R., Birner-Gruenberger, R., Deller, S., Eiteljoerg, I., Remler, P., Weber, T., Siegert, P., Maurer, K.-H., Donelli, I., Freddi, G., Schwab, H., and Guebitz, G. M. (2011)

Hydrolysis of polyethyleneterephthalate by *p*-nitrobenzylesterase from *Bacillus subtilis*. *Biotechnol. Prog. 27*, 951-960.

Rogalska, E., Cudrey, C., Ferrato, F., and Verger, R. (1993) Stereoselective hydrolysis of triglycerides by animal and microbial lipases. *Chirality 5*, 24-30.

Ronkvist, Å. M., Xie, W., Lu, W., and Gross, R. a. (2009) Cutinase-Catalyzed Hydrolysis of Poly(ethylene terephthalate). *Macromolecules 42*, 5128-5138.

Schmeisser, C., Steele, H., and Streit, W. R. (2007) Metagenomics, biotechnology with non-culturable microbes. *Appl. Microbiol. Biotechnol. 75*, 955-962.

Schmidt, B., Ho, L., and Hogg, P. J. (2006) Allosteric disulfide bonds. *Biochemistry 45*, 7429-7433.

Schulenburg, C., Weininger, U., Neumann, P., Meiselbach, H., Stubbs, M. T., Sticht, H., Balbach, J., Ulbrich-Hofmann, R., and Arnold, U. (2010) Impact of the C-terminal disulfide bond on the folding and stability of onconase. *Chembiochem 11*, 978-986.

Schultz, J., Milpetz, F., Bork, P., and Ponting, C. P. (1998) SMART, a simple modular architecture research tool: identification of signaling domains. *Proc. Natl. Acad. Sci. U. S. A. 95*, 5857-5864.

Sebastian, J., and Kolattukudy, P. E. (1988) Purification and characterization of cutinase from a fluorescent Pseudomonas putida bacterial strain isolated from phyllosphere. *Arch. Biochem. Biophys. 263*, 77-85.

Sebastian, J., Chandra, A. K., and Kolattukudy, P. E. (1987) Discovery of a cutinase-producing *Pseudomonas sp.* cohabiting with an apparently nitrogen-fixing *Corynebacterium sp.* in the phyllosphere. *J. Bacteriol. 169*, 131-136.

Shishiyama, J., Araki, F., Akai, S. (1970) Studies on cutin-esterase II. Characteristics of cutin-esterase from *Botrytis cinerea* and its activity on tomato-cutin. *Plant cell Physiol. 11*, 937-945.

Silva, C., Da, S., Silva, N., Matamá, T., Araújo, R., Martins, M., Chen, S., Chen, J., Wu, J., Casal, M., and Cavaco-Paulo, A. (2011) Engineered *Thermobifida fusca* cutinase with increased activity on polyester substrates. *Biotechnol. J. 6*, 1230-1239.

Skamnioti, P., Furlong, R. F., and Gurr, S. J. (2008a) Evolutionary history of the ancient cutinase family in five filamentous Ascomycetes reveals differential gene duplications and losses and in *Magnaporthe grisea* shows evidence of sub- and neo-functionalization. *New Phytol. 180*, 711-721.

Skamnioti, P., Furlong, R. F., and Gurr, S. J. (2008b) The fate of gene duplicates in the genomes of fungal pathogens. *Commun. Integr. Biol. 1*, 196-198.

Soliday, C. L., and Kolattukudy, P. E. (1976) Isolation and characterization of a cutinase from *Fusarium roseum* culmorum and its immunological comparison with cutinases from *F. solani pisi*. *Arch. Biochem. Biophys. 176*, 334-343.

Soliday, C., and Flurkey, W. (1984) Cloning and structure determination of cDNA for cutinase, an enzyme involved in fungal penetration of plants. *Proc. Natl. Acad. Sci. U. S. A. 81*, 3939-3943.

St Leger, R. J., Joshi, L., and Roberts, D. W. (1997) Adaptation of proteases and carbohydrates of saprophytic, phytopathogenic and entomopathogenic fungi to the requirements of their ecological niches. *Microbiology 143*, 1983-1992.

Steele, H. L., Jaeger, K.-E., Daniel, R., and Streit, W. R. (2009) Advances in recovery of novel biocatalysts from metagenomes. *J. Mol. Microbiol. Biotechnol. 16*, 25-37.

Suzuki, K., Sakamoto, H., and Shinozaki, Y. (2012) Affinity purification and characterization of a biodegradable plastic-degrading enzyme from a yeast isolated from the larval midgut of a stag beetle , *Aegus laevicollis*. *Appl. Micrbiol. Biotechnol. 97,* 7679-7688.

Sweigard, J. A., Chumley, F. G., and Valent, B. (1992) Cloning and analysis of CUT1, a cutinase gene from *Magnaporthe grisea*. *Mol. Gen. Genet. 232*, 174-182.

Ternström, T., Svendsen, A., Akke, M., and Adlercreutz, P. (2005) Unfolding and inactivation of cutinases by AOT and guanidine hydrochloride. *Biochim. Biophys. Acta 1748*, 74-83.

Trail, F., and Köller, W. (1993) Diversity of cutinases from plant pathogenic fungi-Purification and characterization of two cutinases from *Alternaria brassicicola*. *Physiol. Mol. Plant Pathol. 42*, 205-220.

Trail, F., Köller, W. (1990) Diversity of cutinases from plant pathogenic fungi: Evidence for a relationship between enzyme properties and tissue specificity. *Physiol. Mol. Plant Pathol. 36*, 495-508.

Tuffin, M., Anderson, D., Heath, C., and Cowan, D. A. (2009) Metagenomic gene discovery: how far have we moved into novel sequence space? *Biotechnol. J. 4*, 1671-1683.

Uchiyama, T., and Miyazaki, K. (2009) Functional metagenomics for enzyme discovery: challenges to efficient screening. *Curr. Opin. Biotechnol. 20,* 616-622.

Vagin, A., and Teplyakov, A. (1997) MOLREP : an Automated Program for Molecular Replacement. *J. Appl. Crystallogr. 30*, 1022-1025.

Van Tilbeurgh, H., Gargouri, Y., Dezan, C., Egloff, M. P., Nésa, M. P., Ruganie, N., Sarda, L., Verger, R., and Cambillau, C. (1993) Crystallization of pancreatic procolipase and of its complex with pancreatic lipase. *J. Mol. Biol. 229*, 552-554.

Vertommen, M. A. M. E., Nierstrasz, V. A., Veer, M. Van Der, and Warmoeskerken, M. M. C. G. (2005) Enzymatic surface modification of poly(ethylene terephthalate). *J. Biotechnol. 120*, 376-386.

Vinther, T. N., Norrman, M., Ribel, U., Huus, K., Schlein, M., Steensgaard, D. B., Pedersen, T. Å., Pettersson, I., Ludvigsen, S., Kjeldsen, T., Jensen, K. J., and Hubálek, F. (2013) Insulin analog with additional disulfide bond has increased stability and preserved activity. *Protein Sci. 22*, 296-305.

Walton, T. J., and Kolattukudy, P. E. (1972) Determination of the structures of cutin monomers by a novel depolymerization procedure and combined gas chromatography and mass spectrometry. *Biochemistry 11*, 1885-1897.

Wang, G. Y., Michailides, T. J., Hammock, B. D., Lee, Y. M., and Bostock, R. M. (2000) Affinity purification and characterization of a cutinase from the fungal plant pathogen *Monilinia fructicola* (Wint.) honey. *Arch. Biochem. Biophys. 382*, 31-38.

Watanabe, K., Chishiro, K., Kitamura, K., and Suzuki, Y. (1991) Proline residues responsible for thermostability occur with high frequency in the loop regions of an extremely thermostable oligo-1,6-glucosidase from *Bacillus thermoglucosidasius* KP1006. *J. Biol. Chem. 266*, 24287-24294.

Wei, Y., Swenson, L., Castro, C., Derewenda, U., Minor, W., Arai, H., Aoki, J., Inoue, K., Servin-Gonzalez, L., and Derewenda, Z. S. (1998) Structure of a microbial

homologue of mammalian platelet-activating factor acetylhydrolases: *Streptomyces exfoliatus* lipase at 1.9 Å resolution. *Structure 6*, 511-519.

West, N. P., Chow, F. M. E., Randall, E. J., Wu, J., Chen, J., Ribeiro, J. M. C., and Britton, W. J. (2009) Cutinase-like proteins of *Mycobacterium tuberculosis*: characterization of their variable enzymatic functions and active site identification. *FASEB J. 23*, 1694-1704.

Woloshuk, C. P., and Kolattukudy, P. E. (1986) Mechanism by which contact with plant cuticle triggers cutinase gene expression in the spores of *Fusarium solani* f. sp. *pisi*. *Proc. Natl. Acad. Sci. U. S. A. 83*, 1704-1708.

Woodruff, M. A., and Hutmacher, D. W. (2010) The return of a forgotten polymer-Polycaprolactone in the 21st century. *Prog. Polym. Sci. 35*, 1217-1256.

Wozniak-Knopp, G., and Rüker, F. (2012) A C-terminal interdomain disulfide bond significantly stabilizes the Fc fragment of IgG. *Arch. Biochem. Biophys. 526,* 181-187.

Yang, S., Xu, H., Yan, Q., Liu, Y., Zhou, P., and Jiang, Z. (2013) A low molecular mass cutinase of *Thielavia terrestris* efficiently hydrolyzes poly(esters). *J. Ind. Microbiol. Biotechnol. 40*, 217-226.

Yoon, M. Y., Kellis, J., and Poulouse, A. J. (2002) Enzymatic modification of polyester. *AATCC Rev 2*, 33-36.

You, D.-J., Chon, H., Koga, Y., Takano, K., and Kanaya, S. (2007) Crystal structure of type 1 ribonuclease H from hyperthermophilic archaeon *Sulfolobus tokodaii*: role of arginine 118 and C-terminal anchoring. *Biochemistry 46*, 11494-11503.

Zakariassen, H., Aam, B. B., Horn, S. J., Vårum, K. M., Sørlie, M., and Eijsink, V. G. H. (2009) Aromatic residues in the catalytic center of chitinase A from *Serratia marcescens* affect processivity, enzyme activity, and biomass converting efficiency. *J. Biol. Chem. 284*, 10610-10617.

Zielenkiewicz, W., Swierzewski, R., Attanasio, F., and Rialdi, G. (2006) Thermochemical, volumetric and spectroscopic properties of lysozyme–poly(ethylene) glycol system. *J. Therm. Anal. Calorim. 83*, 587-595.

Zimmermann, W., and Billig, S. (2010) Enzymes for the biofunctionalization of poly (ethylene terephthalate). *Adv. Biochem. Eng./Biotechnol. 125*, 97-120.

List of publications

1. Sulaiman, S., Yamato, S., Kanaya, E., Kim, J.-J., Koga, Y., Takano, K., and Kanaya, S. (2012) Isolation of a novel cutinase homolog with polyethylene terephthalate-degrading activity from leaf-branch compost by using a metagenomic approach. *Appl. Environ. Microbiol. 78,* 1556-1562.

2. Sulaiman, S., You, D.-J., Kanaya, E., Koga, Y., and Kanaya, S. (2014) Crystal structure and thermodynamic and kinetic stability of metagenome-derived LC-cutinase. *Biochemistry, 53*, 1858-1869.

Acknowledgements

I would like to express my uttermost gratitude to my advisor, Prof. Shigenori Kanaya, who gave the research opportunity and supported me during five years. I realized that it was very difficult to guide unexperience student for the research work but he still supported me, although I had no basic of experimental skills. All over five years, his suggestions guided and showed me how to handle the research plan and create the work as good as possible. In addition, I am truly thankful for his kindness helps for corrections of my writing. Without his helps, I think that I could not accomplish my research within time. Thank you very much sensei.

I would like to extend my gratitude to Prof. Takuya Nihira and Prof. Toshiya Muranaka for valuable comments and advices. Without these suggestions, this thesis would not be possible to be accomplished.

I would express my sincere gratitude to Prof. Hiroyuki Noji, who accepted me for the first year of my Master course in Osaka University and introduced me for the first step of science.

I also would like to thank the Japanese Ministry of Education, Culture, Sports, Science and Technology, for the financial support through the period of my study.

My sincere gratitude is also to Prof. Kazufumi Takano, Assoc. Prof. Yuichi Koga, Assist. Prof. Eiko Kanaya, Assist. Prof. Clement Angkawidjaja and Dr. Dong-Ju You for the supports, guidances and every valuable comments.

Special thanks to Ms. Reiko Matsumoto for motherhood and friendships during the period of my staying in Japan.

I am also thankful to all Kanaya lab members for our friendships. The thankfulness is also to Ms. Saya Yamato, who started this research and provided the valuable data for my study.

My thankfulness also goes to my friends in Japan for sharing every moment, especially Thai friends, who usually stay, share and understand the hard situations. I will remember the happiness and fun through the time that we spent in Japan.

I would like to give the special thanks for my beloved family. All the past of my childhood, whatever the inspiration, motivation and happiness, it is the great impact of my current life.

Last but not the least, thank you for the specials, who always support, share, cheer up and understand every single moment of my life.